

## **ABSTRACT**

Title of Document: SEMI-ACTIVE MAGNETORHEOLOGICAL SEAT SUSPENSIONS FOR ENHANCED CRASHWORTHINESS AND VIBRATION ISOLATION OF ROTORCRAFT SEATS

Gregory J. Hiemenz, Ph.D., 2007

Directed By: Professor N. M. Wereley, Department of Aerospace Engineering

This research focuses on the use of magnetorheological (MR) dampers for enhanced occupant protection during harsh vertical landings as well as isolation of the occupant from cockpit vibrations. The capabilities of the current state-of-the-art in helicopter crew seat energy absorption systems are highly limited because they cannot be optimally adapted to each individual crash scenario (i.e. variations in both occupant weight and crash load level). They also present an unnecessarily high risk of injury by not minimizing the load transmitted to the occupant during a crash. Additionally, current rotorcraft seats provide no means of isolating the occupant from harmful cockpit vibrations.

The objective of this research was to investigate and demonstrate the feasibility and benefits of an MR-based suspension for rotorcraft seats. As such, this research began with an in-depth investigation into design feasibility. Three MR seat suspension design cases are investigated: 1) for only vibration isolation, 2) for adaptive occupant protection, and 3) for combined adaptive occupant protection and

vibration isolation. It is shown that MR-based suspensions are feasible for each of these cases and the performance benefits and tradeoffs are discussed for each case. Next, to further illustrate the occupant protection benefits gained with an MR-based suspension, three control strategies were developed and performance metrics were compared. It was shown that MR dampers can be controlled such that they will automatically adapt to the crash load level as well as occupant weight. By using feedback of sensor signals, MR dampers were adjusted to utilize the full stroke capability of the seat suspension regardless crash level and occupant weight. The peak load transmitted to the occupant and the risk of spinal injury, therefore, was always minimized. Because this control significantly reduced or eliminated injury risk during less severe landings, it is a significant advance over the current state-of-the-art rotorcraft seat suspensions which can provide no better than 20% risk of occupant injury. Finally, an MR-based seat suspension designed solely for the purposes of vibration isolation was designed, analyzed, and experimentally demonstrated. MR dampers were integrated into the current crashworthy SH-60 crew seat with minimal weight impact such that the original crashworthy capabilities were maintained. Then, utilizing semi-active control, experimental vibration testing demonstrated that the system reduced vertical cockpit vibrations transmitted to the occupant by 76%. This is a significant advance over current state-of-the-art rotorcraft seats which provide no attenuation of cockpit vibrations.

SEMI-ACTIVE MAGNETORHEOLOGICAL SEAT SUSPENSIONS FOR  
ENHANCED CRASHWORTHINESS AND VIBRATION ISOLATION OF  
ROTORCRAFT SEATS.

By

Gregory J. Hiemenz

Dissertation submitted to the Faculty of the Graduate School of the  
University of Maryland, College Park, in partial fulfillment  
of the requirements for the degree of  
Doctor of Philosophy  
2007

Advisory Committee:  
Professor Norman Wereley, Chair  
Professor Balakumar Balachandran  
Professor Amr Baz  
Professor Alison Flatau  
Professor Darryll Pines

© Copyright by  
Gregory J. Hiemenz  
2007

## **Acknowledgements**

"At times our own light goes out and is rekindled by a spark from another person. Each of us has cause to think with deep gratitude of those who have lighted the flame within us."

--Albert Schweitzer

The light in which I stand at the culmination of this Ph.D. research has been sparked and fueled by many to which I am very grateful. Such stimulation and inspiration has come to me in many forms, ranging from encouragement and motivation, to technical guidance and advice, to the efforts that financially facilitated my involvement in this research. To all of those who have generously shared the light of their own torches, I send my warmest gratitude.

First, I would like to thank Mr. William Glass and the Naval Air Warfare Center - Aircraft Division (Pax River, MD) for supporting this exciting research and for providing wise direction and feedback throughout. Financial support provided by the Center for Rotorcraft Innovation and the Vertical Flight Foundation Scholarship is also gratefully acknowledged. My deepest gratitude also goes out to Dr. Peter Chen and Techno-Sciences, Inc. (TSi), the Principal Investigator and prime contractor of this research for making it financially possible for me to achieve this educational goal. Dr. Chen's guidance, advice, and motivation have played a large role in the success of this research. I am also very appreciative of the support and suggestions provided by my other colleagues at TSi, including Dr. Gang Wang, Dr. Curt Kothera,

and Dr. Ashish Purekar. Perhaps the most valuable benefit I have enjoyed from all of my TSi colleagues is their friendship.

Next, I would like to thank the students and post-doctoral researchers in the Smart Structures Laboratory at the University of Maryland Department of Aerospace Engineering for their friendship and contributions to my research successes. The support of Ben Woods, Ted Bubert, and Robbie Vocke in the assembly of the shock and vibration testing facility was critical in the success of this project and I am thankful for their hard work and dedication on that effort. Dr. Young-Tai Choi has been a valuable resource throughout my academic career at the University of Maryland. I am very grateful of his suggestions and guidance in MR damper control strategies, MR damper modeling, and experimental implementation. Additionally, I would like to deeply thank Dr. Peter Hu for his support on this project. He is paralleled by few in the field of MR damper design, and his help on this project has been crucial to its success.

Additionally, I would like to thank Prof. Balakumar Balachandran, Prof. Amr Baz, Prof. Alison Flatau, and Prof. Darryll Pines for serving on my dissertation committee and for their guidance and advice on my dissertation research. I am extremely grateful to have such a distinguished committee, both as educators and researchers. Their hard work, dedication, and successful contributions to the field provide continued motivation for me to strive for excellence. I especially would like to thank Prof. Amr. Baz, who despite knowing me as an immature undergraduate at Catholic University, first recommended me to Prof. Wereley. Whether it was sincere or whether it was an attempt to sabotage his research efforts, only Prof. Baz knows.

In the end, however, it has worked out well and has made a lasting effect on my life and career.

My gratitude to my advisor, Prof. Norman Wereley, is immeasurable. He has been an excellent advisor and mentor for over nine years and I am sincerely grateful for the opportunity that he gave me to return to the University of Maryland to complete my doctoral research under his advisement. His knowledge, hard work, dedication, and successes as both an educator and researcher will always stand as a model to which I strive. I feel very lucky to have had the opportunity to learn from him, work with him, and earn his friendship. I hope for these continued opportunities in the future.

Finally, without a strong and loving family, I would be nowhere. I am extremely grateful to have been constantly motivated and guided by my Mother and Father throughout my life. They have raised me to have an open, yet practical mindset and have prepared me well for a successful life and career. Finally, my deepest gratitude and love to my wife, Vanessa, who was a major stimulus for completing my Ph.D. She always encourages me to strive to be my best, she makes me a better person, and she selflessly supported me throughout this very demanding and stressful time. With her flame forever burning warmly nearby, I know mine will never go out.

# Table of Contents

<b>List of Tables .....</b>	<b>viii</b>
<b>List of Figures.....</b>	<b>ix</b>
<b>Nomenclature .....</b>	<b>xiv</b>
<b>List of Abbreviations .....</b>	<b>xvii</b>
<b>Chapter 1: Introduction.....</b>	<b>1</b>
1.1 Research Objective & Organization of the Dissertation.....	1
1.2 Rotorcraft Seat Suspension Design.....	3
1.2.1 Crashworthy Seat Suspension Design .....	3
1.2.2 Whole-Body Vibration.....	7
1.3 Semi-Active Magnetorheological Seat Suspensions .....	8
1.3.1 Magnetorheological Fluid Dampers .....	8
1.3.2 Dynamic Behavior of Systems Utilizing MR Dampers.....	10
1.3.3 Semi-Active Control .....	12
1.3.4 Prior Work with ER & MR Seat Suspensions .....	16
1.4 Mathematical Modeling.....	17
1.4.1 Lumped Parameter Biodynamic Model for Crash Simulations .....	19
1.4.2 SDOF Model for Vibration Simulations.....	21
1.5 Fundamental Contributions of the Present Research .....	22
1.5.1 Adaptive Crashworthiness .....	22
1.5.2 Vibration Isolation Combined with Crashworthiness.....	24

<b>Chapter 2: Investigation of MR Dampers for Enhanced Crashworthiness and Vibration Isolation of Helicopter Crew Seats .....</b>	<b>45</b>
2.1 MR Seat Suspension Design Principles .....	45
2.2 Case 1: Designing MR Dampers Solely for Vibration Isolation .....	49
2.3 Case 2: Designing MREAs for Adaptive Occupant Protection .....	52
2.4 Case 3: Dual-Goal MREA Design .....	56
2.5 Summary and Conclusions .....	60
<b>Chapter 3: Control of MREAs for Enhanced Crashworthiness .....</b>	<b>78</b>
3.1 Load Limiting or VLEA Control .....	78
3.1.1 Analytical Results .....	79
3.1.2 Effect of MR Damper Time Response .....	80
3.2 Notched-Profile or VPEA Control .....	82
3.2.1 Analytical Results .....	83
3.2.1 Effect of MR Damper Time Response .....	84
3.3 Crash Load Adaptive (CLA) Control .....	85
3.3.1 Analytical Results .....	87
3.3.2 Effect of MR Damper Time Response .....	89
3.4 Summary and Conclusions .....	90
<b>Chapter 4: Semi-Active Magnetorheological Helicopter Crew Seat Suspension for Vibration Isolation .....</b>	<b>108</b>
4.1 Integration into the Unarmored SH-60 Seahawk Crew Seat .....	108
4.2 MR Damper Characterization .....	109
4.3 Semi-Active Control .....	111
4.4 Experimental Setup .....	113

4.5	Experimental Results and Discussion.....	114
4.6	Summary and Conclusions .....	118
<b>Chapter 5: Summary, Conclusions, &amp; Recommendations for Future Work</b>		<b>138</b>
5.1	Original Contributions .....	138
5.1.1	Investigation of MR Dampers for Enhanced Crashworthiness and Vibration Isolation of Helicopter Crew Seats.....	139
5.1.2	Control of MREAS for Adaptive Crashworthiness .....	141
5.1.3	Semi-Active Magnetorheological Helicopter Crew Seat Suspension for Vibration Isolation .....	142
5.2	Future Work.....	143
5.2.1	MREA Design.....	144
5.2.2	MREA Control Experimentation & Refinement .....	145
5.2.3	Refinement of MR Seat Suspension for Vibration Isolation .....	146
5.2.4	Applicability to Other Vehicle Seats .....	147
<b>Bibliography .....</b>		<b>149</b>

## List of Tables

Table 1.1: Preliminary Lumped Parameter Biodynamic MR Seat Suspension Model Parameters.....	43
Table 2.1: Summary of MR Seat Suspension Trade Study .....	77
Table 4.1: Summary of Key Response Reductions Compared to Unmodified SH-60 Crew Seat.....	137

## List of Figures

Figure 1.1: Energy Absorbers Attenuate Input Deceleration and Limit the Deceleration of the Seat/Occupant [1].....	25
Figure 1.2: Inversion Tube FLEA Utilized in the Unarmored SH-60 Seahawk Crew Seat [3].....	26
Figure 1.3: Wire Bender FLEA Utilized in the EH101 Foldable Troop Seat [4].....	27
Figure 1.4: Crushable Composite Column FLEA Utilized in the Bell 230/430 Pilot Seat [4].....	28
Figure 1.5: FPEA Load-Stroke Characteristic [3] .....	29
Figure 1.6: Conceptual Explanation of the Fixed Profile Energy Absorber Process [3] .....	30
Figure 1.7: Schematic of Example FPEA [3] .....	31
Figure 1.8: VLEA Load-Stroke Adjustment Range [3].....	32
Figure 1.9: Wire Bender VLEA Utilized in the V-22 Osprey Armored Crew Seat [4] .....	33
Figure 1.10: Force vs. Velocity Profile for the Bingham Plastic Force Model .....	34
Figure 1.11: MR Damper Dynamic Range vs. Reynold's Number [16].....	35
Figure 1.12: SDOF Frequency Response for Varying $\beta$ [18].....	36
Figure 1.13: Comparing Bingham-plastic, Biviscous, and Hysteretic Biviscous Force Models [13].....	37
Figure 1.14: Comparison of Control Capability for Passive, Semi-Active, and Active Control .....	38

Figure 1.15: Physical Representation of skyhook Control Algorithm.....	39
Figure 1.16: Physical Representation of Groundhook Control Algorithm.....	40
Figure 1.17 - Comparing State-of-the-Art Rotorcraft Seat Suspension Schematic Diagrams with the MR Based Seat Suspensions Presented in this Dissertation.....	41
Figure 1.18: Lumped Parameter Biodynamic MR Seat Suspension Model for Design and Performance Evaluations of MREAs for Enhanced Occupant Protection.....	42
Figure 1.19: SDOF MR Seat Suspension Model for Vibration Isolation Design and Performance Predictions .....	44
Figure 2.1: Transmissibility for SDOF System to Base Excitation for Varying Viscous Damping Levels .....	63
Figure 2.2: Semi-Active Control Objective .....	64
Figure 2.3: Unarmored SH-60 Seahawk Crew Seat Produced By Armor Holdings ..	65
Figure 2.4: Reduction in Vibration Due to 0.2 g Amplitude 4P Floor Excitation vs. MREA Viscous Damping Ratio.....	66
Figure 2.5: MR Damper Optimized for Vibration Isolation.....	67
Figure 2.6: MR Dampers Retrofitted into SH-60 Crew Seat (Patent Pending) .....	68
Figure 2.7: MR Damper Response for a 95th Percentile Male Occupant and a 12.8 m/s (42 ft/s) Sink Rate Crash .....	69
Figure 2.8: Lumbar Time Response for 95th Percentile Male and a 12.8 m/s (42 ft/s) Sink Rate Crash with MREA .....	70
Figure 2.9: Preliminary Design of an MREA for Adaptive Crashworthiness .....	71
Figure 2.10: Crashworthy MREAs Retrofitted into SH-60 Seahawk Crew Seat .....	72

Figure 2.11: MR Damper Time Response for Load Limiting Control and Varying Occupant Weight .....	73
Figure 2.12: Dual-goal MREA Utilizing Bi-fold MR Valve (Patent Pending) .....	74
Figure 2.13: Standard Methods for Accounting for Rod Volume .....	75
Figure 2.14: Dual-Goal MREAs Integrated in Unarmored SH-60 Seahawk Seat.....	76
Figure 3.1: MREA Time Response for Passive Viscous, Constant Yield Force, and Load Limiting Control .....	92
Figure 3.2: MREA Time Response for Load Limiting Control and Varying Occupant Weight.....	93
Figure 3.3: MREA Time Response for Load Limiting Control and 10 ms Time Constant .....	94
Figure 3.4: MREA Time Response for Load Limiting Control and 20 ms Time Constant .....	95
Figure 3.5: Notched Profiles for VPEA Control.....	96
Figure 3.6: MREA Time Response for VPEA (Notched-Profile) Control.....	97
Figure 3.7: Effect of 10 ms Time Delay on Notched Load-Stroke Profile.....	98
Figure 3.8: MREA Time Response for VPEA Control with 10 ms Time Delay.....	99
Figure 3.9: Effect of 20 ms Time Delay on Notched Load-Stroke Profile.....	100
Figure 3.10: MREA Time Response for VPEA Control with 20 ms Time Delay....	101
Figure 3.11: MREA Time Response for Crash Load Adaptive Control.....	102
Figure 3.12: Load-Stroke Profile Resulting from Crash Load Adaptive Control.....	103
Figure 3.13: Correlation between EA Limit Load (g) and Spinal Injury Risk [4]....	104

Figure 3.14: MREA Time Response for Crash Load Adaptive Control for Varying Occupant Weight and Crash Level .....	105
Figure 3.15: MREA Time Response for Crash Load Adaptive Control with a 10 ms Time Delay.....	106
Figure 3.16: MREA Time Response for Crash Load Adaptive Control with a 20 ms Time Delay.....	107
Figure 4.1: MR Dampers Retrofitted into SH-60 Crew Seat in Series with Inversion Tube FLEAs* .....	120
Figure 4.2: Raw Force vs. Displacement Data for 1 Hz, 2.5 mm Amplitude Excitation .....	121
Figure 4.3: Force vs. Piston Velocity Data for 1 Hz, 2.5 mm Amplitude Excitation	122
Figure 4.4: Fitting Bingham Plastic Model to MR Damper Results for 1 Hz, 5 mm Amplitude Excitation .....	123
Figure 4.5: Fitting Cubic Function to Yield Force, $F_y$ , vs. Applied Current .....	124
Figure 4.6: Fitting a Cubic Function to Post-yield Damping, $C_p$ , vs. Applied Current .....	125
Figure 4.7: SDOF skyhook Control Performance Prediction for 50 <sup>th</sup> Percentile Male Crew Seat Occupant.....	126
Figure 4.8: Crew Seat Installed in Vertical Axis Shock and Vibration Test Stand ..	127
Figure 4.9: Accelerometer Placement on Seat.....	128
Figure 4.10: Rear Seat Pan Vertical Transmissibility for 50th Percentile Male, 0.2 g Excitation .....	129
Figure 4.11: Seat Top Longitudinal Coupling Transmissibility for 50th Percentile Male, 0.2 g Excitation.....	130

Figure 4.12: Front Seat Pan Vertical Transmissibility for 50 <sup>th</sup> Percentile Male, 0.2 g Excitation .....	131
Figure 4.13: Time History Data near Resonance, 50 <sup>th</sup> Percentile Male, 0.2 g Amplitude Floor Excitation .....	132
Figure 4.14: Rear Seat Pan Vertical Transmissibility for 5th Percentile Female, 0.2 g Excitation .....	133
Figure 4.15: Rear Seat Pan Vertical Transmissibility for 95th Percentile Male, 0.2 g Excitation .....	134
Figure 4.16: Rear Seat Pan Vertical Transmissibility for 50th Percentile Male, 0.4 g Excitation .....	135
Figure 4.17: Rear Seat Pan Vertical Transmissibility for 50th Percentile Male, 0.2 g Excitation, with Cushion.....	136

## Nomenclature

$f_d$	Desired control input
$f_{d_f}$	Filtered / delayed control input
$g$	Acceleration of gravity
$t$	Time
$t_m$	Time to reach peak deceleration input into seat
$v$	Piston velocity (relative velocity between seat and floor for seat suspension)
$v_o$	Initial vertical landing velocity of floor (sink rate)
$v_s$	Absolute velocity of seat
$z$	Absolute position of sprung mass in suspension model
$z_0$	Absolute position of base / floor
$z_s$	Absolute position of seat
$z_{st}$	Free suspension travel
$C_{grnd}$	Groundhook control gain
$C$	Viscous damping
$C_o$	Off-state viscous damping
$C_p$	Post-yield viscous damping
$C_{sky}$	skyhook control gain
$D$	MR damper dynamic range (ratio of on-state damping force to off-state damping force)
$F_{on}$	Maximum on-state total MR damper force at piston velocity $v$
$F_{st}$	Seat suspension end-stop impact force
$F_y$	MR damper yield force

$F_{CLA}$	Desired control force for crash load adaptive control
$F_{EA}$	Constant passive energy absorber force
$F_L$	Energy absorber limit load
$F_{MR}$	Total MR damper force
$F_{sky}$	skyhook control force
$F_{VPEA}$	Desired control force for VPEA control
$G_s$	Desired deceleration value at the spike portion of VPEA load-stroke profile
$G_n$	Desired deceleration value at the notch portion of VPEA load-stroke profile
$G_h$	Desired deceleration value at the hold portion of VPEA load-stroke profile
$G_L$	Deceleration limit for seat/occupant system
$G_M$	Peak deceleration input into seat
$I$	Current applied to MR damper
$K$	Suspension stiffness
$K_{CLA}$	Control gain for crash load adaptive control
$M$	Effective occupied seat mass
$Z$	Stroking distance tuning parameter for CLA control
$\alpha_{limit}$	Energy absorber limit load factor
$\beta$	Non-dimensional parameter for combined Coulomb and viscous damping
$\delta_n$	Stroke threshold for notch load in VPEA load-stroke profile
$\delta_h$	Stroke threshold for hold load in VPEA load-stroke profile
$\tau$	MR damper time constant for first-order low-pass filter
$\omega_n$	Fundamental resonance of seat suspension system
$\zeta$	Viscous damping ratio

- $\zeta_{sky}$  Equivalent viscous damping ratio for skyhook control
- $(\dot{\cdot})$  First time derivative
- $(\ddot{\cdot})$  Second time derivative
- $(\cdot)_i$  Denotes number of lumped parameter in multi-degree-of-freedom model

## **List of Abbreviations**

CLA:	Crash Load Adaptive control strategy
EA:	Energy Absorber
FLEA:	Fixed Load Energy Absorber
FPEA:	Fixed Profile Energy Absorber
MR:	Magnetorheological
MREA:	Magnetorheological Energy Absorber
RPM:	Revolutions per Minute
SDOF:	Single-Degree-of-Freedom
VLEA:	Variable Load Energy Absorber
VPEA:	Variable Profile Energy Absorber
WBV:	Whole Body Vibration
1P:	1/rev, main rotor frequency
4P:	4/rev, blade passing frequency for 4 bladed rotorcraft
8P:	8/rev, 2 <sup>nd</sup> harmonic of blade passing frequency for 4 bladed rotorcraft

# **Chapter 1: Introduction**

## *1.1 Research Objective & Organization of the Dissertation*

The objective of this research is to investigate and demonstrate the feasibility and benefits of an MR-based suspension for rotorcraft seats. As will be discussed in the following sections, MR dampers have the capability of providing enhanced occupant safety to both harmful cockpit vibrations during normal operation and lethal shock loads during harsh vertical or crash landings. As the research presented herein is the first known effort to implement an MR suspension into rotorcraft seats, after a thorough review of the state-of-the-art (Chapter 1), the research begins with an in-depth investigation into the feasibility of designing such a system for both enhanced crashworthiness and vibration isolation. In this study (presented in Chapter 2) design principles to which an MR seat suspension should be designed to maximize performance are presented, and three MR seat suspension cases are investigated: 1) MR dampers for only vibration isolation, 2) MR energy absorbers (MREAs) for adaptive occupant protection, and 3) dual-goal MREAs for combined adaptive occupant protection and vibration isolation. The performance benefits and tradeoffs are discussed for each.

One of the results from Chapter 2 is that, using conventional MR damper technology, achieving enhanced crashworthiness with an MREA-based seat suspension tends to increase the weight of the seat, which is undesirable. In order to further illustrate the benefits gained and to justify this increased suspension weight, a second study (Chapter 3) was undertaken. In Chapter 3, strategies are investigated to control the MREAs to provide enhanced crashworthiness and performance metrics

such as lumbar load and the amount of stroke utilized are compared. These control strategies are intended to advance the state-of-the-art in rotorcraft seat suspensions by providing automatic and unattended adaptation to both occupant weight and crash level. By using feedback of sensor signals, MR dampers can be adjusted to utilize the full stroke capability of the seat suspension regardless of crash level and occupant weight. The peak load transmitted to the occupant and the risk of spinal injury, therefore, are always minimized. Because this control significantly reduces or eliminates injury risk during less severe landings, it is a significant advance over the current state-of-the-art rotorcraft seat suspensions which can provide no better than 20% risk of occupant injury. For each of these control schemes, the effect of MREA time response is also investigated and performance metrics (tracking error, spinal loads, stroke utilized, etc.) are compared.

Next, since current rotorcraft seat suspensions provide no means of attenuating harmful cockpit vibrations, the goal of vibration isolation using MR dampers is addressed in Chapter 4. It is shown in Chapter 2 that an MR damper designed solely for the purposes of vibration isolation can be integrated into the current crashworthy SH-60 crew seat with minimal weight impact. This option, therefore, was deemed the most practical goal for near-term implementation into the fleet. MR dampers were designed, fabricated, tested, characterized, and integrated into the unarmored SH-60 crew seat such that the original crashworthy capabilities were maintained. Then, utilizing semi-active control, experimental vibration testing was performed to evaluate the system performance in isolating cockpit vibrations.

Finally, in Chapter 5, the final conclusions of these studies are collected together and presented. A summary of results as well as a list of original contributions to the state-of-the-art are presented. Recommendations for future research are also presented in this final chapter.

## *1.2 Rotorcraft Seat Suspension Design*

In order to effectively improve rotorcraft seats with a semi-active magnetorheological suspension, it is important to understand the limitations of the state-of-the-art seats. The following two sections summarize the evolution of crashworthy seat suspension designs and illustrate their limitations for both occupant protection during harsh or crash landings as well as whole body vibration.

### 1.2.1 Crashworthy Seat Suspension Design

A very important issue in helicopter seat design is occupant protection during harsh vertical or crash landings. The primary goal in occupant protection is to minimize the potential for occupant spinal and pelvic injuries. While a significant amount of energy is absorbed through the compression of the landing gear and crushing of vehicle substructure, the cockpit floor can still transmit lethal loads into the seat and spine. The floor deceleration during such events is typically approximated as a triangular pulse with peak deceleration,  $G_M$ , as shown in Figure 1.1 [1]. This peak deceleration and the duration of the pulse are functions of the helicopter sink rate at impact and the energy absorption properties of the landing gear and/or base frame. Most helicopter seats currently utilize energy absorption systems such as a seat suspension to attenuate the vertical shock loads that are transmitted

from the base frame of the aircraft and imparted into the human body. The use of these energy absorption systems increases the chances of occupant survival during these events [2].

Most crashworthy crew seat designs currently employ fixed-load energy absorbers (FLEAs) to limit an occupant's spinal load to within a tolerable range. The load-stroke profile of these FLEAs are tuned to a factory-established, constant load throughout their entire operating range (i.e., passive). Examples of these FLEAs are inversion tube energy absorbers (Figure 1.2), used in the unarmored SH-60 Seahawk crew seat discussed herein, wire bender energy absorbers (Figure 1.3), crushable composite columns (Figure 1.4), etc. [1], [3]. FLEAs are tuned only for one occupant weight/type (typically a 50<sup>th</sup> percentile male) and one crash level (typically to the highest crash design level). FLEAs are typically designed to provide a 14.5 g seat deceleration limit for the occupant to whom they are tuned. This deceleration limit was determined through analysis and cadaveric testing in the 1960s and 1970s and corresponds to a 20% risk of injury to U.S. Army Aviators per Ref. [4]. Lighter occupants, however, tend to have weaker spines and the FLEA factory established stroking load tends to be too high, which can result in an increased injury risk [4]. Moreover, for heavier occupants, this fixed stroking load is too low – potentially resulting in the full use of the system's stroke capability and a hard end-stop impact leading to increased injury risk.

Next, fixed-profile energy absorbers (FPEAs) were developed. These devices aim to more efficiently utilize stroke by taking advantage of the dynamic response of the human body. FPEAs use a “notched” load-stroke profile (Figure 1.5) with an

initial load spike to quickly compress the “springs” in the human body [3]. Then, the load is lowered rapidly to minimize the overshoot as the body “springs” are loaded up, thereby limiting the maximum load on the occupant’s spine. The energy absorber (EA) load would then be again increased to a sustainable plateau for the rest of the stroke. A simplified illustration of this effect is presented in Figure 1.6 [1], [3]. This type of load-stroke profile allows the body to be decelerated at a higher average acceleration than FLEAs by minimizing the overshoot typical of rapid loading of such a spring-mass system. Since the peak spinal loads typically occur during this overshoot, minimizing the overshoot allows the average load to be raised while keeping the spinal load within human tolerance limits [1], [3]. An example of such an FPEA is shown in Figure 1.7 [1], [3]. This embodiment includes a shear plug to provide the initial load spike, and two inversion tubes in series: one for the notch load and one for the hold load [3]. While these FPEAs were found to use stroke more efficiently, they are still tuned for one occupant weight and one crash level, and therefore, they suffer similar limitations as the FLEAs discussed above.

Finally, variable load energy absorbers (VLEAs) have been developed that allow the occupant to manually adjust the constant stroking load by setting a dial for their weight. The stroking load of the VLEA is then selected *a priori* to be proportional to the occupant weight, so that each occupant will undergo similar acceleration (typically 14.5 g) and use similar stroking space during a crash. These VLEAs exploit the fact that the strength of an occupant’s spine is nearly proportional to occupant weight, so that the injury risk is low (~20%) regardless of occupant weight [1], [3], [4]. In Figure 1.8, an example of a VLEA load-stroke adjustable

range is shown. An example of a VLEA design is the wire bender energy absorber used in the armored V-22 Osprey pilot seat (Figure 1.9) [3]. In this VLEA design, the stroking load is adjusted by changing the location of the center roller [3]. VLEA technology was also applied in programs to retrofit new seats for the U.S. Navy's CH-53 Sea Stallion and SH-3 Sea King aircraft [3]. Since these devices rely on plastic deformation of material, however, their weight adjustment range is limited and they are only adjustable in preset increments (typically 45-90 N [10-20 lb]).

FLEAs, FPEAs, and VLEAs, however, are all passive in that they cannot automatically adapt their load-stroke profile as a function of occupant weight or as a function of real-time environmental measurements such as crash levels. Because the load-stroke profile for FLEAs, FPEAs, and VLEAs are fixed during flight, the occupant has the same 20% risk of injury during a lower sink rate or lower energy crash as the highest sink rate or highest energy crash. This is because the EA force (and thus the amount of force transmitted to the occupant) remains constant, but the amount of stroke utilized is reduced during a lower sink rate crash. The capabilities of these EAs, therefore, are highly limited because they cannot optimally adapt to the individual crash scenario. An optimal EA would utilize the same (full) stroke in each crash, regardless of occupant weight or crash level, to transmit the lowest load possible to the occupant, and therefore, minimize the risk of injury. The risk of injury during a lower sink rate or lower energy crash would then be much less than the 20% risk associated with current EA technology. Moreover, because these devices all rely on plastic deformation of a material, these EAs do not begin to stroke until the EA load reaches the tuned threshold and therefore act as a stiff coupling between the floor

and the seat. For these reasons, these systems provide only limited occupant protection to harsh vertical loads and no isolation to rotorcraft vibration during normal operation.

### 1.2.2 Whole-Body Vibration

Whole body vibration (WBV) has become an increasingly significant area of concern in helicopter seat design. Chronic exposure to cockpit vibration levels can fatigue crew, shorten mission duration, and cause significant health problems [5],[6]. Military studies and hazard reports have shown that back pain and spinal abnormalities are prevalent amongst helicopter pilots [5]. Such pain has been identified as extreme localized pain and becomes chronic as rotary wing flight exposure increases [5], [6]. Hazard reports have indicated that such pain in the lumbar region, buttocks, and legs begins 2 to 4 hours into the flight and increases with time [6]. Growing operational demands and evolving military strategies have significantly increased the frequency of extended duration missions (> 6 hours) [6], exacerbating the problem. Studies have also shown that such physical discomfort leads to inattention and distraction – contributing to a loss of situational awareness and poor decision making in both training and missions [6],[7].

While seat suspension technology is available that can significantly minimize the rotor-induced vibration transmitted to the occupant, such designs have not been explored because crash safety has been the design priority [6], [8]. That is, all available stroke has been devoted to mitigating crash loads, and no stroke has been allocated to vibration mitigation. Energy absorbers such as FLEAs, FPEAs, or VLEAs minimize the potential for occupant spinal and pelvic injuries during harsh

vertical or crash landings of these aircraft [1],[3]. These FLEAs, however, will not stroke until a tuned load threshold is reached and therefore act as a stiff link between the seat and the floor during normal rotorcraft vibration. Because of this, these systems provide no isolation to rotor-induced vibration [8]. While crash safety is a critical issue, pilot fatigue and chronic health problems, as well as reduced mission effectiveness, are also serious concerns [6].

### *1.3 Semi-Active Magnetorheological Seat Suspensions*

#### 1.3.1 Magnetorheological Fluid Dampers

Magnetorheological (MR) fluid dampers are semi-active devices in which the damping forces are controlled by magnetic field [9], [10]. These dampers are well suited for semi-active seat suspensions because of their low power requirements (can be run on batteries), high force capacity [11], high dynamic range (large difference between off and on conditions), and mechanical simplicity (no moving parts). They are also attractive for this application because in the case of power loss (as may happen during crash events), they can be safely powered with batteries. An advantage of MR dampers over active actuators is that they have an inherent failsafe mode. That is, even if battery power is lost, MR dampers will still provide passive hydraulic damping, albeit at a lower level than for non-zero field.

This study uses the Bingham plastic model for the MR dampers because it provides the most general case and is the simplest in form. Prior work has shown that while the Bingham plastic model may not exactly match real damper characteristics, its response in dynamic systems is nearly identical to the more complex models [12]. At the fluid level, the Bingham plastic model assumes a fluid with a constant plastic

viscosity and a non-zero yield stress. At the damper level, the force becomes essentially a yield force added to a linear damping model.

When field is applied to the fluid, the yield stress of the fluid increases, which in turn increases the yield force of the damper [9],[10],[13]. If the input force to the damper is less than this yield force, the damper is rigid or the damper locks. When the input force is greater than the yield force, the damper force is the superposition of forces due to a viscous damper and a Coulomb friction element. The damper force can be expressed as:

$$F_{MR}(v) = C_p v + F_y \text{sign}(v) \quad (1.1)$$

where,  $v$  is the piston velocity,  $C_p$  is the post yield damping, and  $F_y$  is the yield force of the damper that is controlled by the magnetic field. This force vs. velocity relation is shown in Figure 1.10.

A number of studies have been undertaken to aid in the design of MR dampers. In 1998, Wereley and Pang utilized parallel plate assumptions to develop a non-dimensional analysis of MR dampers [14]. This analysis identifies key non-dimensional parameters such as the Bingham number (the ratio of the dynamic yield stress to the shear stress due to Newtonian viscosity), area ratio (ratio of the annular gap area to the piston area), and non-dimensional plug thickness (ratio of the plug thickness to the annular gap distance) which can be used to determine preliminary design geometry for shear mode, flow mode, and mixed mode MR dampers [14]. In 2005, Hong *et al.* developed a non-dimensional design scheme for mixed-mode MR dampers based upon the Bingham plastic constitutive equations [15]. By using four parameters; namely, the Bingham number, the non-dimensional damping force,

dynamic range (ratio of the on-state force to the off-state force), and geometric ratio (ratio of the piston radius to the annular gap distance), sequential design steps identifying key design geometry for MR dampers have been formulated [15]. Finally, in 2005, Mao and Wereley developed an effective design strategy for MR dampers using a nonlinear flow model to describe laminar and turbulent flow [16]. In this study, MR damper force is related to non-dimensional parameters such as Bingham number, dynamic range, and Reynold's number over a wide operating range of shear rates. An important result from this study is the fact that the MR damper dynamic range decreases exponentially with the Reynold's number of the flow within the MR valve (Figure 1.11) [16]. Since this Reynold's number is a function of the piston velocity, a given MR damper design will see reduced dynamic or controllable range as piston velocity increases. As will be discussed in Section 2.1, this directly affects the design of MR dampers for use in crashworthy seat suspensions.

### 1.3.2 Dynamic Behavior of Systems Utilizing MR Dampers

As stated above, MR dampers exhibit Bingham plastic behavior, which is the superposition of a viscous damping term and a Coulomb or yield force,  $F_y$ , that is dependent on magnetic field (Eq. 1.1) [9],[13]. This damping force is similar to the system studied by Hartog [17], that is, a viscous damping combined with Coulomb friction/damping. In a mass-spring-damper system with Coulomb damping, if the yield force is higher than the input force, the system will experience stopped motion. In this case, there will be no damping because the damper will be locked and there will be no displacement [18]. To help with this issue, a non-dimensional group suggested by Hartog is used, which is the ratio of the Coulomb force of the damper to

the input force. For a base excited system, this non-dimensional group can be expressed as follows:

$$\beta = \frac{F_y}{M\ddot{z}_0}, \quad (1.2)$$

where  $M$  is the mass supported by the MR damper and  $z_o$  is the base motion [18]. For a constant input acceleration,  $\beta$  becomes a function of the applied magnetic field to the damper. If the yield force should become greater than the input force (i.e.,  $\beta > 1$ ), the damper will lock and the sprung mass will essentially have a stiff connection to the base. While having the MR damper in this locked condition will remove the resonance condition resulting from the spring in the system, any desired higher frequency isolation effects will also be lost. Thus, for isolation, it is important to prevent stopped damper motion by maintaining  $\beta < 1$  when the excitations frequencies are above a system resonance [18]. Furthermore, in 1999, Hiemenz and Wereley [18] showed that for a single degree of freedom (SDOF) system utilizing MR dampers, the system begins experiencing stopped motion and changes resonance frequency when  $\beta > \pi / 4$ . When  $\beta < \pi / 4$ , the additional magnetic field dependent Coulomb damping decreases the transmissibility,  $T$ , at resonance while not affecting the resonant frequency as shown in Figure 1.12. It has been shown that  $\beta$  can be a useful parameter for both MR damper design and semi-active control algorithm design [18].

Finally, as was noted in Section 1.3.1, the Bingham-plastic force model does not exactly capture the real MR damper characteristics; that is, experimental testing results show that the pre-yield region is not rigid as predicted using the Bingham-

plastic force model. This is illustrated in Figure 1.13b, where the solid line represents typical MR damper force vs. velocity characteristics and the dashed line represents the Bingham-plastic model [13]. MR damper pre-yield behavior is, however, more accurately modeled using the biviscous and hysteretic biviscous force model shown in Figure 1.13c and Figure 1.13d [13]. This is why the phenomena of drift, usually associated with systems having high Coulomb (friction) damping, is typically not seen in the dynamics of MR systems.

Furthermore, in 1999, Kamath and Wereley studied the effect of pre-yield behavior on dynamic response of MR dampers [12]. In this study, the method of slowly varying parameters was used to approximate closed form solutions for SDOF systems incorporating the Bingham-plastic, biviscous, and hysteretic biviscous MR damper models [12]. The results showed that the differences in dynamic amplitude and phase were relatively minor. The Bingham-plastic model, therefore, is sufficient for the design and performance predictions of MR suspension systems.

### 1.3.3 Semi-Active Control

There are three main methods of motion control: passive, active, and semi-active control. Passive vibration control is the most simple and widely used strategy because it involves no control logic or effort and the control/damping properties remain constant. Passive control/damping removes energy from a system, and cannot inject energy into the system, thereby assuring stability. While passive vibration control is attractive because it requires no control effort, is low maintenance, and is inherently stable, its performance is limited because the damping profile (force vs.

velocity) is fixed as shown in Figure 1.14 and cannot adapt to changing system parameters or excitation levels [19].

Active vibration control, on the other hand, involves actuators that strategically inject a desired input into a system to optimally control its motion. Such actuators include hydraulic systems, air pumps, motor systems, and piezoelectric actuators [19]. Active controllers will process signals from sensors within the system and designate the location and amount of force injected by these actuators. Referring again to Figure 1.14, active control has the capability of providing control input anywhere within all four quadrants of the force vs. velocity plane (limited only by the force limits of the actuator). Active vibration control gives the best performance of these three categories, but also has some drawbacks. Because active control injects energy into the system, there is the potential of the system becoming unstable and worsening the vibration response. In addition, active control requires that net energy be injected into the system, and therefore uses a high amount of energy. Finally, many of these actuators are very bulky, require large-scale power sources, and/or can be very high maintenance.

Semi-active vibration control aims to combine the adaptive nature of active control with the low maintenance, low energy consumption, and stability characteristics of passive control. A semi-active control device is defined as one that cannot increase the mechanical energy in the controlled system, but has properties that can be dynamically varied [20]. For dynamically variable dampers, the semi-active control force is limited to anywhere within the upper right and lower left quadrants of the force vs. velocity plane (Figure 1.14) when the control force is the

same sign as velocity. For the most part, semi-active actuators are in the form of dynamically variable dampers, and have fewer moving parts than active actuators. This lends them to be lower maintenance and higher reliability than active control actuators. Because semi-active devices cannot inject and can only remove energy from a system, the system cannot become unstable due to control action. In semi-active vibration control, the properties of the actuators are dynamically varied to optimally damp the vibration of a system [21]. The control logic used is similar to that in active vibration control, but the control action is limited since the actuator cannot inject energy [21]. Additionally, because semi-active control does not need to input any forces, the energy consumption is low when compared to active vibration control.

A number of semi-active control algorithms have been developed for various applications. One of the most basic and widely used is the skyhook control algorithm which was developed in 1974 by Karnopp *et al.* This simple, yet effective vibration isolation strategy is realized by a fictitious damper connecting between the sprung mass and the stationary sky (see Figure 1.15). [22]. In this control scheme, the damper exerts a force tending to reduce the *absolute* velocity of the sprung mass. This differs from conventionally position dampers (positioned between the sprung mass and the base), which exert forces that tend to reduce the *relative* velocity between the sprung mass and the base. While conventional dampers reduce the resonant response, it is at the cost of increased high frequency response. This is because, at high frequency inputs, they tend to harden the suspension when a soft suspension is desired. The skyhook algorithm, however, effectively achieves a

combination of resonance suppression and high frequency isolation [22]. For an MR damper installed in place of a conventional damper, this control strategy essentially adjusts the damper to the desired force (linearly proportional to sprung mass absolute velocity) when it is the same sign as relative velocity and turns the damper off when they are opposite, ensuring that the force is always dissipative:

$$F_{sky} = \begin{cases} C_{sky} \dot{z} & \text{if } \dot{z} \cdot (\dot{z} - \dot{z}_o) \geq 0 \\ 0 & \text{if } \dot{z} \cdot (\dot{z} - \dot{z}_o) < 0 \end{cases} \quad (1.3)$$

where  $C_{sky}$  is the skyhook control gain.

Following this, Groundhook control was developed [23],[24]. Rather than suppressing vibration of the sprung mass, Groundhook control is intended to reduce the vibration of the unsprung mass, essentially assuming an additional inertia damper between the unsprung mass and the ground (Figure 1.16). In terms of practical use, Groundhook control adjusts the damper to the desired force (linearly proportional to unsprung mass absolute velocity) when it is the opposite sign as relative velocity and turns the damper off when they are the same sign:

$$F_{grnd} = \begin{cases} C_{grnd} \dot{z}_2, & \text{if } -\dot{z}_2 (\dot{z}_1 - \dot{z}_2) \geq 0 \\ 0 & \text{if } -\dot{z}_2 (\dot{z}_1 - \dot{z}_2) < 0 \end{cases} \quad (1.4)$$

where  $C_{grnd}$  is the Groundhook control gain. For vehicle applications, skyhook control is designed to reduce the vibration experienced by the rider, while Groundhook is intended to stabilize the vehicle by reducing tire-axle assembly vibration [25].

A myriad of control strategies have been proposed to implement and modify skyhook and Groundhook control. These address topics ranging from combining skyhook and Groundhook control to merge their benefits [26], incorporating gain

scheduling and state estimation [27], reducing the dynamic jerk that tends to be induced by these types of control [28], imposing force limits preventing damper lock-up, and combination with other control algorithms [29]. The following section describes semi-active control algorithms used specifically for the purposes of seat suspensions.

#### 1.3.4 Prior Work with ER & MR Seat Suspensions

Many researchers have been motivated to investigate innovative seat suspensions showing improved shock and/or vibration mitigating performance by controlling stiffness and/or damping. In 1997, Wu and Griffin studied several semi-active control algorithms to reduce the severity of seat suspension end-stop impacts [30]. This two-state (on-off) control algorithm switches between states based upon the stroking deflection. If the deflection exceeds a preset stroke threshold, the damper is turned on to a “hard” state. If the deflection is less than the stroke threshold, the damper remains in the off or “soft” state [30]. It was shown that, using such an algorithm, a compromise can be made between vibration isolation and end-stop impact reduction [30].

In 2000 and 2003, Choi et al. investigated attenuating seat vibration using skyhook and sliding mode control algorithms on both electrorheological (ER) and MR seat suspensions for a commercial vehicle [31], [32]. For the skyhook control implementation, it was shown through full-vehicle HILS testing that the seat vibration levels were significantly reduced for both bump and random road profiles [31]. For the sliding mode control implementation, the governing equation was derived by treating the occupant mass as a parametric uncertainty. The sliding mode controller,

which has inherent robustness to parametric uncertainties, was shown to significantly improve ride comfort quality [32].

In 2002, Park and Jeon developed a Lyapunov-based robust control algorithm to compensate for actuator time delay and experimentally evaluated it for vibration control performance of an MR seat suspension [33]. Analytical predictions using this control algorithm are compared with a passive system, and semi-active systems using skyhook and standard Lyapunov control. It is shown that the Lyapunov-based robust control considering time delay suppresses the vibration most effectively.

Finally, in 2005, Choi and Wereley analytically evaluated the biodynamic response of the seated human occupant protected by a controlled MR rotorcraft seat suspension to both sinusoidal vibration and crash loads, and compared these results with passive hydraulic seat suspensions [1]. For the sinusoidal excitation case, it was observed that the controlled MR seat suspension shows significantly better vibration attenuation performance than the passive seat suspensions [1]. For the crash load cases using the same controller, only minor improvements in critical injury metrics were made. This study showed, however, that vibration attenuation performance can be substantially improved using a semi-active MR seat suspension without sacrificing crashworthiness [1].

#### *1.4 Mathematical Modeling*

In this section, the two mathematical dynamic models utilized in this dissertation are presented: one, a lumped-parameter biodynamic model for use in crashworthy seat suspension design, and another, a single-degree-of-freedom (SDOF) model for use in designing seat suspensions for vibration isolation. Before discussing

these models, however, it is important to first explain the differences between the two excitation cases. Referring to Figure 1.17a and b, it can be seen that for the crash design cases, the occupant and seat have an initial velocity equal to the descent rate of the helicopter. Upon impact with the ground, the seat and occupant system begin to rapidly decelerate. The deceleration profile is dependent upon the descent rate and the structure being crushed underneath the cockpit (landing gear, airframe, etc.) and, as mentioned in Section 1.2.1, is typically approximated as the triangular pulse shown in Figure 1.1. For such crash simulations, it is typically desirable to use a dynamic model of the seat/occupant that has enough fidelity to estimate lumbar loads. Such a dynamic model might be a simple lumped-parameter representation as the one used in this study (see Section 1.4.1, below) or more complicated models such as the commercially available SOMLA and MADYMO software. Figure 1.17a shows a system representing the current state-of-the-art seat suspension systems with a passive crash energy absorber providing a constant frictional force,  $F_{EA}$ . In Figure 1.17b, the EA is replaced with an MREA that provides a damping force,  $F_{MR}(t)$ , which can be controlled based upon real-time sensor feedback. This condition represents the case studied in Section 2.3 as well as Chapter 3.

Figure 1.17c and d illustrate the assumptions for the vibration isolation design conditions. In these cases, the seat/occupant system is initially at rest and is excited by the floor motion,  $z_0(t)$ . In the current state-of-the-art rotorcraft seat suspensions (Figure 1.17c), the constant passive energy absorber force,  $F_{EA}$ , is much higher than the excitation force, therefore the EA does not stroke and all floor vibration is transmitted directly to the seat/occupant system. Figure 1.17d shows a spring and

MR damper implemented in series with the passive energy absorber. In this case, the spring and MR damper dampen/isolate the floor vibrations transmitted from the passive EA. The amplitude of the MR damper force,  $F_{MR}(t)$  is on the order of the vibration forces and is dependent upon real-time motion sensor feedback. This condition represents the case studied in Section 2.2 and Chapter 4.

#### 1.4.1 Lumped Parameter Biodynamic Model for Crash Simulations

Occupant spinal/lumbar loading is a prime factor in determining occupant injury and survivability during harsh vertical or crash landing scenarios. In order to evaluate MREA designs and performance, it is therefore necessary to use a mathematical model with enough fidelity to predict lumbar loads. This study uses a model originally developed in 1998 by Liu *et al.* via cadaveric testing [34] and further verified by Zong and Lam in 2002 [35]. In 2005, Choi and Wereley added an MR seat suspension to this model [1]. In the biodynamic MR seat suspension model (Figure 1.18), a nonlinear lumped parameter representation of a seated occupant was coupled with the nonlinear Bingham-plastic force model for an MREA. The seat, denoted by  $M_I$ , is fixed to the floor through the MREA,  $F_{MR}$ , and spring,  $K_I$ . In addition, an end-stop buffer is implemented, which produces a nonlinear spring reaction force,  $F_{st}$ , when the suspension stroke exceeds its free-suspension travel,  $z_{st}$ . The soft seat cushion is simply represented as a stiffness and damping ( $K_{2c}$  and  $C_{2c}$ , respectively). The body is divided into four parts: pelvis, upper torso, viscera, and head, represented by mass  $M_i$ , stiffness  $K_i$ , and damping  $C_i$ , where  $i = 2, 3, 4$ , and  $5$ , respectively. The motion of this system is governed by the following five equations [1]:

$$M_1\ddot{z}_1 = -K_1(z_1 - z_0) + K_{2t}(z_2 - z_1) + C_{2t}(\dot{z}_2 - \dot{z}_1) - F_{MR} - F_{st} \quad (1.5)$$

$$M_2\ddot{z}_2 = -K_{2t}(z_2 - z_1) - C_{2t}(\dot{z}_2 - \dot{z}_1) + K_3(z_3 - z_2) + C_3(\dot{z}_3 - \dot{z}_2) \quad (1.6)$$

$$M_3\ddot{z}_3 = -K_3(z_3 - z_2) - C_3(\dot{z}_3 - \dot{z}_2) - K_4(z_3 - z_4) - C_4(\dot{z}_3 - \dot{z}_4) + K_5(z_5 - z_3) + C_5(\dot{z}_5 - \dot{z}_3) \quad (1.7)$$

$$M_4\ddot{z}_4 = K_4(z_3 - z_4) + C_4(\dot{z}_3 - \dot{z}_4) \quad (1.8)$$

$$M_5\ddot{z}_5 = -K_5(z_5 - z_3) - C_5(\dot{z}_5 - \dot{z}_3) \quad (1.9)$$

where,

$$K_{2t} = \frac{K_2 K_{2c}}{K_2 + K_{2c}}, \text{ and } C_{2t} = \frac{C_2 C_{2c}}{C_2 + C_{2c}} \quad (1.10, 1.11)$$

In Eq. 1.5,  $z_0$  is the displacement of the floor. The initial conditions for this problem are  $z_i = 0$  and  $\dot{z}_i = -v_o$ , where  $i = 0, 1, 2, 3, 4$ , and  $5$ , and  $v_o$  is the initial vertical landing velocity (or sink rate) of the helicopter. The stiffness of the pelvis,  $K_2$ , is modeled by the nonlinear function [1], [34], [35]:

$$K_2 = 8.1075e7(z_2 - z_1)^2 \quad (1.12)$$

The stiffness of the upper torso is also nonlinear [1], [34], [35]:

$$K_3 = \begin{cases} 3.78e6 + 1.09e7\delta_3 - 2.69e7\delta_3^2, & \text{if } \delta_3 \geq 0.04 \\ 77044, & \text{if } \delta_3 < 0.04 \end{cases} \quad (1.13)$$

where  $\delta_3 = x_2 - x_3$ .

The damping  $C_i$  is given by

$$C_i = 2\zeta_i \sqrt{M_i K_i}, \quad \text{if } i = 2, 3, 4, 5 \quad (1.14)$$

where  $\zeta_i$  is the damping ratio of each part of the human body. Because  $K_2$  and  $K_3$  are nonlinear functions,  $C_2$  and  $C_3$  are also nonlinear. Lastly, the nonlinear spring reaction force,  $F_{st}$ , due to the end-stop buffer is given by [1]:

$$F_{st} = \begin{cases} 0 & \text{if } \delta_1 < z_{st} \\ 8.0e4[\delta_1 - z_{st} \operatorname{sgn}(\delta_1)] + 3.4e8[\delta_1 - z_{st} \operatorname{sgn}(\delta_1)]^3 & \text{if } \delta_1 \geq z_{st} \end{cases}, \quad (1.15)$$

where,  $\delta_j = z_1 - z_0$ .

The parameters of the MR seat suspension model used for this study are specified in Table 1.1 [1], [34], [35]. The biodynamic parameters represent those obtained from dynamic tensile tests for an approximate 90th percentile male [34], [35]. It is also assumed that 29% of the occupant's body weight is supported by the floor, and therefore not part of the total effective seat mass [36]. When considering varying occupant weights, these mass values are scaled linearly by total occupant weight. In addition to these masses, 11 kg of body worn equipment has been added to the upper torso, and 2.25 kg has been added to the head to account for a helmet. Based upon studies performed by Boileau et al. [37], the biodynamic stiffnesses have been assumed to remain constant over varying occupant weights. Finally, it should be noted that the coil spring stiffness,  $K_I$ , has been set to zero. This is because for a harsh vertical loading event, an energy storing device (spring) will produce an undesirable rebound lumbar load. Such a one-dimensional model provides an economic means of optimizing MREA design and evaluating control performance by predicting lumbar load response [1], [38].

#### 1.4.2 SDOF Model for Vibration Simulations

Because the nonlinear stiffnesses used in the previously presented lumped parameter biodynamic model have been generated for high amplitude excitations, this model is not well suited for vibration isolation design and performance predictions. Experimental testing at the University of Maryland, however, has shown that a simple

single-degree-of-freedom (SDOF) MR seat suspension model (Figure 1.19) is a valuable tool in design and performance predictions for low amplitude excitations [39]. The equation of motion for this SDOF MR seat suspension model is simply:

$$M\ddot{z}_s + K(z_s - z_0) + F_{MR} = 0 \quad (1.16)$$

Here,  $M$  is the effective occupied seat mass (seat mass plus the percent of occupant weight supported by the seat -71% [36]),  $K$  is spring stiffness used in the suspension, and  $z_s$  is the absolute seat position. This SDOF model remains accurate during these low amplitude excitations because the suspension stiffness,  $K$ , is much lower than the nonlinear biodynamic stiffnesses and the nonlinear pre-compressed cushion stiffness. The body and seat, therefore, resemble one lumped mass at these excitation levels and frequencies of interest.

## 1.5 Fundamental Contributions of the Present Research

### 1.5.1 Adaptive Crashworthiness

In Section 1.2, the current state-of-the-art for crashworthy aircraft seat suspension designs was discussed. It was explained that FLEAs and FPEAs used widely throughout industry for military and commercial applications are tuned only for one occupant weight/type (typically a 50<sup>th</sup> percentile male) and one crash level (typically to the highest crash design level). For lighter occupants, this factory established stroking load is too high, which can result in increased injury risk. Moreover, for heavier occupants, this fixed stroking load is too low – potentially resulting in the rapid utilization of the system’s stroke capability and a hard end-stop impact – leading to increased injury risk. VLEAs have been developed to help

address this by manually adjusted for occupant weight. Since these devices rely on plastic deformation of material, however, their weight adjustment range is limited and they are only adjustable to set increments (typically 45-90 N [10-20 lb]). Furthermore, because the load-stroke profile for FLEAs, FPEAs, and VLEAs are fixed during flight, the occupant sees the same risk of injury during a lower sink rate or lower energy crash as it does the highest sink rate or highest energy crash. This is because the EA force (and thus the amount of force transmitted to the occupant) remains constant, but the amount of stroke utilized is reduced during a lower sink rate crash. The capabilities of these EAs, therefore, are highly limited because they cannot optimally adapt to the individual crash scenario.

In Chapter 3, it will be shown that, using real-time feedback of sensors mounted on the seat, MREAs can be controlled such that the same (full) stroke is optimally utilized in each crash, regardless of occupant weight or crash level, to transmit the lowest load possible to the occupant and therefore minimize the risk of injury. The risk of injury during a lower sink rate or lower energy crash is significantly reduced below the 20% risk associated with current EA technology. Additionally because the MREAs are electronically controllable, the adaptation to occupant weight can be performed automatically (using on-seat sensors) and will be tuned for the exact occupant weight (as opposed to discrete increments). These capabilities for automatic and optimal adaptation to occupant weight and crash severity are significant advances over the current state of the art in occupant crash protection.

### 1.5.2 Vibration Isolation Combined with Crashworthiness

As noted in Section 1.2, current passive EAs act as stiff members until their tuned load threshold is reached – thereby providing no means of isolating the occupant from harmful cockpit vibrations. Rotorcraft seat manufacturers are focused solely on crash safety. Vibration isolation systems for rotorcraft seats are considered to be infeasible because it is thought that they would sacrifice crash safety, would not perform well under the broad spectrum of vibration typically experienced by rotorcraft, or would incur a significant weight penalty. Because of this, rotorcraft seats rarely meet military vibration specifications and the crew must therefore suffer with the resulting discomfort, adverse health effects, and loss in situational awareness resulting from whole-body vibration.

In Chapter 4, however, it will be shown that MR dampers for vibration isolation can be implemented into tactical rotorcraft seats such that the crash safety is maintained. It is shown that by implementing the MR dampers in series with the passive EAs in such a manner that the original load path is restored once a crash load threshold is met, significant vibration isolation performance can be attained while preserving crashworthiness. Using semi-active control, it is shown that the MR-based solution provides a significant vibration performance improvement across a wide spectrum of frequencies and provides over a 70% reduction in primary rotor-induced vibration. It is further shown that this performance improvement comes at a minimal weight penalty. Thus, this MR damper / EA arrangement detailed in Chapter 4 is a significant advance over the current state-of-the-art rotorcraft seats.

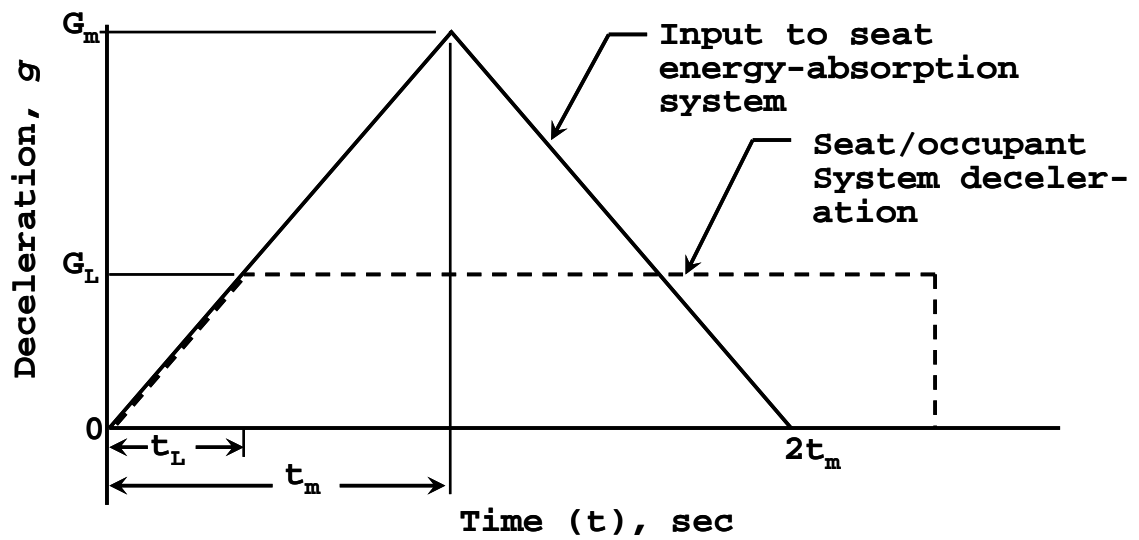


Figure 1.1: Energy Absorbers Attenuate Input Deceleration and Limit the Deceleration of the Seat/Occupant [1]

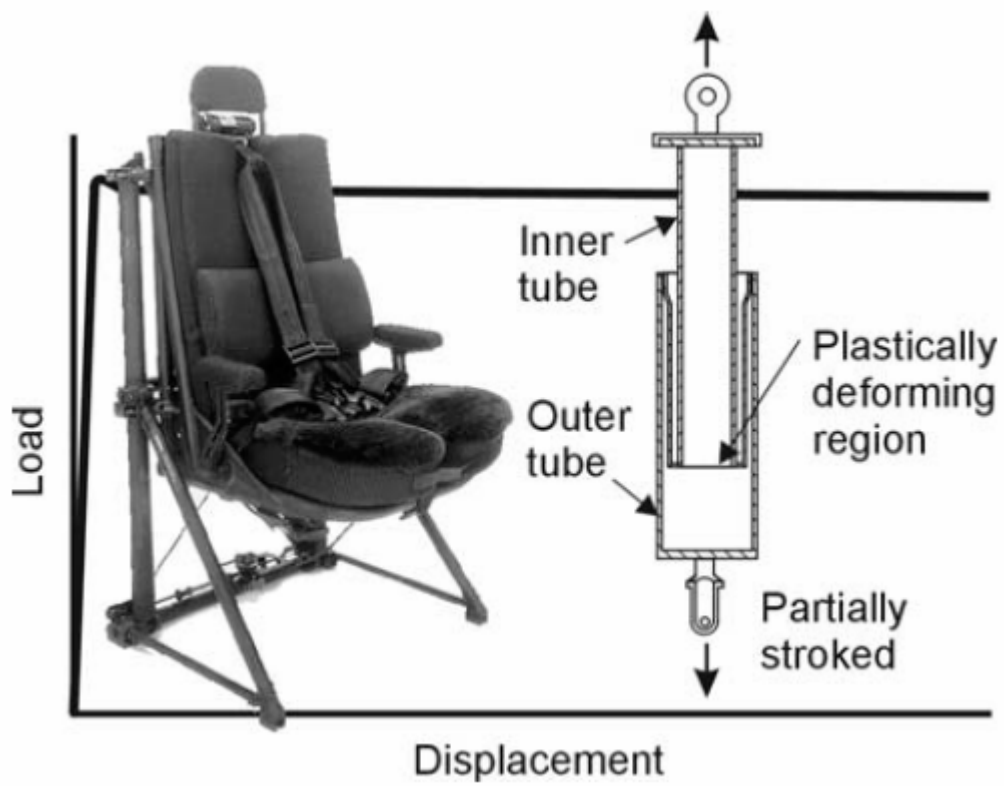


Figure 1.2: Inversion Tube FLEA Utilized in the Unarmored SH-60 Seahawk Crew

Seat [3]

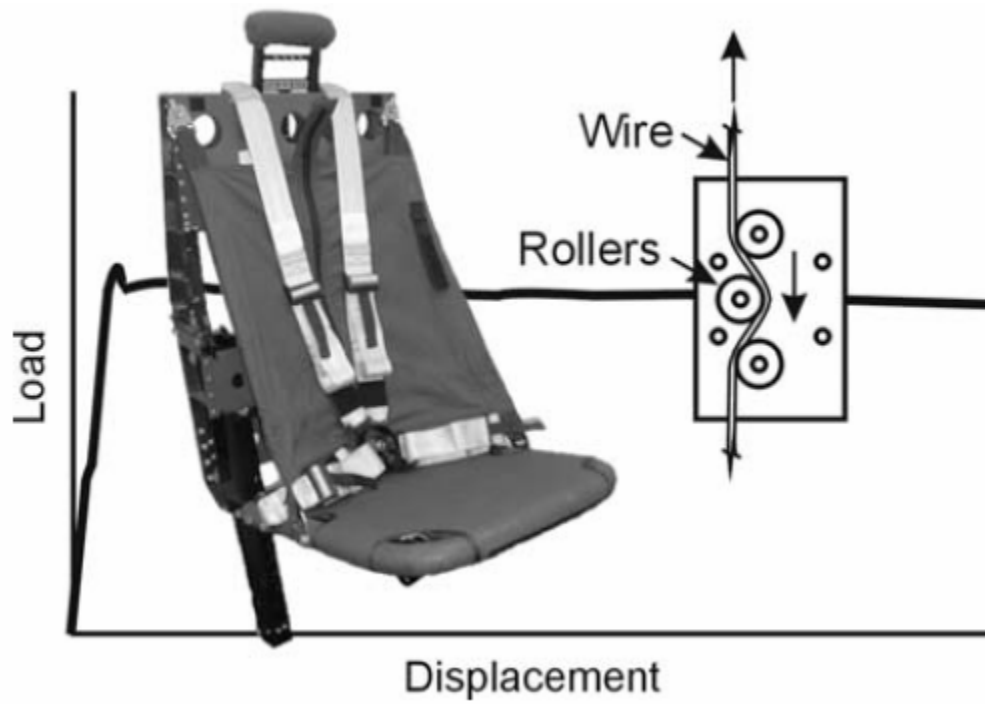


Figure 1.3: Wire Bender FLEA Utilized in the EH101 Foldable Troop Seat [4]

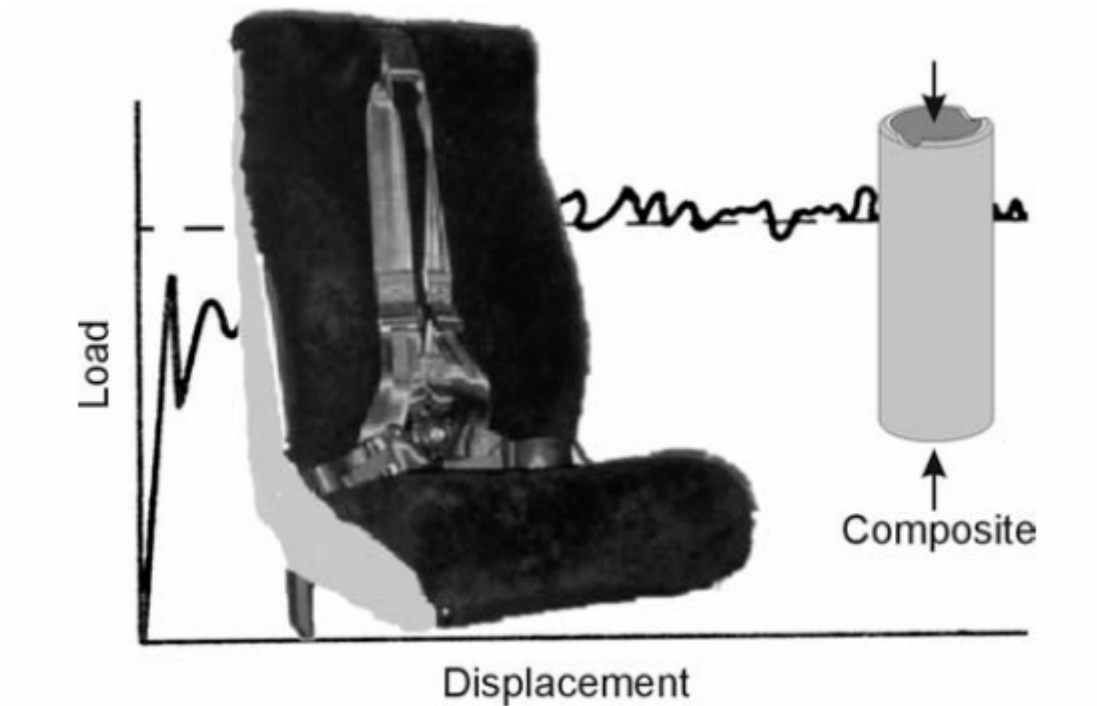


Figure 1.4: Crushable Composite Column FLEA Utilized in the Bell 230/430 Pilot

Seat [4]

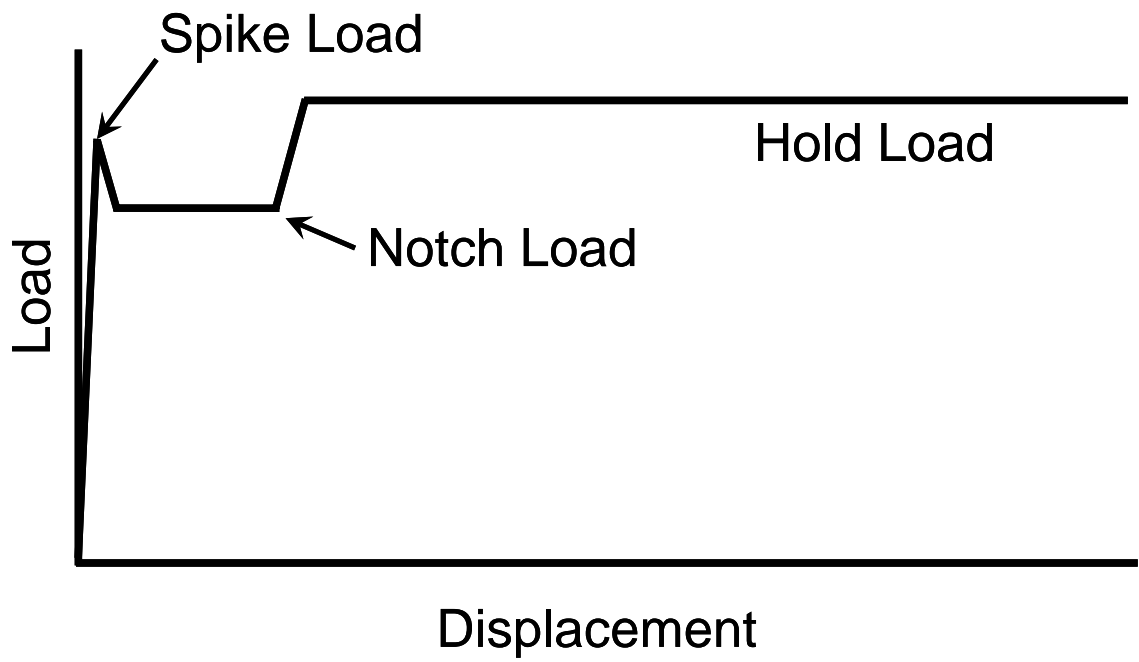


Figure 1.5: FPEA Load-Stroke Characteristic [3]

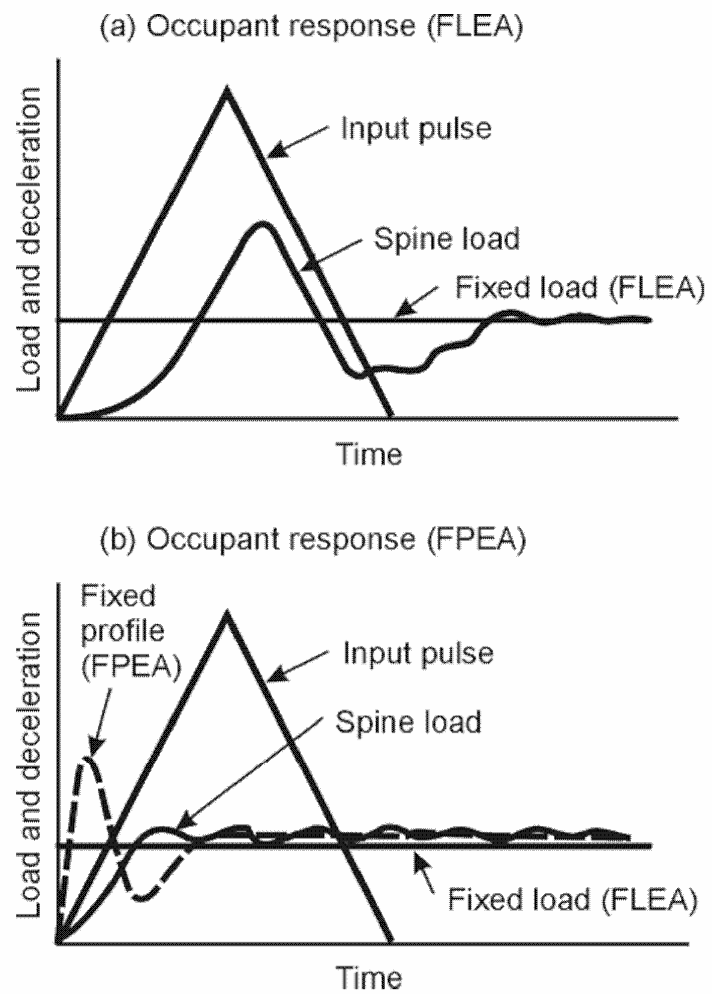


Figure 1.6: Conceptual Explanation of the Fixed Profile Energy Absorber Process [3]

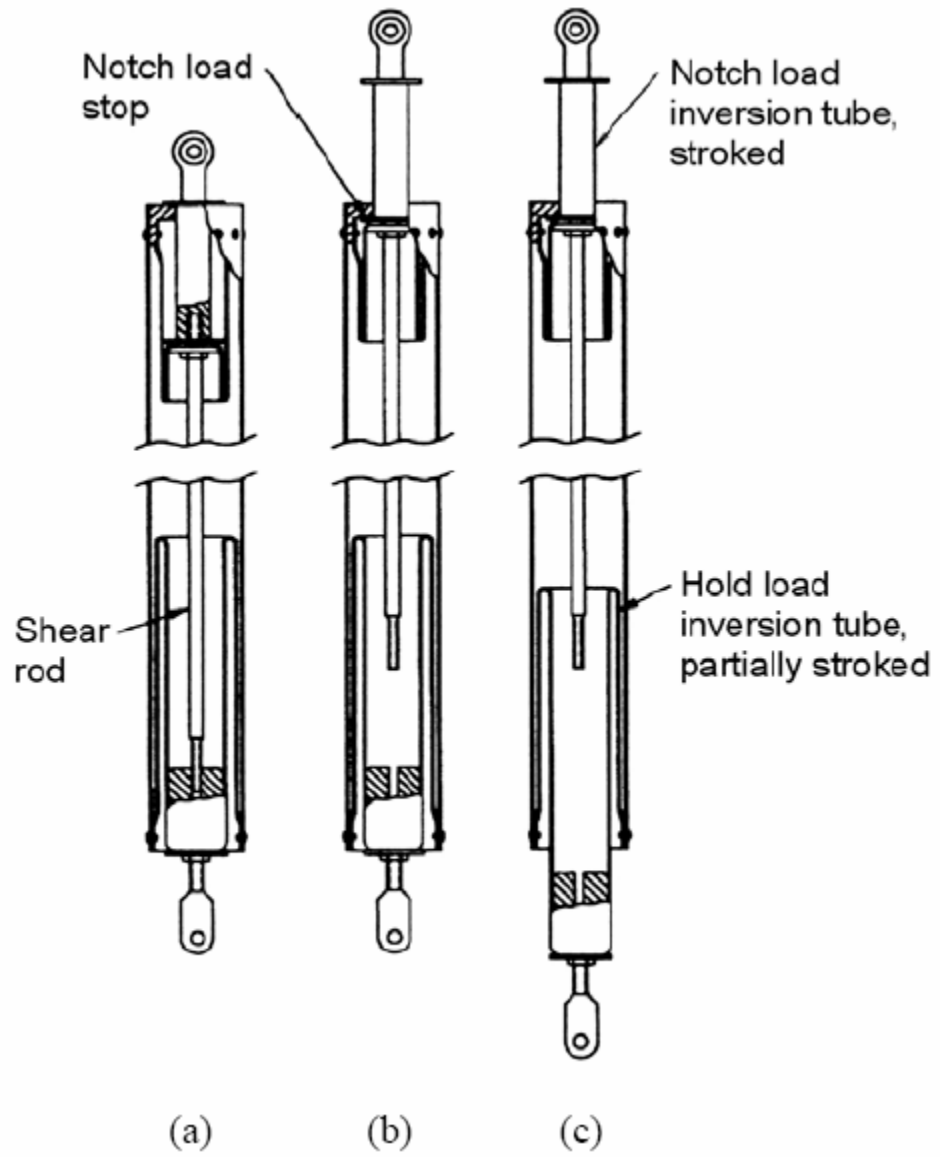


Figure 1.7: Schematic of Example FPEA [3]

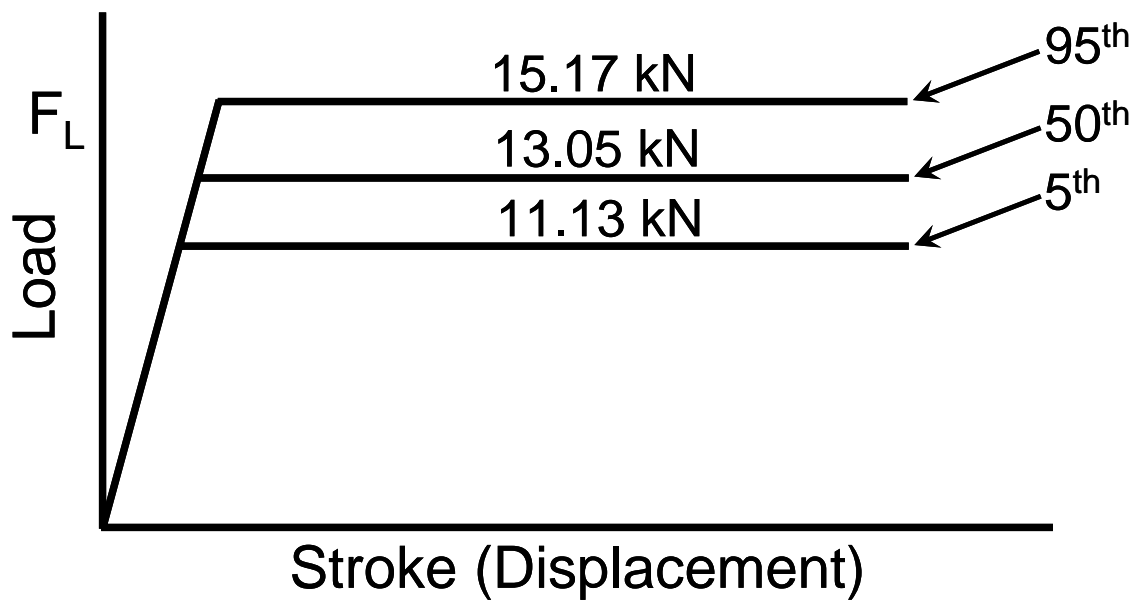


Figure 1.8: VLEA Load-Stroke Adjustment Range [3]

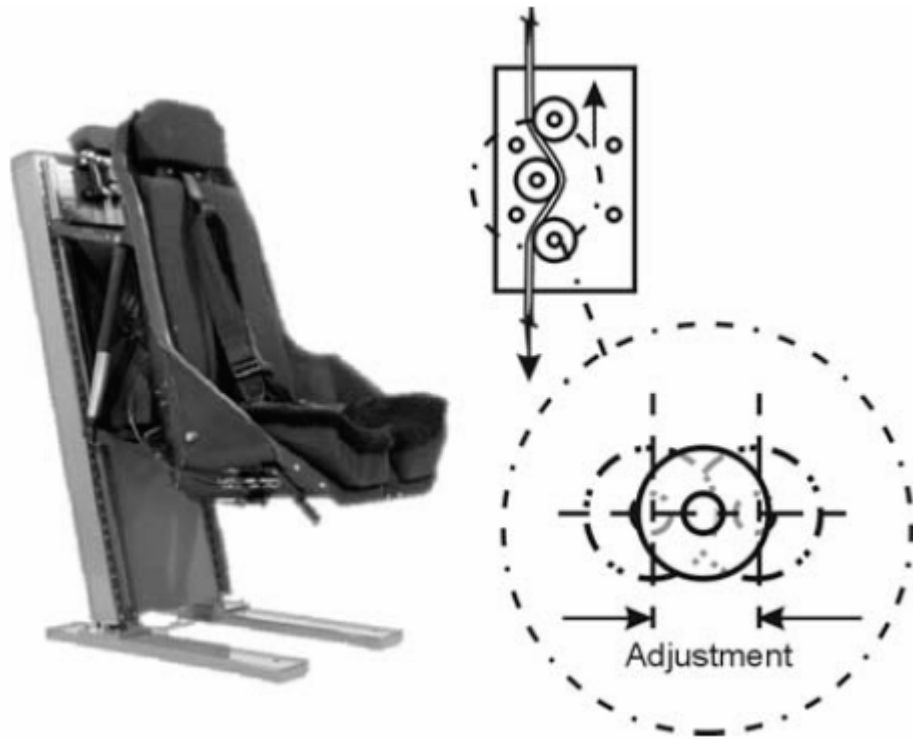


Figure 1.9: Wire Bender VLEA Utilized in the V-22 Osprey Armored Crew Seat [4]

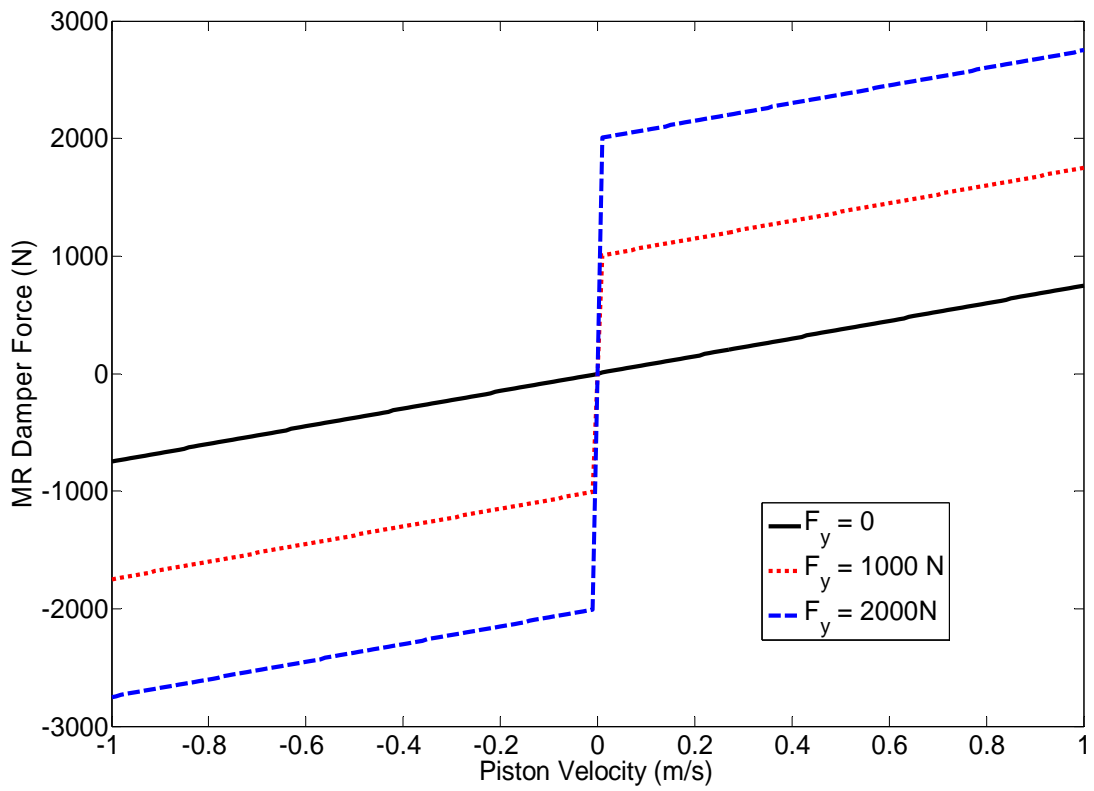


Figure 1.10: Force vs. Velocity Profile for the Bingham Plastic Force Model

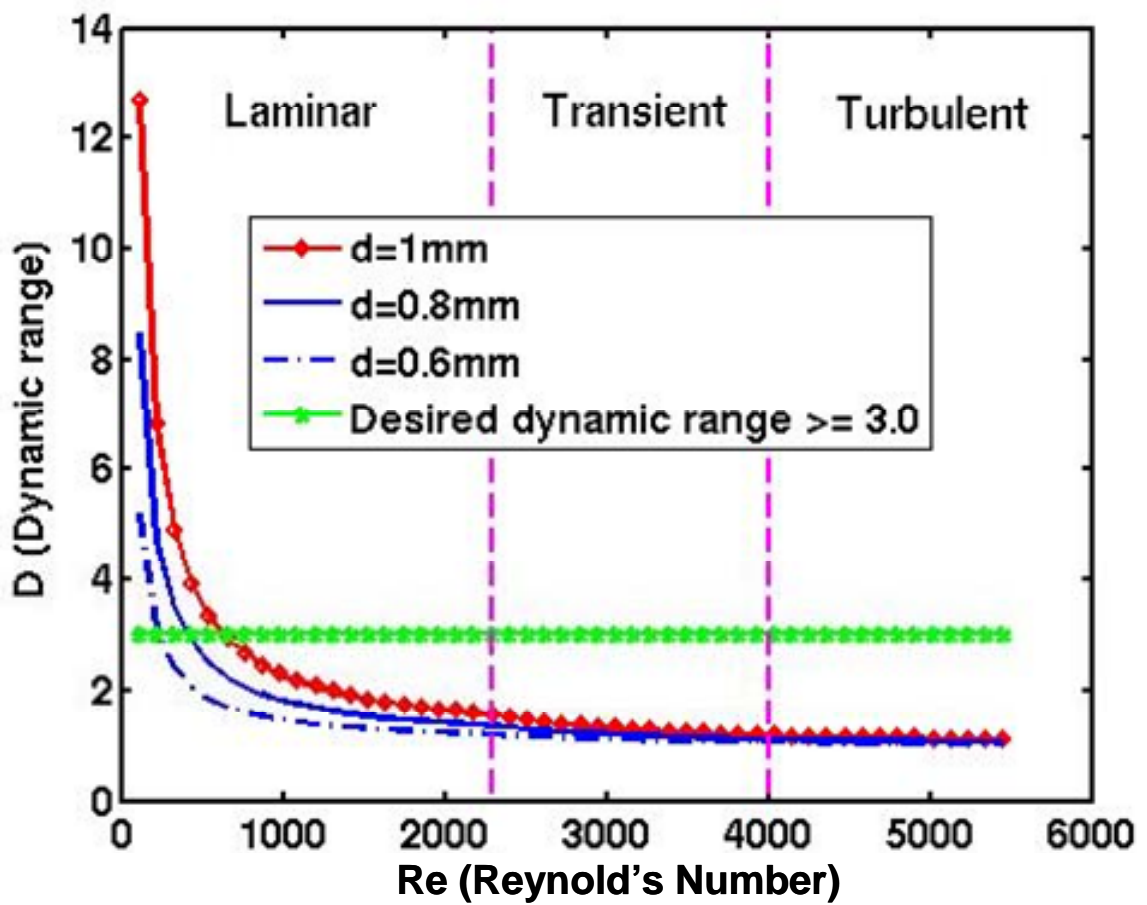


Figure 1.11: MR Damper Dynamic Range vs. Reynold's Number [16]

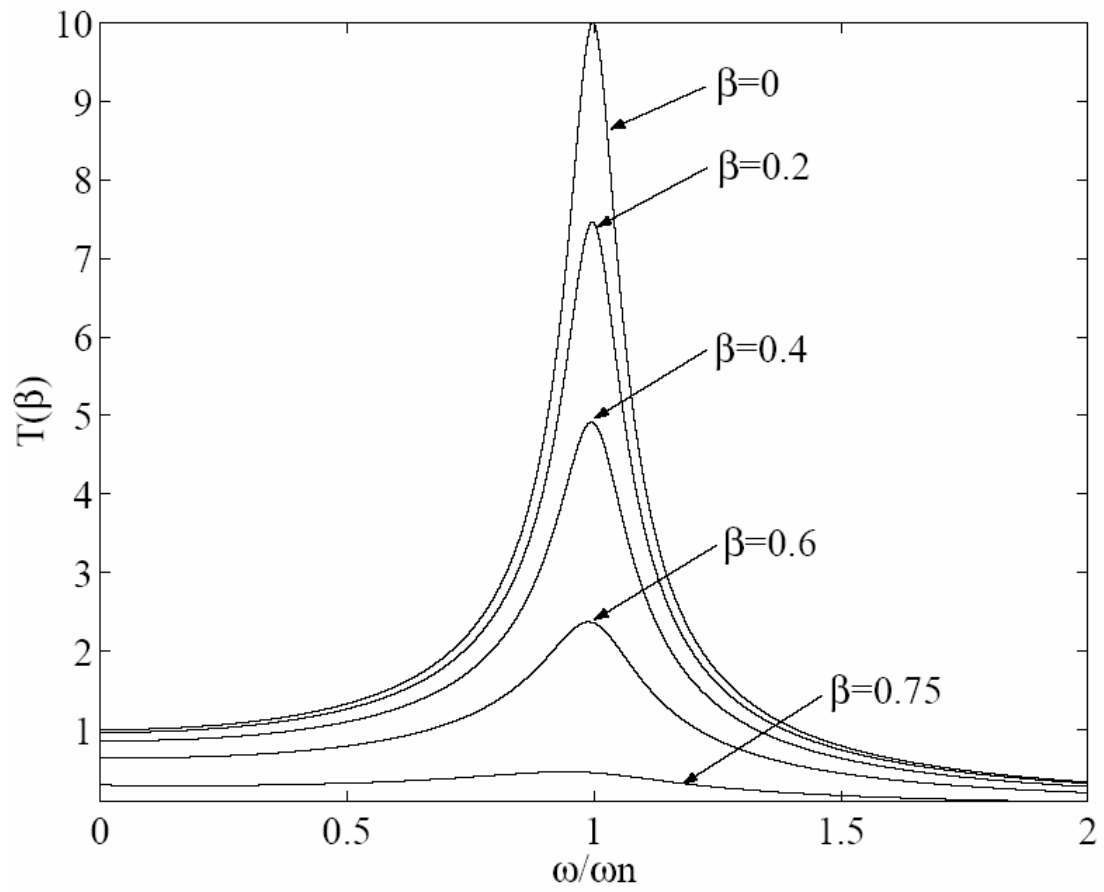


Figure 1.12: SDOF Frequency Response for Varying  $\beta$  [18]

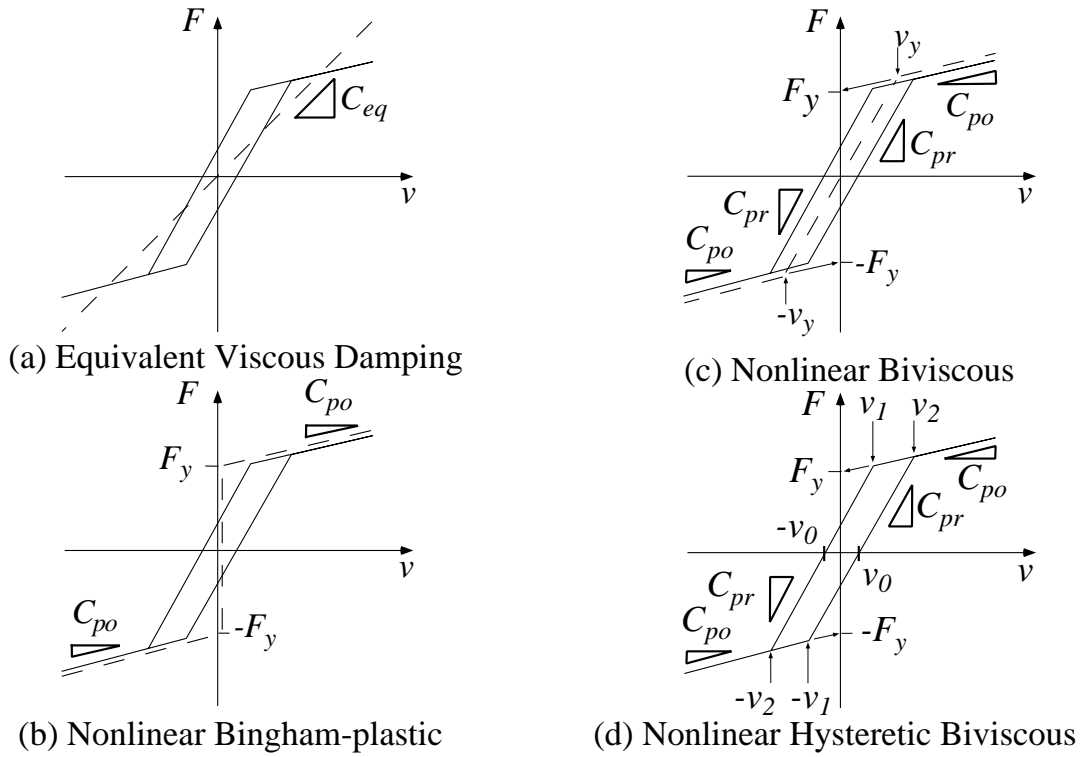


Figure 1.13: Comparing Bingham-plastic, Biviscous, and Hysteretic Biviscous Force

Models [13]

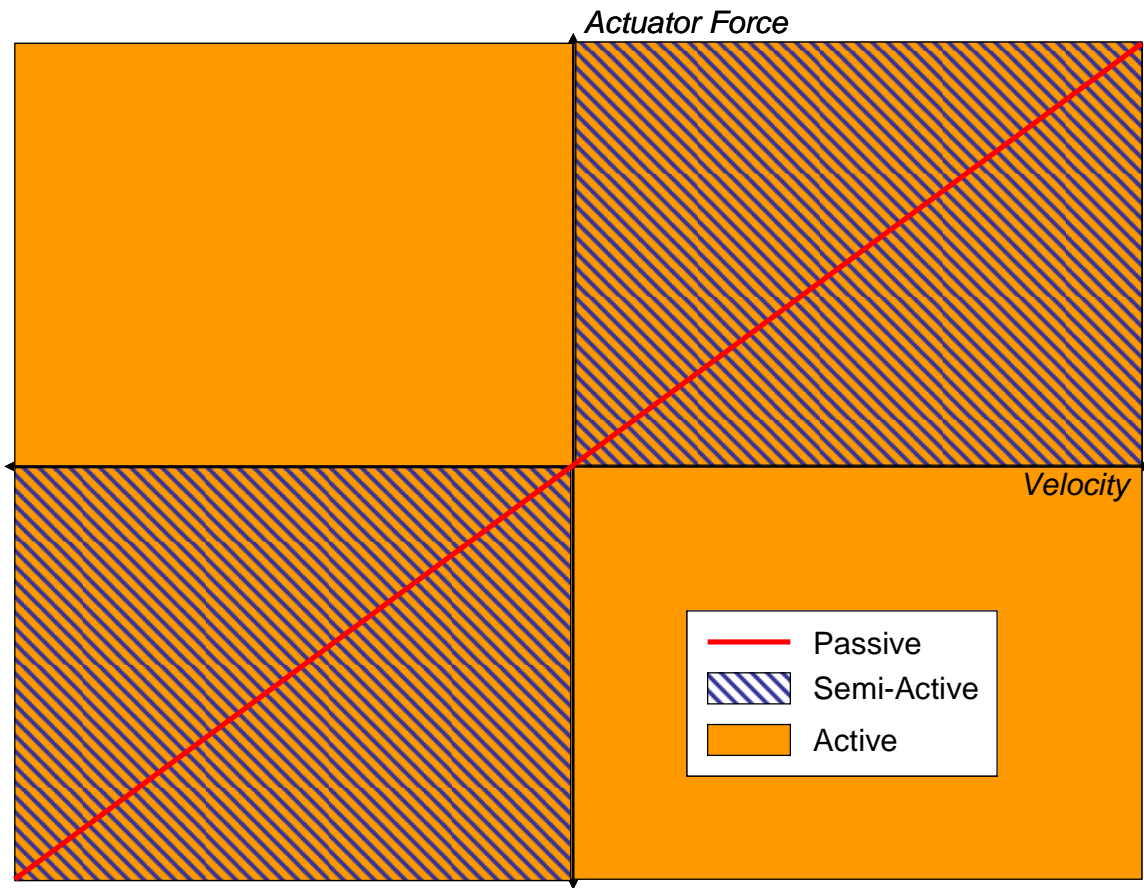


Figure 1.14: Comparison of Control Capability for Passive, Semi-Active, and Active Control

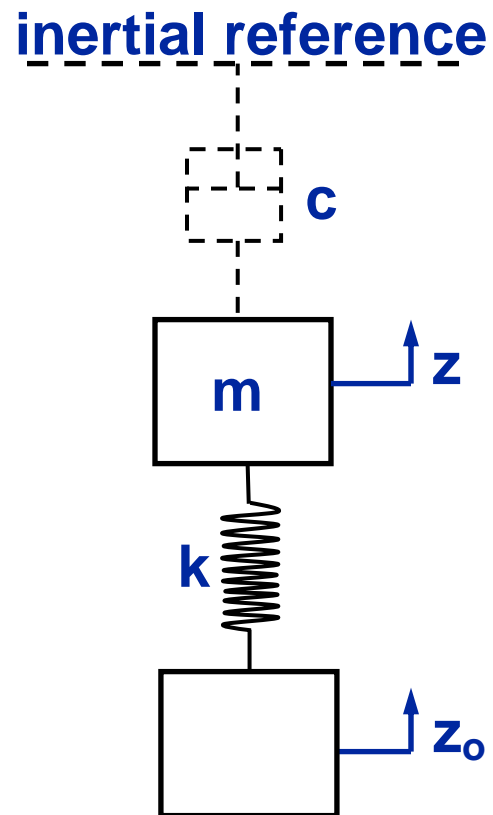


Figure 1.15: Physical Representation of skyhook Control Algorithm

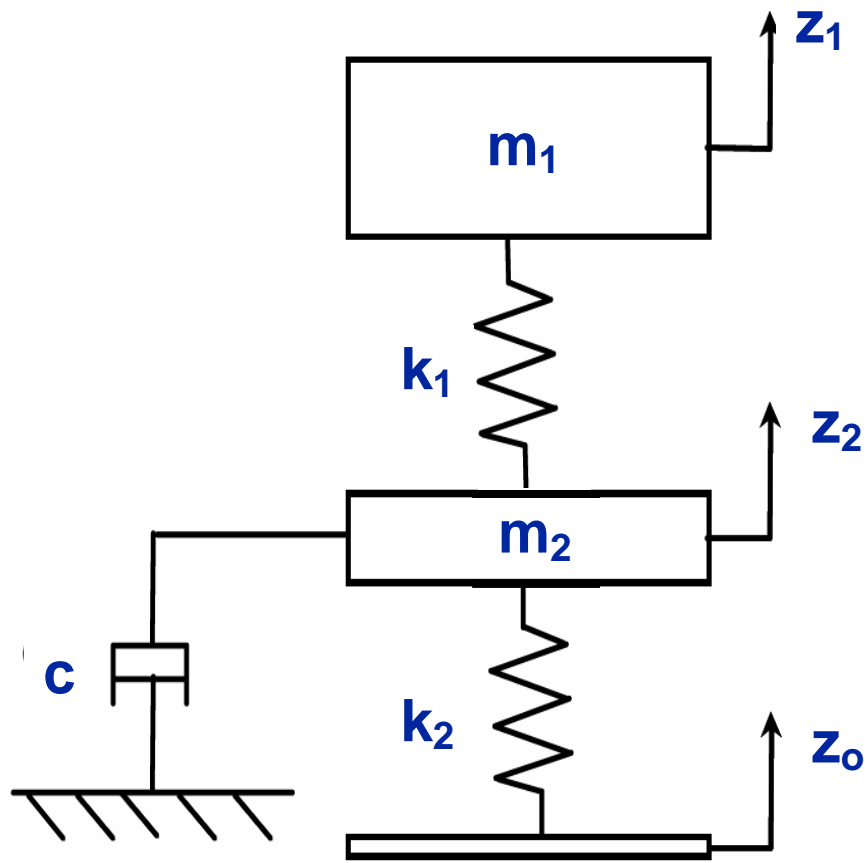


Figure 1.16: Physical Representation of Groundhook Control Algorithm

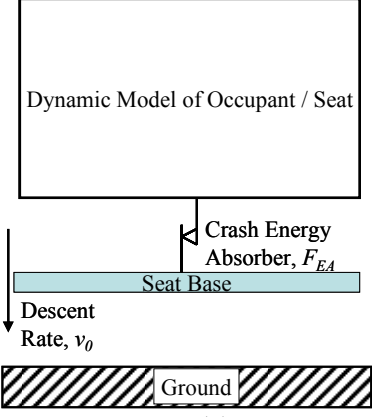
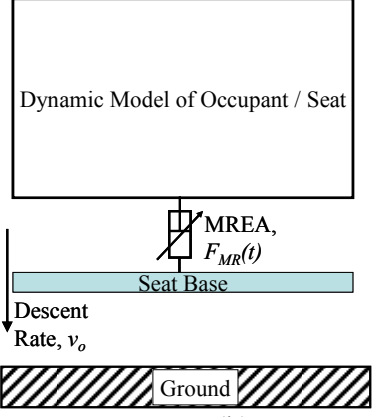
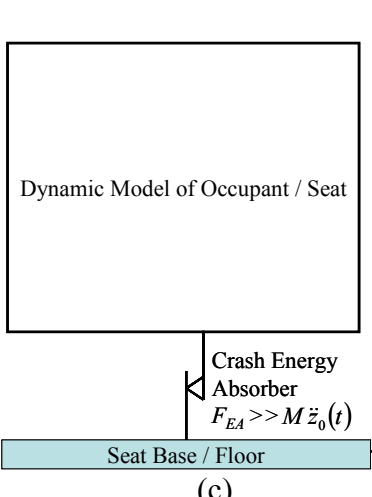
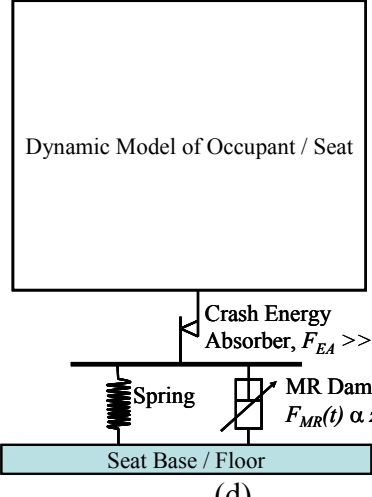
Goal	State-of-the-Art Rotorcraft Seat Suspensions	MR Based Seat Suspension
<p><b>Crash Protection</b></p>	 <p>(a)</p>	 <p>(b)</p>
<p><b>Vibration Isolation</b></p>	 <p>(c)</p>	 <p>(d)</p>

Figure 1.17 - Comparing State-of-the-Art Rotorcraft Seat Suspension Schematic Diagrams with the MR Based Seat Suspensions Presented in this Dissertation

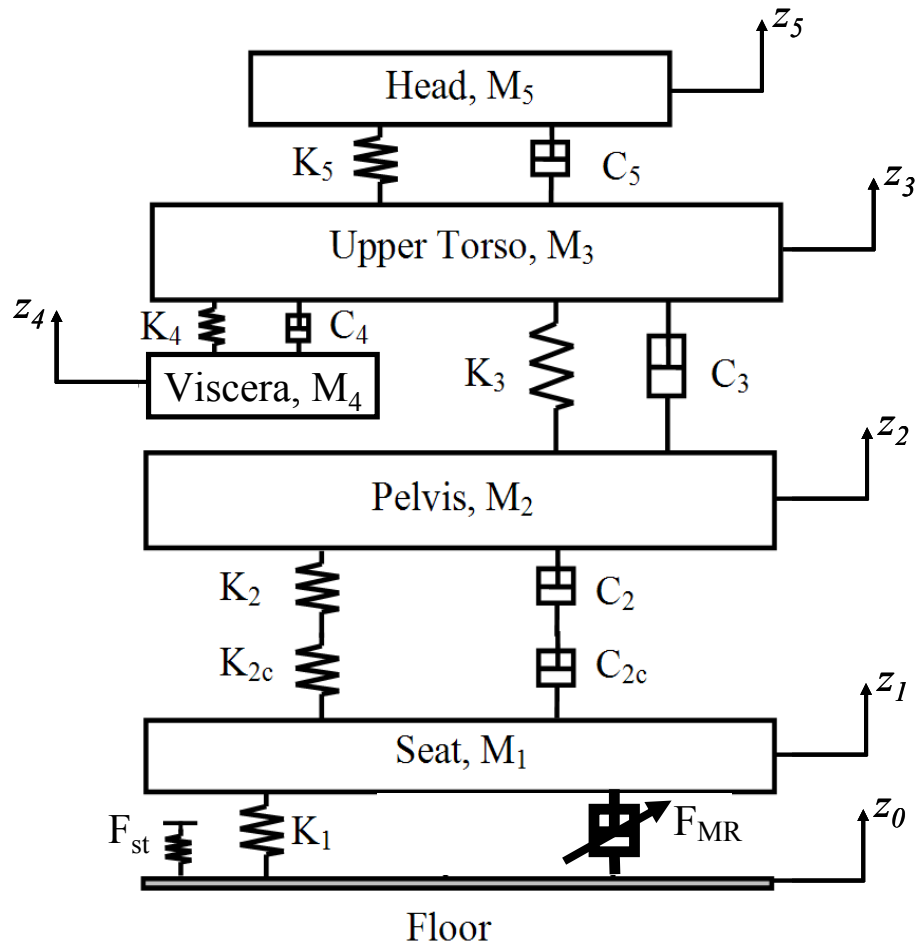


Figure 1.18: Lumped Parameter Biodynamic MR Seat Suspension Model for Design and Performance Evaluations of MREAs for Enhanced Occupant Protection

Table 1.1: Preliminary Lumped Parameter Biodynamic MR Seat Suspension Model

Parameters

Quantity	Symbol	Value	Units
Mass of seat	$M_1$	11.5	kg
Mass of pelvis	$M_2$	29	kg
Mass of upper torso	$M_3$	21.8	kg
Mass of viscera	$M_4$	6.8	kg
Mass of head	$M_5$	5.5	kg
Stiffness of coil spring	$K_1$	0.0	kN/m
Stiffness of soft seat cushion	$K_{2c}$	37.7	kN/m
Stiffness of viscera	$K_4$	2.84	kN/m
Stiffness of head	$K_5$	202.3	kN/m
Cushion Damping	$C_{2c}$	159	N·s/m
Pelvis Damping	$\zeta_2$	0.25	-
Torso Damping	$\zeta_3$	0.11	-
Viscera Damping	$\zeta_4$	0.5	-
Head Damping	$\zeta_5$	0.1	-

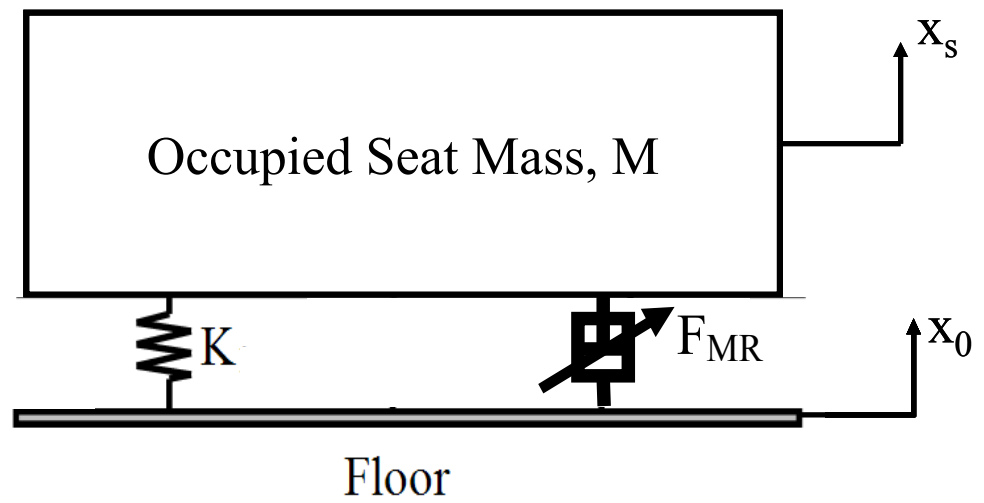


Figure 1.19: SDOF MR Seat Suspension Model for Vibration Isolation Design and Performance Predictions

## Chapter 2: Investigation of MR Dampers for Enhanced Crashworthiness and Vibration Isolation of Helicopter Crew Seats

In this chapter, design principles to which an MR seat suspension should be designed to maximize performance are presented and key challenges are identified. Then, three MR seat suspension cases are investigated: 1) MR dampers for only vibration isolation, 2) MREAs for adaptive occupant protection, and 3) dual-goal MREAs for combined adaptive occupant protection and vibration isolation. The performance benefits and tradeoffs are discussed for each and key conclusions are made regarding the feasibility of MREA-based rotorcraft seat suspensions.

### 2.1 *MR Seat Suspension Design Principles*

There are significant challenges associated with designing an MR suspension system for the dual goals of enhanced occupant protection and vibration isolation. The main challenges explored herein are the conflicting force requirements between these dual goals and the geometric restrictions associated with retrofitting these systems into existing helicopter seats.

One of the most simple and widely used force models for MR dampers is the Bingham-plastic model:

$$F_{MR}(v) = C_p v + F_y \text{sign}(v), \quad (2.1)$$

where  $F_{MR}$  is the total force dissipated by the MR damper,  $F_y$ , is the controllable yield force,  $C_p$ , is the post-yield viscous damping and  $v$  is the piston velocity. This behavior is essentially a combination of viscous and coulomb friction damping [18].

Physical constraints on MR fluid properties, electromagnetic coil performance, geometry, etc., however, often limit the maximum achievable controllable yield force for an MR damper. Because of this, supplemental force via viscous damping may be necessary in order to reach high MR damper force levels such as those necessary for harsh vertical or crash landings.

The problem with augmenting viscous damping is that it degrades high frequency vibration isolation performance. This is most simply explained by considering a base-excited single-degree-of-freedom (SDOF) system. For vibration isolation, the fundamental resonance of a seat suspension system is typically tuned to be lower than the excitation frequencies to take advantage of the low transmissibility at higher frequencies. As shown in the non-dimensionalized frequency response for an SDOF system (Figure 2.1), when the excitation frequencies are greater than the fundamental resonance, the transmissibility of the base excitation is less than one. In this plot, the off-state viscous damping ratio,  $\zeta$ , is a function of the off-state viscous damping:

$$\zeta = \frac{C_o}{2\omega_n M}, \quad (2.2)$$

where  $C_o$  is the off-state viscous damping ( $C_p$  when there is no current applied to MR damper) and  $\omega_n$  is the tuned fundamental resonance of the system. For isolation of these higher excitation frequencies, best performance is achieved when  $\zeta$  is very small – meaning viscous damping is minimized. As viscous damping is increased, the resonant peak is reduced, but high frequency transmissibility increases. Thus, if an MR damper's off-state viscous damping component is very large, the high frequency

vibration isolation performance is limited. It is therefore desirable to have the MR damper's off-state viscous damping component as low as possible.

It is most advantageous to tune the fundamental resonance of the system as far below excitation frequencies as possible to take advantage of the low transmissibility. There are practical limitations, however, to how low this fundamental resonance can be tuned for a seat suspension system. If the tuned spring stiffness is too low, the static deflection may cause problems with the pilot's line-of-sight. This study uses an assumed maximum static deflection of 13mm for the 95<sup>th</sup> percentile male aviator (96.1 kg per [1]). It is also assumed that 29% of the occupant's weight is supported by the floor (legs) [35], that there is 13.6 kg of body worn equipment, and that the stroking seat mass is 11.5 kg. The resulting design spring stiffness that gives this static deflection is 70 N/mm, setting the fundamental resonance at 4.4 Hz for the 95<sup>th</sup> male aviator. Since it is possible that this resonance may be excited by the rotor 1/rev (1P) vibrations, turbulence, and/or occupant motion, utilization of semi-active control is very beneficial. The objective of semi-active control is to combine the resonance response of a highly damped system with a high frequency response of a lightly damped system as illustrated in Figure 2.2.

In order to further quantify the effect of an MREA's off-state viscous damping component on vibration isolation performance, the above SDOF system is assumed for an MR seat suspension in an unarmored SH-60 Seahawk crew seat (Figure 2.3). The SH-60 has four blades and a main rotor frequency of 4.3 Hz. Primary rotor-induced vibrations, therefore, occur at the blade passing frequency (17.2 Hz – 4/rev) and harmonics thereof (34.4 Hz – 8/rev, etc.) [40]. By using this SDOF assumption,

in Figure 2.4 the amount of isolation (in percent reduction) that an MR seat suspension can provide is plotted for a 0.2 g amplitude 4/rev (4P) vertical floor excitation as a function of off-state viscous damping ratio. It can be seen that for an ideal system, the MR suspension provides 93% vibration reduction assuming zero off-state viscous damping. As off-state viscous damping ratio is increased, this vibration isolation performance drops significantly – down to 45% reduction for  $\zeta = 1.0$ . In such a system, however, this vibration performance can be degraded because of friction in the system. Friction in MR dampers is typically due to contact in rod seals and piston rings and can range from 20 N to 200 N depending upon the damper design. MR dampers designed for high fluid pressures (e.g., high piston velocities and high force) typically have higher friction because of the increased fluid sealing required. The dashed line in Figure 2.4 shows the response reduction assuming 80 N of friction in the system. It can be seen that isolation performance now ranges from 60% reduction down to 8% reduction. This further emphasizes the need to maintain the off-state viscous damping ratio as low as possible and illustrates the importance in keeping system friction as low as possible.

When designing MREAs with high on-state forces for enhanced occupant protection, maintaining low off-state damping for vibration isolation means prescribing a high dynamic range,  $D$ , which is the ratio of the on-state damping force to the off-state damping force. In 2005, Mao *et al.* showed that the dynamic range decreases exponentially with the Reynold's number for the flow within the MR damper [16]. Since this Reynold's number is a function of the piston velocity, it is therefore difficult to achieve a high dynamic range when designing MREAs for high

speed applications such as enhanced occupant protection from harsh vertical and crash landings. Increasing the dynamic range in these cases must be achieved by increasing the overall size of the MR valve. Therefore, as will be evidenced in the following three design cases, achieving a dynamic range high enough to effectively address both vibration isolation and adaptive occupant protection carries a tradeoff of device size and weight.

## 2.2 Case 1: Designing MR Dampers Solely for Vibration Isolation

As discussed above, the off-state viscous damping ratio is a key parameter in vibration isolation performance. When designing for vibration isolation, the viscous damping ratio, therefore, becomes an important design parameter. Up to this point, however, damping ratio has not been considered in MR damper design strategies. To address this, we can combine Eq. 2.2 with that for MR damper's dynamic range:

$$D = \frac{F_{on}}{C_o v} \quad (2.3)$$

$$= \frac{F_{on}}{2\xi\omega_n Mv} \quad (2.4)$$

By using this equation, one can determine the necessary dynamic range based on system properties (resonant frequency, stroking mass) and desired vibration isolation performance. Plots such as Figure 2.4 can be used to aid in the selection of the off-state viscous damping ratio. This dynamic range can then be used as a design parameter in MR damper design strategies such as that proposed by Mao *et al.* [16].

For effective semi-active control, the off-state viscous damping ratio should ideally be less than 0.2. Beyond this level, there begins to be a significant loss in high frequency isolation performance, as is shown in Figure 2.1. For this study, a viscous

damping ratio of 0.15 is chosen as the desired design parameter. Using Eq. 2.2 and the seat resonant frequency and effective seat mass for a 95<sup>th</sup> male aviator discussed above, this gives an off-state viscous damping ratio,  $C_o$ , of 0.77 N-s/mm. Assuming two MR dampers per seat, this gives a viscous damping ratio of 0.38 N-s/mm per damper.

In order to determine dynamic range, the maximum total MR damper force,  $F_{on}$ , necessary for resonance mitigation must also be determined. As can be seen in Figure 2.2, the peak transmissibility at resonance for viscous damping ratios of 0.15 and 1.0 are 3.51 and 1.16, respectively. The difference between these transmissibilities (2.35) multiplied by the effective occupied seat mass,  $M$ , and the maximum expected vibration at the floor of the cockpit (assumed to be 0.2 g for this study) gives the additional damping force necessary to mitigate the resonance to be 430 N. This value was further verified using a simple SDOF simulation where the control force was varied using the skyhook control algorithm where the rate-feedback gain was set to be the viscous damping calculated for  $\zeta=1$  [22], [39]. In this simulation, the relative velocity between the base and the effective mass (the piston velocity) at resonance was determined to be 30 mm/s.

For two MR dampers per seat, the designed field-off MR damper force,  $F_{off}$ , is 11 N (0.38N-s/mm x 30mm/s), the necessary field-on MR damper force,  $F_{on}$ , is then 226 N ( $F_{off} + 430N \div 2$ ), and the dynamic range,  $D$ , is 19.6 (per Eq. 2.3) at a piston velocity of 30 mm/s. With these key parameters, the design strategy discussed in [16] was then utilized to design the MR damper depicted in Figure 2.5. This design has a piston diameter of 25mm, and the MR valve has an annular duct with a gap distance

of 0.35 mm and an active length of 2.1 mm. The total stroke capability is 65 mm, which allows for vibration magnitudes up to 2.5 g. These MR dampers have a 38 mm outer diameter, only a 114 mm body length, and have a prototype weight of 1 kg each (using a steel body). Simply replacing the steel body with an aluminum body, the MR damper weight would reduce 0.45 kg. When integrated to an unarmored SH-60 crew seat (23 kg), this yields a net weight increase (with integration hardware) of 8%. For an armored SH-60 crew seat (53 kg), this yields a 3% net weight increase. It should be noted that for this design, low cost and widely available AISI 1018 steel is utilized for the electromagnetic circuit. This same material is also used for the electromagnetic circuit for the two following MREA designs in order to demonstrate the effect of the MR device design requirements on the resulting size and weight. Materials with higher magnetic permeability and/or lower density may be utilized with each of these designs to further reduce size and weight for a production system.

According to Figure 2.4, this configuration (with  $\zeta = 0.15$ ) would ideally provide 89% reduction of the 4P vibration. Assuming 80 N of friction, however, this performance is reduced to 53% reduction. As is discussed in [39], this MR damper design was fabricated and retrofitted into an unarmored SH-60 Seahawk crew seat. This system had approximately 60 N of friction and experimental test results showed that it reduced 4P vertical vibration levels by 76%, which is a 70% improvement over the unmodified SH-60 crew seat [39].

While these MR dampers significantly reduce vibration, they are not capable of mitigating high sink rate landing loads. These MR dampers, therefore, must be coupled with crashworthy energy absorbers such as FLEAs, VLEAs, or MREAs so

that occupant protection is ensured during a crash event. An example of such an arrangement in the unarmored SH-60 Seahawk crew seat is shown in Figure 2.6 [39].

### 2.3 Case 2: Designing MREAs for Adaptive Occupant Protection

In the early 1970s, analyses and testing were performed to determine a limit load for seat energy absorption systems, that is, the load at which an FLEA would start and continue to stroke during a vertical shock event. Relating the seat performance to tolerance data and cadaveric testing, a seat/occupant system deceleration limit,  $G_L$ , of 14.5 g was determined to keep the load-duration in the humanly tolerable range [1], [3]. This means that the FLEA would stroke at 14.5 times the occupied effective seat weight ( $M \times g$ ) to attenuate the input floor deceleration (which is typically approximated as a triangular pulse with peak deceleration  $G_M$ ) as shown in Figure 1.1 [1]. By using the effective occupied seat mass for the 95<sup>th</sup> percentile male condition discussed above, the FLEA design force would be 13.3 kN. Similarly, for a 5<sup>th</sup> percentile female aviator (46.6 kg per [1]) and proportional amount of body worn equipment (7 kg), the FLEA design force would be 7.4 kN. Applying this FLEA design strategy to MREAs gives a design force,  $F_{on}$ , of 13.3 kN when the applied field is at a maximum, a off-state force,  $F_{off}$ , of 7.4 kN, and a dynamic range,  $D$ , of 1.8 to account for varying occupant weight.

In order to verify these MREA force requirements, the lumped parameter biodynamic MR seat suspension model discussed above was employed. Using this model, a simulation of a high speed seat qualification test (12.8 m/s [42 ft/sec] vertical sink rate,  $G_M=51$  g,  $t_m=0.051$  sec, per [1], pp. 165) was performed. Assuming the Bingham Plastic model for MR fluid behavior (Eq. 2.1), it can be reasoned that

the constant MREA yield force (controllable portion of MREA force) would be 5.9 kN (13.3 kN – 7.4 kN). Figure 2.7 shows the MREA response in these simulations for the 95<sup>th</sup> percentile male aviator condition discussed above with a constant yield force of 5.9 kN and an off-state viscous damping of 2.5 N-s/mm. The top plot in this figure shows that a total stroke of 290 mm is utilized. The middle plot in this figure shows that the total MREA force reaches a maximum of 13.3 kN when the piston velocity (bottom plot) reaches a maximum of 3.0 m/s. Finally, Figure 2.8 plots the time response of the occupant lumbar spine force calculated using the biodynamic model. It can be seen that the calculated peak lumbar force, 6.7 kN, does not exceed the tolerance levels specified in [4] and [41] (6.7 kN and 11.3 kN, respectively). This simulation verified the MREA force requirements determined using the 14.5 g criteria and also gives the design MREA piston velocity.

This study examines retrofitting the FLEAs in the unarmored SH-60 Seahawk crew seat (Figure 2.3), with adaptive MREAs. Such a retrofit requires two MREAs at a 22.5° angle from vertical. In addition to this, a load factor of 1.25 was applied to the field-on design force to allow for additional controllability. This configuration and added load factor give the following MREA design parameters (per damper):  $F_{on} = 9.0$  kN,  $F_{off} = 4.0$  kN, and  $D = 2.25$  @  $v = 3.0$  m/s. By using these MREA design parameters, the design strategy of [16] was again utilized to determine a preliminary design geometry. The resulting MREA design (Figure 2.9) has a piston diameter of 38 mm, and the MR valve has an annular duct with a gap distance of 1.2 mm and an active length of 43 mm. The total body length of this design is 450 mm, which allows for 290 mm total stroking capability during a crash. This prototype design

would weigh approximately 9 kg (using all steel components). Simply changing the body material to aluminum reduces the device weight to 3.6 kg. This yields a net weight increase of 29% and 12% for the unarmored SH-60 crew seat and the armored SH-60 crew seat, respectively. Figure 2.10 depicts these MREAs retrofitted into the unarmored SH-60 Seahawk crew seat. As mentioned above, AISI 1018 steel is assumed for the electromagnetic circuit for all three damper designs studied herein for the purposes of comparison. By using higher permeability and/or lower density materials, one can reduce the size and weight of the MREAs for a production system.

With this MREA, a seat suspension system that adapts to occupant weight could be implemented using the controller identified in [38]\*. The controller would determine the effective occupied seat mass,  $M$ , by a weight sensor in the seat, static deflection of the seat, or via manual setting and then adjust the limit load,  $F_L$ , as shown below:

$$\begin{aligned} F_L &= G_L \times M \\ &= G_L \times K \delta_{static} \end{aligned} \tag{2.5}$$

Here,  $K$  is the tuned spring stiffness, and the limit factor,  $G_L$ , is the injury tolerance criteria of choice (in g), such as the 14.5 g criteria discussed above. The control can then modulate MREA yield force real time to keep the damper force at this constant limit load. MREA yield force modulation may be performed using a simple load tracking control algorithm or by using the MREA force model. For example, using the Bingham plastic force model, the yield force would be varied using the following simple equation:

---

\* Patent Pending

$$F_y = F_L - C_o(\dot{z}_1 - \dot{z}_0), \quad (2.6)$$

where  $F_y$  is the MREA yield force and  $F_L$  is the load limit. Knowing the instantaneous velocities of the seat and floor, the controller then uses Eq. 2.6 to determine the desired MREA yield force. Figure 2.11 shows an example of a simulation using this controller for varying occupant weights. In this figure, it can be seen that the controller modulates the yield force (middle plot) in order to prevent the total force transmitted to the occupant (bottom plot) from exceeding the load limit.

Vibration isolation using this device, however, is not ideal. Firstly, the 290 mm stroke capability is reduced by the stroke necessary for vibration. This reduced stroke capability will not be adequate for high sink rate crashes for heavier occupants. Adding in additional stroke to this design complicates the retrofit of the device into the crew seat. Additionally, as discussed above, vibration isolation performance with this MREA is limited because it has a very high off-state damping force. The off-state viscous damping for the crashworthy MREA designed above is 1.3 N-s/mm (4.0 kN ÷ 3.0 m/s). Using this value for the arrangement discussed above (2 MREAs @ 22.5° from vertical), Eq. 2.2 yields an off-state viscous damping ratio of 0.50 for a 95<sup>th</sup> percentile male aviator. According to Figure 2.4, this design would provide a 71% reduction in 4P vibrations assuming no friction, and only 35% reduction in vibration assuming 80 N of friction. Realistically, the piston rings and rod seals for such a high speed, high fluid pressure design would yield friction values in excess of 80N, which means that the practical vibration reduction would be less than 35%.

#### 2.4 *Case 3: Dual-Goal MREA Design*

The previous two sections describe design processes for MR seat suspensions optimized solely for vibration isolation or enhanced occupant protection, respectively. Additional complications arise when the MREAs are designed to achieve both vibration isolation and adaptive occupant protection goals simultaneously. In order to design such a dual-goal MR seat suspension system, three primary considerations must be made.

The first of these considerations is stroke capability. The MREA must have enough stroke capability for both high speed crashes and vibration isolation. In the prior section, it was determined that 290mm of stroke was needed to safely mitigate 12.8 m/s sink rate landings. To ensure that this capability is maintained, the MREA must have enough stroke capability for this plus the stroke needed for vibration. While the stroke needed for vibration is dependent upon the spring stiffness chosen, this study assumes the same vibration stroke as mentioned above (65 mm). The total stroke for such a dual-goal MREA is then 355 mm. Since the overall MREA length is directly related to the stroke capability (stroke capability = cylinder length – piston length), the overall device length must be increased. Such increases in device length may complicate the retrofit of MREAs into existing crew seats.

A second consideration is the spring stiffness. As discussed above, a soft stiffness element is necessary to provide a low tuned resonance and thereby allowing for high frequency vibration isolation. Typically for crash safety, however, energy storing devices such as springs are undesirable. This is because they generate a potentially injurious rebound reaction to the occupant. To account for this, provisions

must be made in the design for the stiffness to be present during normal operation, but removed during a harsh vertical loading event. This may be done by mounting the spring in such a manner that it will break away during a harsh vertical loading scenario [42].

The last, and possibly the most challenging of these design considerations, is achieving the low off-state viscous damping necessary for good vibration isolation performance. Reducing the viscous damping while maintaining the high MREA force requirements means that the dynamic range must be increased. Because of physical limitations of MR fluids and electromagnetic circuits, reaching these high dynamic ranges at high piston velocities is very challenging. Increasing the dynamic range typically results in the need to increase the active length of the MR valve. For standard MR valves (electromagnetic coil and annular duct in piston), this means that the piston length grows significantly. Because increasing the piston length affects the stroke capability as discussed above, this either leads to reduced stroke capability or complications in retrofitting the MREA into the crew seat. MR damper configurations such as a bypass damper [43] or bi-fold MR valve [44], [45] help this issue by decoupling the relationship between MR valve active length and piston length. While these designs allow for a small piston length, they both have some geometric drawback such as overall girth or length which may also complicate the retrofit into the seat.

Taking these design points into consideration, a dual-goal MREA was designed (Figure 2.12) [42]. This MREA design has a maximum force,  $F_{on}$ , of 9 kN and a dynamic range,  $D$ , of 3.0 at a piston velocity,  $v$ , of 3.0 m/s. The off-state

viscous damping is therefore 1 N-s/mm – yielding an off-state viscous damping ratio of 0.20 for the above system with a 95<sup>th</sup> percentile male aviator. According to Figure 2.4, this design would provide an 86% reduction in 4P vibrations assuming no friction, and 50% reduction in vibration assuming 80 N of friction. As discussed for the crash-only design, realistically, the piston rings and rod seals for such a high speed, high fluid pressure design may yield friction values in excess of 80N, which means that the practical vibration reduction may be less than 50%.

This design has a number of additional unique features. Firstly, this design uses the bi-fold MR valve configuration on one end to increase the dynamic range without having a huge impact on overall length. Secondly, a coil spring is included in the design which is compressed by a spring-cap that is attached to the rod. When the load reaches a desired threshold, this spring cap breaks away from the rod, decoupling the spring from the MREA during a harsh vertical loading scenario [42]. Finally, this MREA uses a “clipped double rod” design to account for changes in rod volume. For typical hydraulic shock absorbers, variation in rod volume within the cylinder is compensated for compressing gas in an accumulator (Figure 2.13a). Compressing this gas accumulator stores energy and provides stiffness in the MREA which is undesirable for occupant protection during a high vertical loading event. The alternative method of accounting for rod volume is a double-rod design (Figure 2.13b) in which the rod passes through both ends of the cylinder, thereby maintaining constant rod volume within the cylinder. The main drawback to this method is geometry. When the device is compressed the full length of the rod extrudes through the other end of the cylinder. The “clipped double rod” method used in this design

allows for constant rod volume during vibration, but then the end of the rod pulls through the cylinder during shock, thereby drawing air into the cylinder\*. Since the air being drawn into the cylinder will not reach the MR valve, this has no ill effect on adaptive occupant protection.

While this MREA design successfully addresses the issues associated with combined vibration isolation and adaptive occupant protection, these capabilities come at the expense of geometry and weight. This MREA design has a piston diameter of 45mm, and the MR valve has an annular duct with a gap distance of 1.0 mm and an active length of 51 mm. The total stroke capability is 355 mm, which allows for vibration magnitudes up to 2.5 g plus the necessary stroke capability for a 12.8 m/s sink rate crash. These MREAs have a maximum outer diameter of 114 mm outer diameter, and a 635 mm body length, which necessitates additional components/modifications to retrofit into the SH-60 Seahawk crew seat as shown in Figure 2.14. Furthermore, the weights of these MREAs using a steel and aluminum body are 22 kg and 10.9 kg each, respectively. These yield a net weight increase of 93% and 40% for the unarmored SH-60 crew seat and the armored SH-60 crew seat, respectively. As mentioned above, this electromagnetic circuit in this design again uses AISI 1018 steel for comparison purposes. Using higher permeability and/or lower density materials will reduce the size and weight of the MREAs for a production system. The trend that is shown, however, is that geometric and weight penalties that are encountered when designing MREAs for these dual goals – leading to the idea that it may be more beneficial to utilize two separate MR suspension

systems in series (one designed for vibration and one designed for adaptive occupant protection).

## 2.5 *Summary and Conclusions*

This chapter has explored the use of magnetorheological (MR) fluid dampers in a semi-active seat suspension system for helicopter crew seats. FLEAs and FPEAs currently used for rotorcraft seats provide only limited occupant protection to harsh or crash landings because they are designed to have a factory-established load-stroke profile and are thus tuned for only one occupant weight and one loading scenario. These devices, therefore, do not provide optimal protection for all occupant weights and crash/landing load levels. VLEAs have been used to accommodate varying occupant weight based upon a manual setting prior to use, but are also only tuned for one loading scenario. Furthermore, because these devices do not stroke until the tune stroking load threshold is reached during a crash, they are very stiff during normal operation and therefore transmit all floor vibrations directly to the occupant.

In this chapter, the benefits to utilizing a magnetorheological energy absorber (MREA)-based seat suspension system have been identified. MREAs allow for unattended, automatic adaptability to occupant weight (from the 5<sup>th</sup> percentile female to 95<sup>th</sup> percentile male) and crash/landing load level. With a real-time feedback controller, this allows the suspension to safely use the full stroke capability for each crash or harsh landing – regardless of occupant weight or crash/landing speed – thus transmitting the lowest force to the occupant at all times. Furthermore, MREAs have a secondary benefit during normal operation as they can be used to isolate the occupant from harmful cockpit vibrations. Key challenges in designing a magnetorheological

energy absorber (MREA)-based seat suspension system for both enhanced occupant protection and vibration isolation were identified. Furthermore, relations were made between MREA design parameters (maximum force, dynamic range, etc.) and resulting performance. Three MREA design options are considered: one optimized solely for vibration isolation, one for enhanced occupant protection, and one that is simultaneously capable of both enhanced occupant protection and vibration isolation. Resulting metrics such as performance, capabilities, weight, and size are compared, and the benefits and sacrifices associated with each of these designs were discussed. The summary of these results is shown in Table 2.1.

Key conclusions of this study are:

1. Using a single-degree-of-freedom (SDOF) seat suspension model, it can be shown that low off-state viscous damping and low friction are key elements in effective design of MR seat suspensions for vibration isolation. It has been shown that using such a design strategy, an MR damper can be designed to significantly reduce the vibration transmitted to the occupant with minimal weight impact. Experimental results have shown that such a system will reduce 4P floor vibrations by 76% of 4/rev floor vibrations while only adding 1.8 kg (4.0 lb) to the seat. This is only a net weight gain of 8% and 3% for the unarmored and armored SH-60 Seahawk crew seats, respectively. Furthermore, it has been shown that such MR dampers can be retrofit into current rotorcraft seat designs in such a manner (in series with FLEA/VLEAs) that their crashworthy capabilities are preserved.

2. Using a lumped-parameter biodynamic seat model with the capability of estimating occupant lumbar load response, an MR seat suspension can be designed for the purposes of enhanced occupant protection. It was shown that MREAs can be designed to retrofit FLEAs and VLEAs in rotorcraft seats and provide enhanced occupant protection by adapting to occupant weight and load level. These MREAs can utilize the full stroking capability of the seat for each harsh landing in order to minimize the load transmitted into the occupant. Using conventional MR valve designs, however, this enhanced performance comes at a cost of a slightly higher weight penalty of 6.7 kg (14.7 lb), which is an increase of 29% and 12% to the unarmored and armored SH-60 Seahawk crew seats, respectively. Because of stroke limitations and high viscous damping levels, however, such a design has reduced capability to isolate the occupant from cockpit vibrations.

3. It was shown that, with an increase in MREA dynamic range and stroke capability, an MR seat suspension is capable of achieving the dual goals of enhanced occupant protection and vibration isolation. An MREA has been designed which will provide the capability of adapting to occupant weight and load levels during a crash or harsh landing and also provide 50% reduction in 4P cockpit vibrations. Using conventional MR damper technology, however, this enhanced performance comes at a cost of increased weight penalty – 21.4 kg (47 lb) or 93% and 40% of the unarmored and armored SH-60 crew seat, respectively. Practical implementation, therefore, is hindered by a sacrifice to size and weight resulting from conventional MR damper technology.

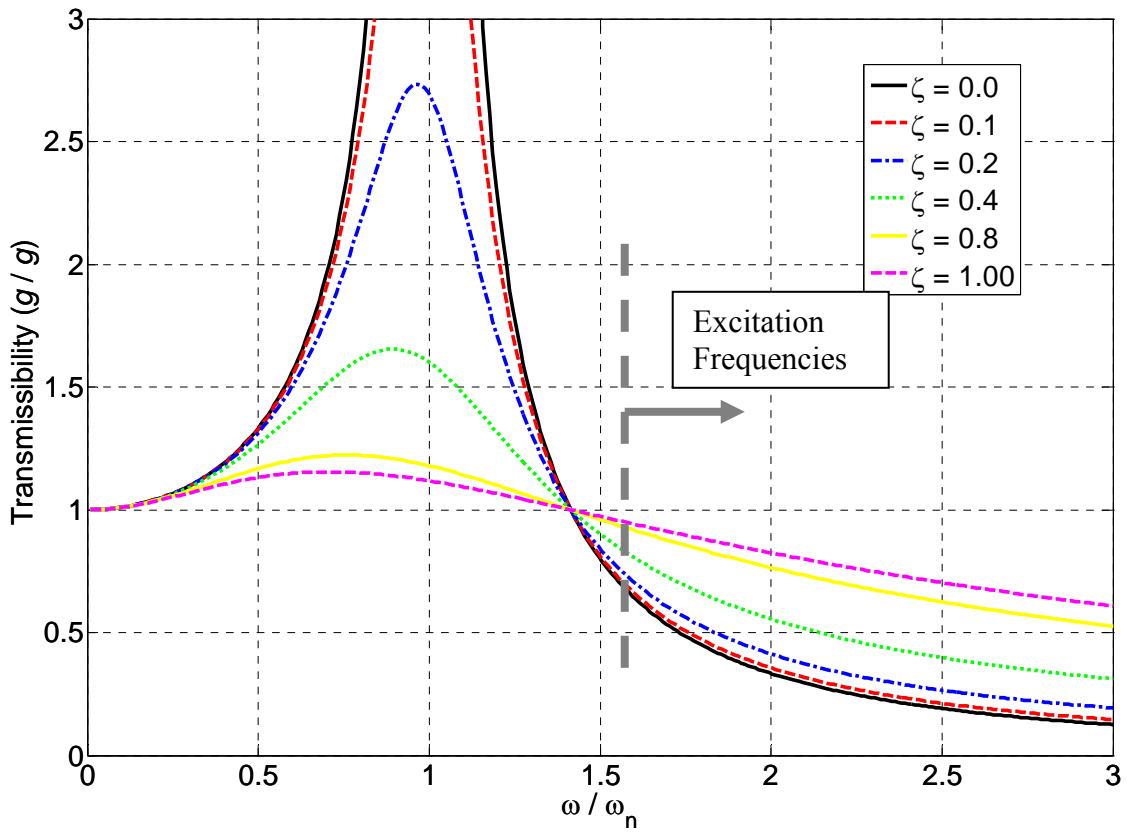


Figure 2.1: Transmissibility for SDOF System to Base Excitation for Varying Viscous Damping Levels

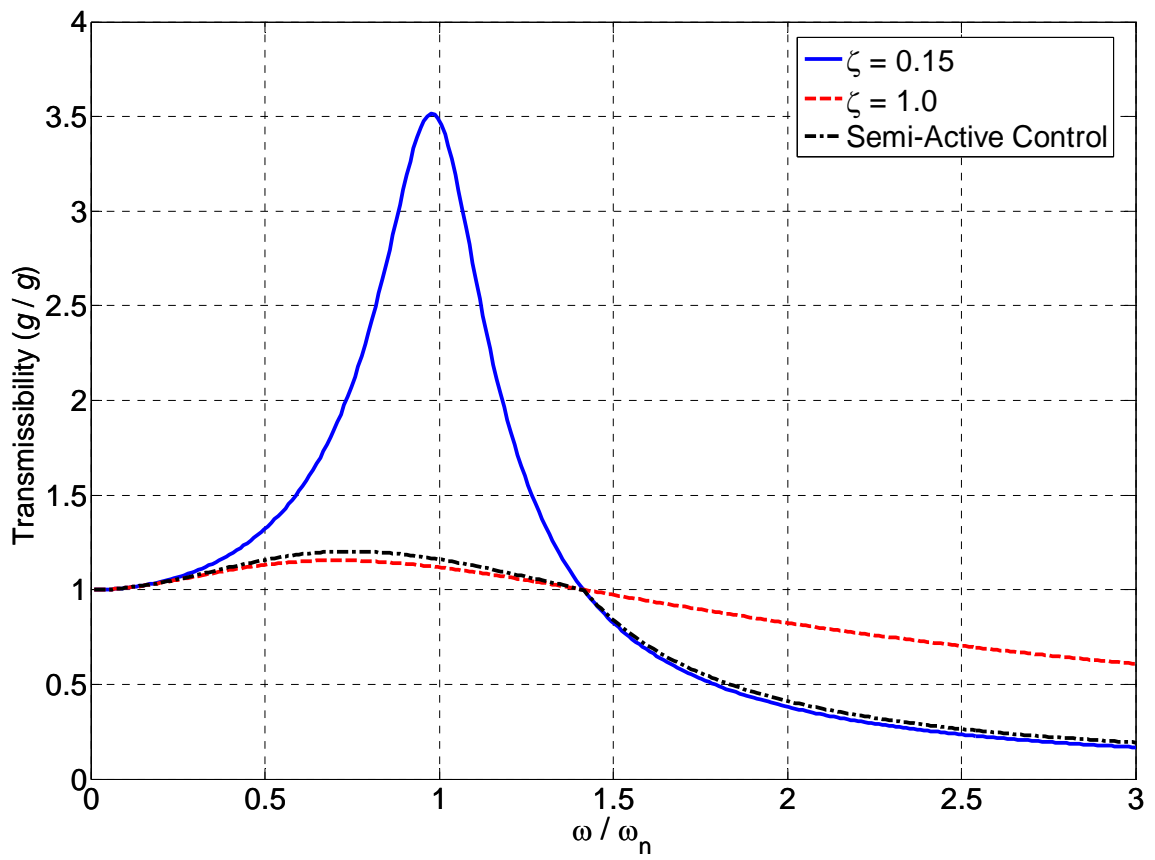


Figure 2.2: Semi-Active Control Objective

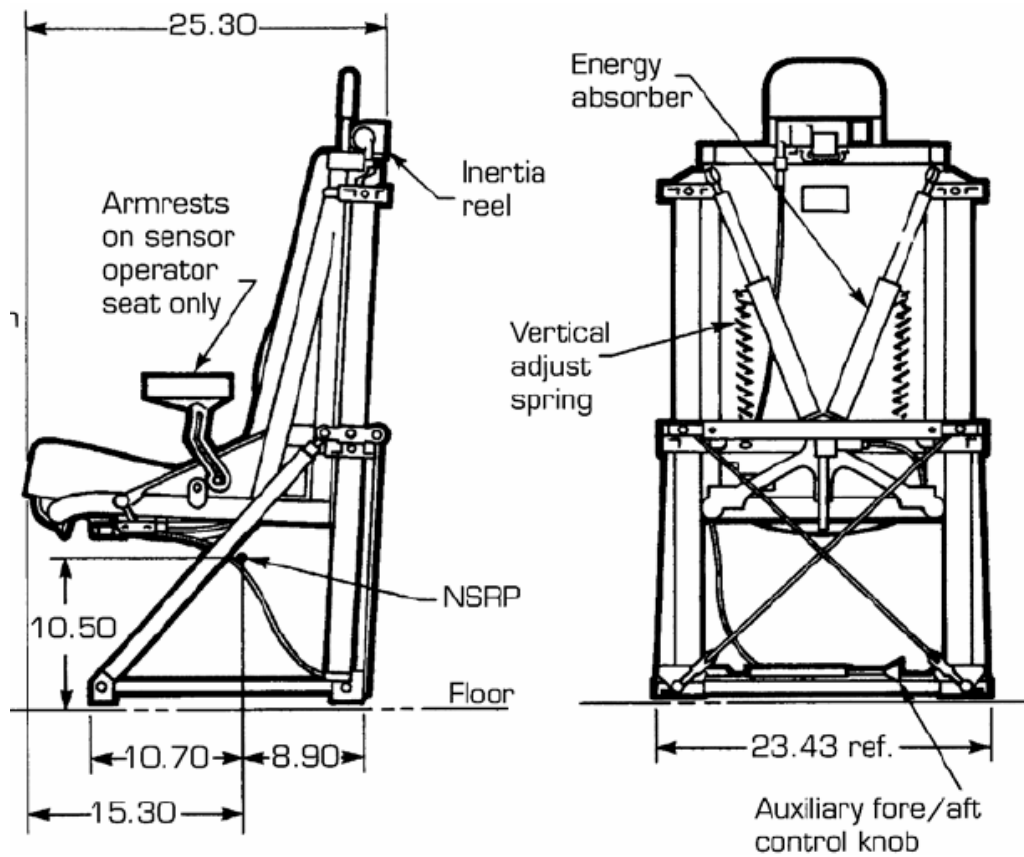


Figure 2.3: Unarmored SH-60 Seahawk Crew Seat Produced By Armor Holdings

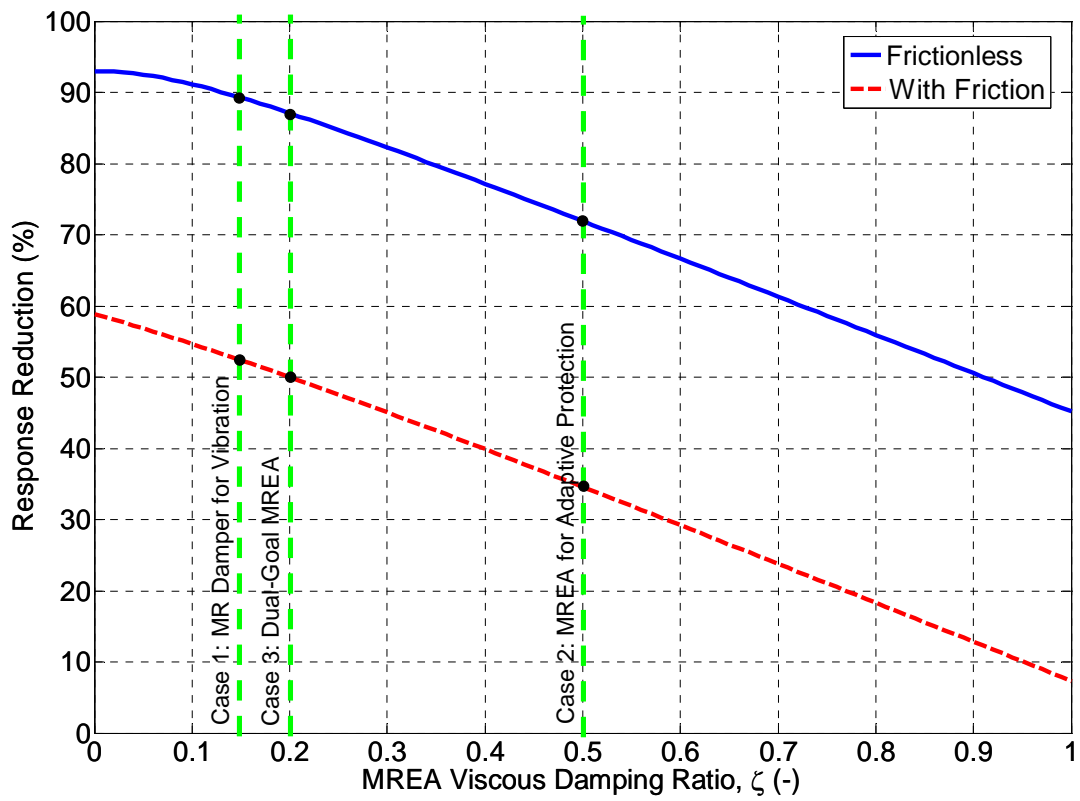


Figure 2.4: Reduction in Vibration Due to 0.2 g Amplitude 4P Floor Excitation vs. MREA Viscous Damping Ratio

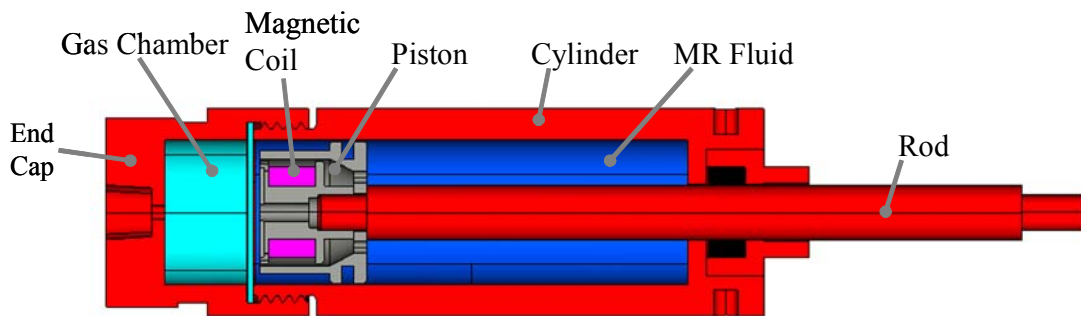


Figure 2.5: MR Damper Optimized for Vibration Isolation

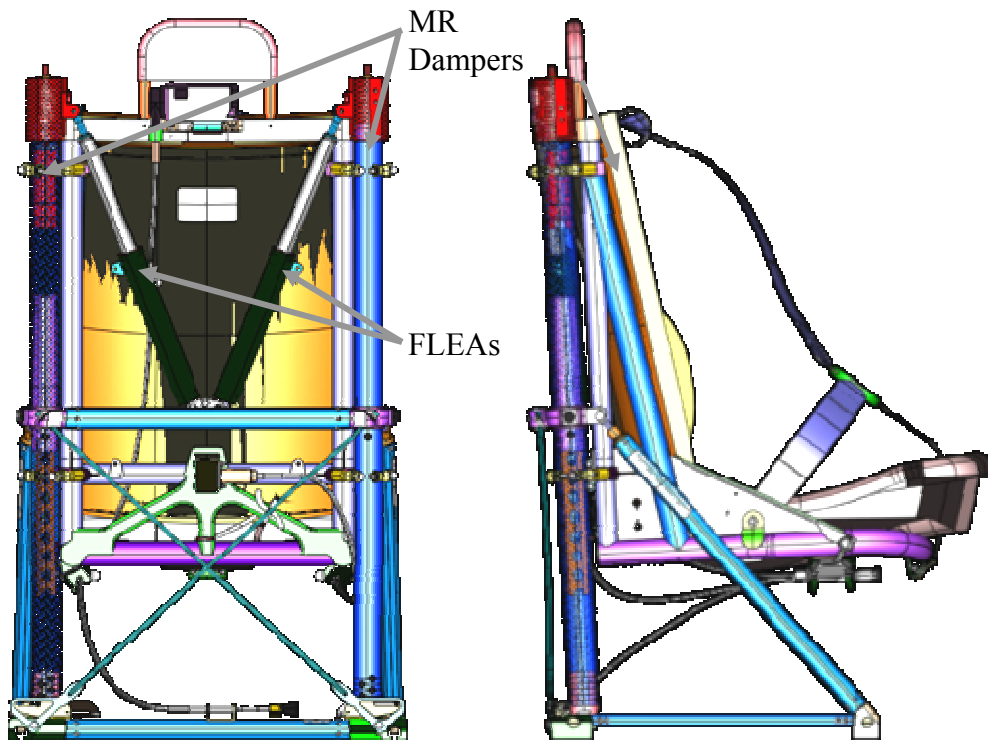


Figure 2.6: MR Dampers Retrofitted into SH-60 Crew Seat (Patent Pending)

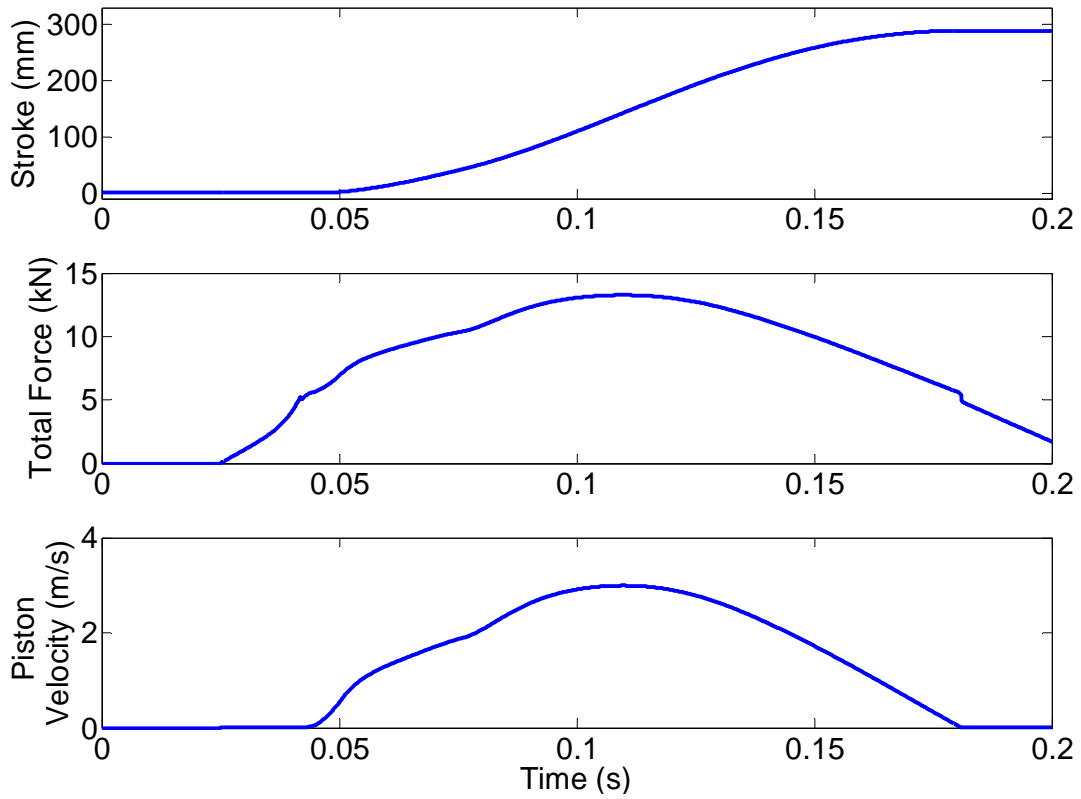


Figure 2.7: MR Damper Response for a 95th Percentile Male Occupant and a 12.8 m/s (42 ft/s) Sink Rate Crash

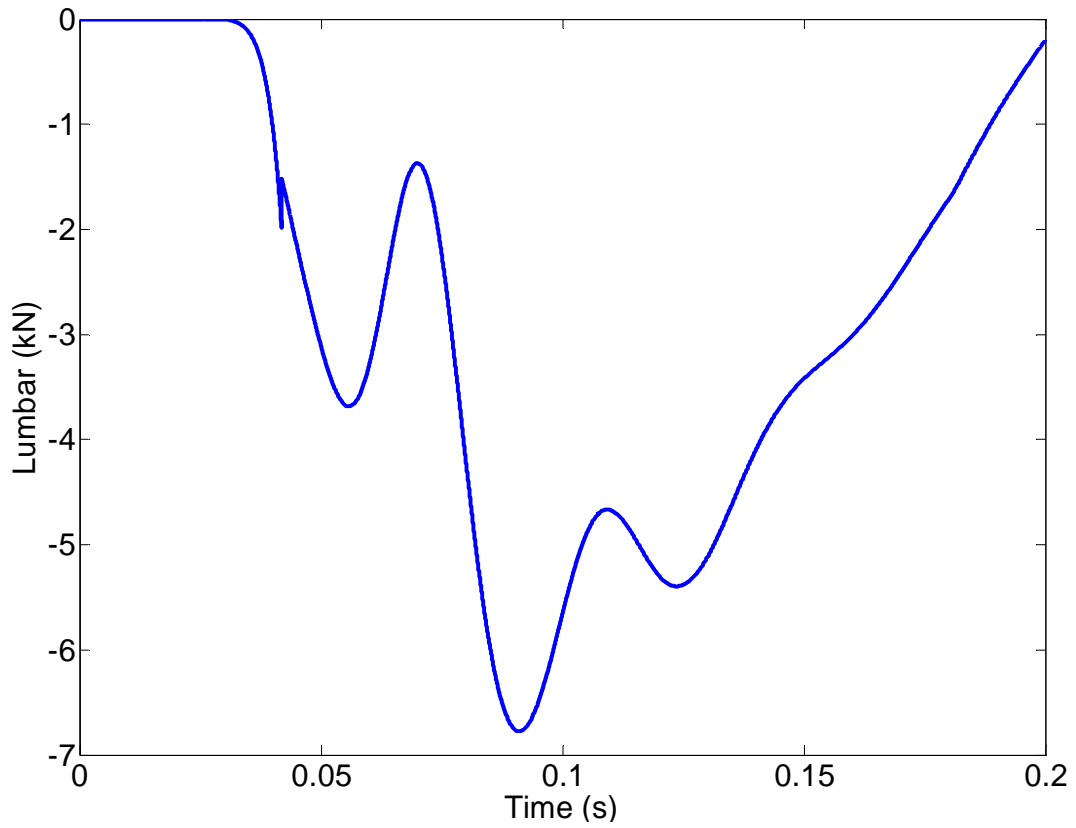


Figure 2.8: Lumbar Time Response for 95th Percentile Male and a 12.8 m/s (42 ft/s)

Sink Rate Crash with MREA

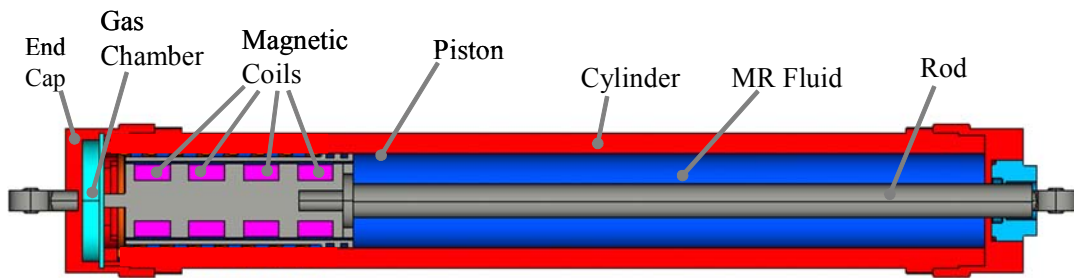


Figure 2.9: Preliminary Design of an MREA for Adaptive Crashworthiness

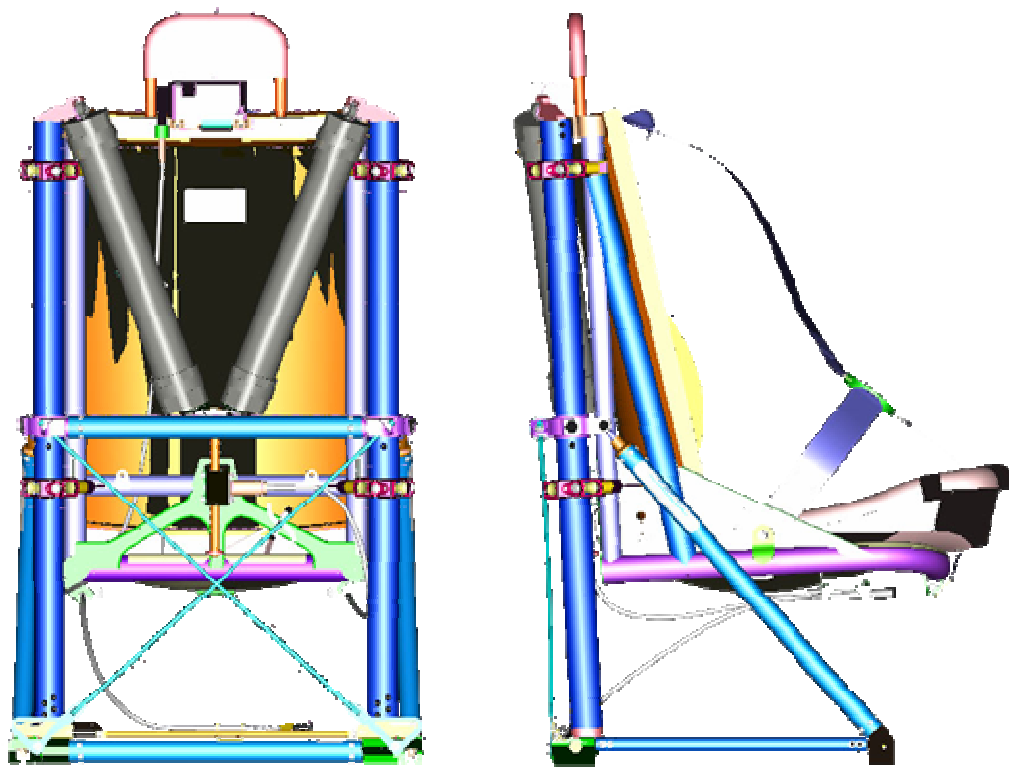


Figure 2.10: Crashworthy MREAs Retrofitted into SH-60 Seahawk Crew Seat

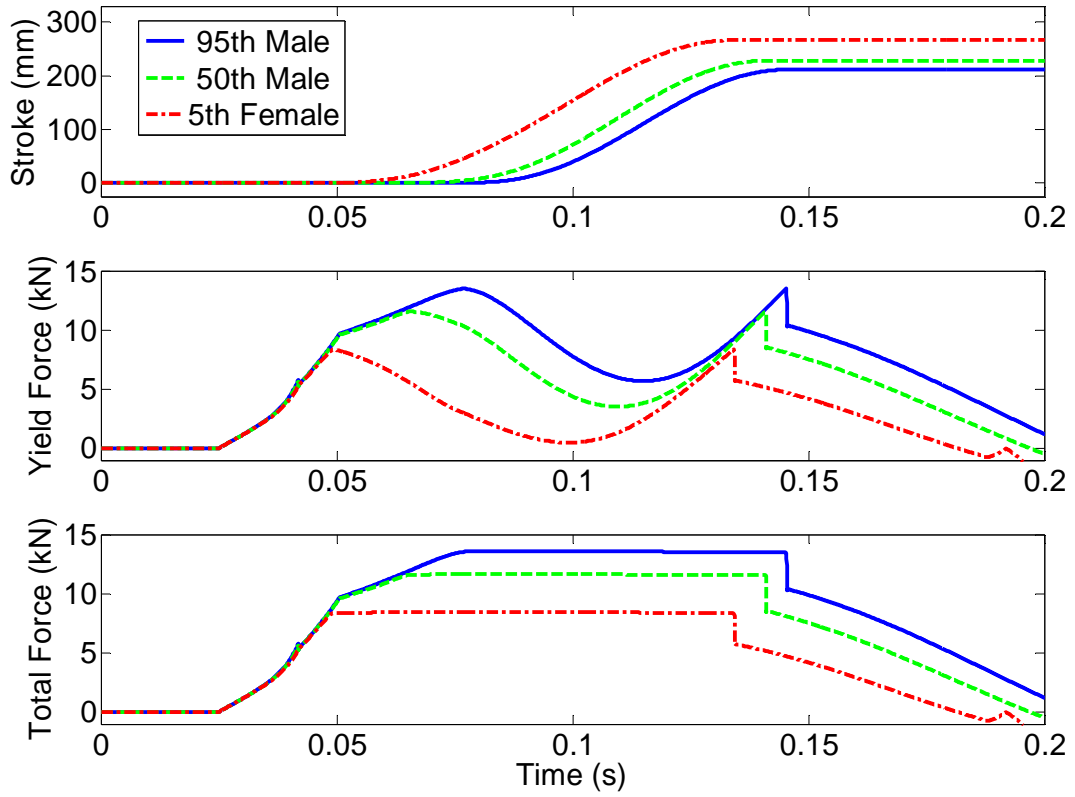


Figure 2.11: MR Damper Time Response for Load Limiting Control and Varying Occupant Weight

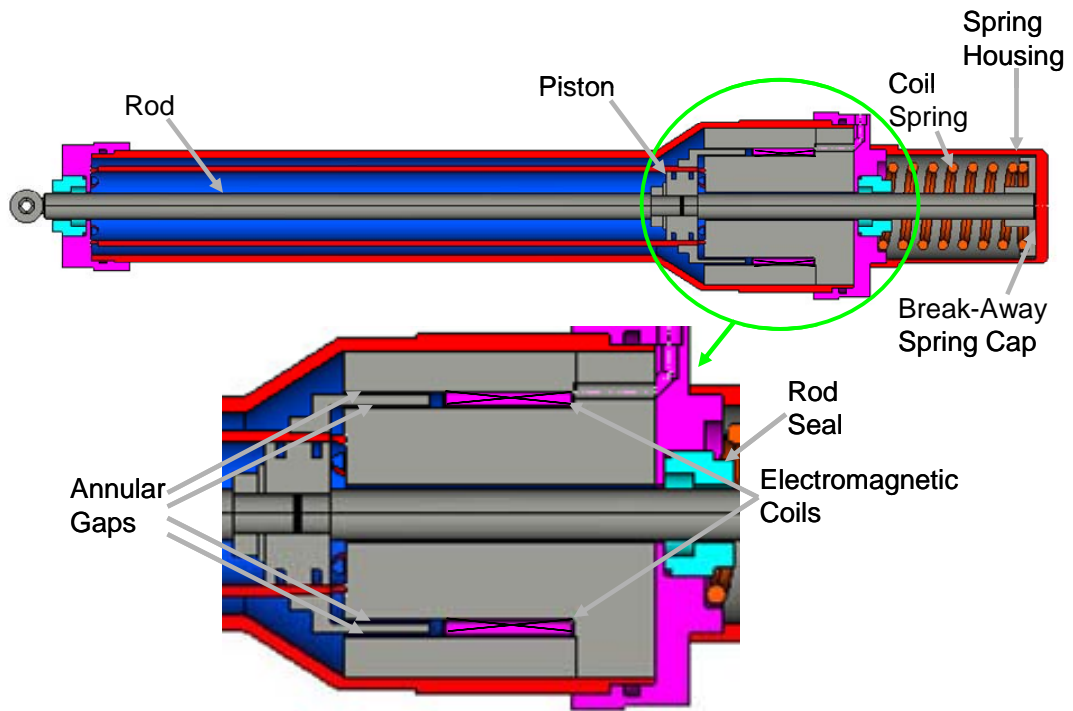


Figure 2.12: Dual-goal MREA Utilizing Bi-fold MR Valve (Patent Pending)

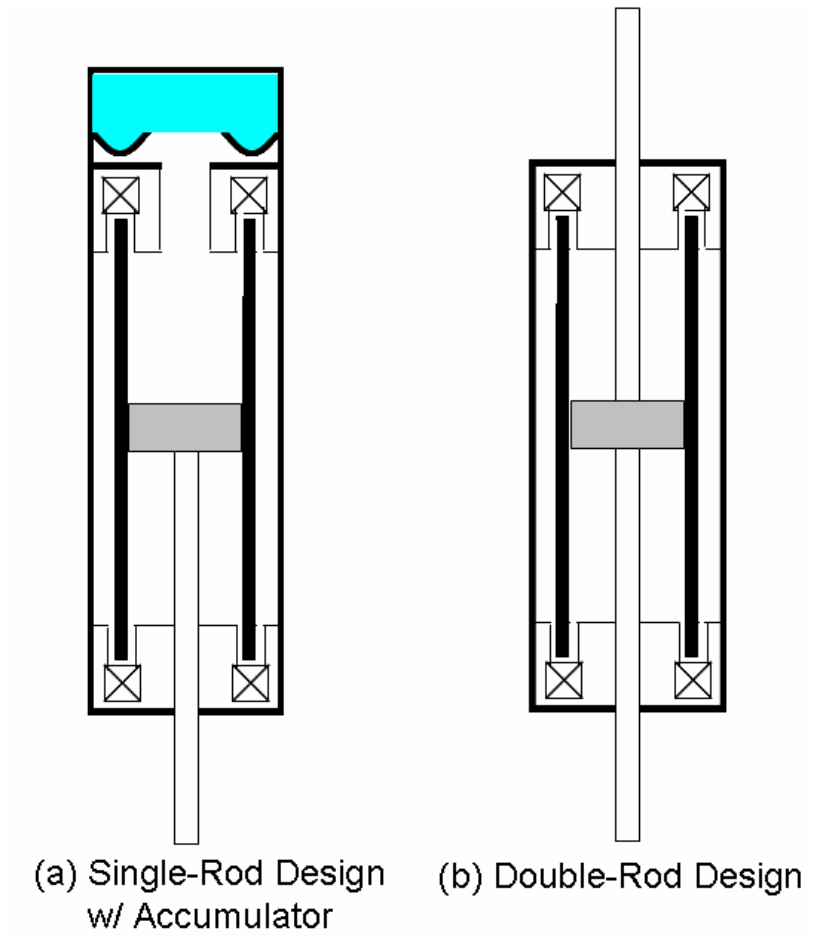


Figure 2.13: Standard Methods for Accounting for Rod Volume

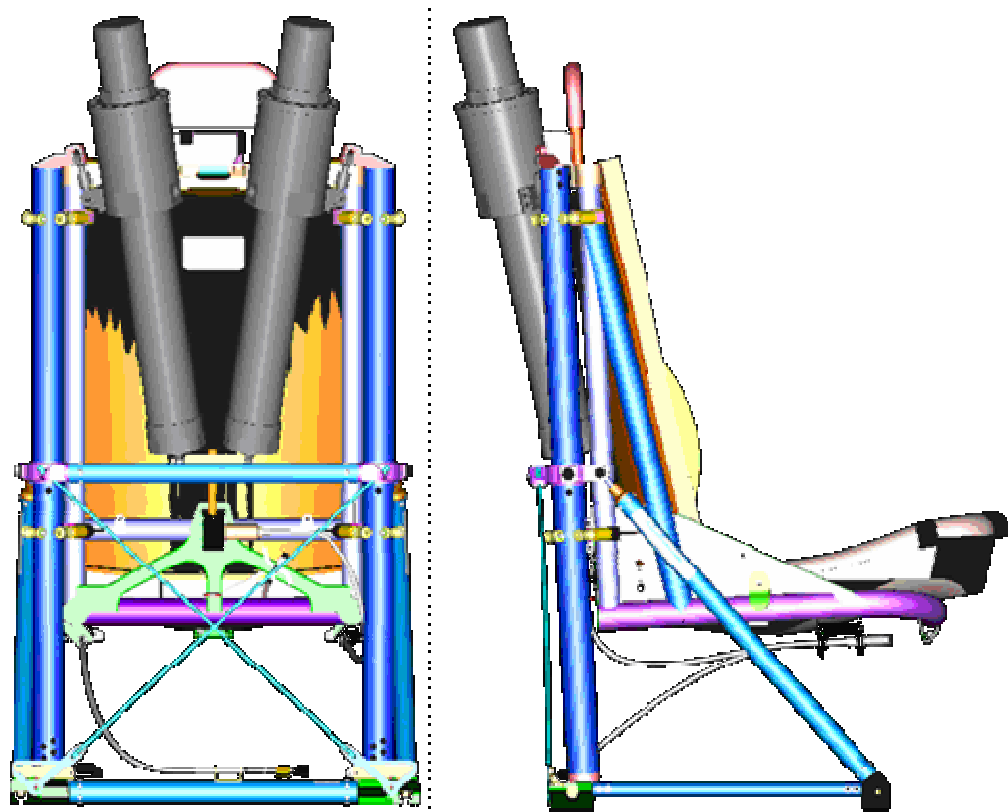


Figure 2.14: Dual-Goal MREAs Integrated in Unarmored SH-60 Seahawk Seat

Table 2.1: Summary of MR Seat Suspension Trade Study

<b>MR Design Goal</b>	<b>4P Vibration Reduction<sup>1</sup></b>	<b>Adaptive Crash.?</b>	<b>MR Device Mass [kg (lb)]</b>	<b>Net Percentage Weight Increase: Unarmored SH-60 Seat</b>	<b>Net Percentage Weight Increase: Armored SH-60 Seat</b>
<b>Vibration-only MR Damper</b>	76% [15]	No	0.45 (1)	8	3
<b>Adaptive MREA</b>	30% <sup>2</sup>	Yes	3.6 (8)	29	12
<b>Dual-Goal MREA</b>	50% <sup>3</sup>	Yes	10.9 (24)	93	40

<sup>1</sup> Assuming friction in system and 0.2 g amplitude floor excitation

<sup>2</sup> Assuming 80 N friction in system, performance will degrade for higher friction values

<sup>3</sup> Assuming 80 N friction in system, performance will degrade for higher friction values

## Chapter 3: Control of MREAs for Enhanced Crashworthiness

A key from Chapter 2 is that, using conventional MR damper technology, achieving enhanced crashworthiness with an MREA-based seat suspension tends to increase the weight of the seat. This study is intended to further illustrate the benefits gained with this increased suspension weight. In this chapter, various methods to control the MREAs to provide enhanced crashworthiness are investigated and performance metrics, such as lumbar load and the amount of stroke utilized, were compared.

### *3.1 Load Limiting or VLEA Control*

In the early 1970s, analysis and testing were performed to determine a limit load for seat energy absorption systems, that is, the load at which an FLEA would start and continue to stroke. Relating the seat performance to tolerance data and cadaveric testing, an energy absorbing limit load of 14.5 g was determined to keep the load-duration in the humanly tolerable range. This means that the FLEA would stroke at 14.5 times the effective occupant weight (% of body weight not supported by floor plus weight of body worn items) plus the weight of the stroking portion of the seat [1], [3]. This 14.5 g stroking limit corresponds to a 20% risk of injury to U.S. Army Aviators per Ref. [4].

Given this, an MR VLEA seat system (that is, an MR seat energy absorption system which varies its limit load based upon occupant weight) can be realized. A simple controller can be designed to determine the effective occupied seat mass,  $M$ ,

by a weight sensor in the seat, static deflection of the seat, or via manual setting. Once this value is determined, the controller then adjusts the limit load,  $F_L$ , as shown below:

$$\begin{aligned} F_L &= \alpha_{\text{limit}} \times M \\ &= \alpha_{\text{limit}} \times \frac{K(z_1 - z_0)_{\text{static}}}{g} \end{aligned} \quad (3.1)$$

The limit factor,  $\alpha_{\text{limit}}$ , is the injury tolerance criteria of choice (in  $g$ ). In this study, the 14.5  $g$  criteria discussed above is used. The controller can then modulate the MREA yield force real time to keep the damper force at this constant limit load. MREA yield force modulation may be performed using a simple load tracking control algorithm or by using the MREA force model. In this study, the Bingham plastic force model is used as an example, therefore the yield force is varied using the following simple equation:

$$F_y = F_L - C_p v, \quad (3.2)$$

where  $F_y$  is the MREA yield force,  $F_L$  is the load limit,  $C_p$  is the MREA post-yield viscous damping, and  $v$  is the stroking velocity. Knowing the instantaneous velocities of the seat and floor, the controller then uses Eq. 3.2 to determine the desired MREA yield force. This MR yield force modulation equation can become more complex if other MREA or MR damper force models are used (those including hysteresis, compressibility, etc.).

### 3.1.1 Analytical Results

Figure 3.1 shows the resulting time response of the MREA from a 12.8 m/s (42 ft/s) sink rate crash assuming a symmetric triangular acceleration pulse with 51

ms duration, 292 mm (11.5 in.) of available stroke, and a 95<sup>th</sup> percentile male occupant (96.15 kg [212 lb]) [4]. The top plot shows that, in the passive, viscous-only case, the MREA bottoms-out quickly – which leads to an increased reaction into the occupant’s spine. In the constant yield force case, the total damper force (bottom plot) quickly increases to the 14.5 g yield force setting. As piston velocity increases, the total MREA force further increases beyond the 14.5 g load due to the viscous force component. The load limiting control, however, prevents the total force imparted into the seat (bottom plot) from exceeding the limit value by modulating the yield force (middle plot). It can also be seen that limiting the load to 14.5 g efficiently uses more of the available stroke than the constant yield force case.

Figure 3.2 shows these MREA time response plots for load limiting control and varying occupant weight. It can be seen that the load limiting control effectively limits the load imparted into the seat to the respective 14.5 g level for the 5<sup>th</sup> percentile female (46.62 kg [102.8 lb]) as well as the 50<sup>th</sup> and 95<sup>th</sup> percentile males (77.55 kg [171 lb] and 96.15 kg [212 lb]), respectively [4]. It can also be seen that the controller prevents the MREA from bottoming out in each of these cases. Additionally, note that the peak lumbar loads predicted by the biodynamic model are 7,570 N, 6,405 N, and 4,137 N for the 95<sup>th</sup> percentile male, 50<sup>th</sup> percentile male, and 5<sup>th</sup> percentile female, respectively. These are well below the respective limits of 11,271 N, 7,161 N, and 5,698 N published in [41].

### 3.1.2 Effect of MR Damper Time Response

The previous simulations assume an ideal MREA and control system, so that the practical effect of delay in the MREA time response is now considered. To

emulate this time response, the control action, or desired damper force  $f_d$ , is assumed to pass through a first-order low-pass filter given by:

$$\dot{f}_{d\_f} = \frac{f_d - f_{d\_f}}{\tau} \quad (3.3)$$

where  $f_{d\_f}$  is the filtered control input and  $\tau$  is the time constant [2], [46]. Choi and Wereley [46] have experimentally calculated the response time of their MR dampers (or MREAs) to be 7-8 milliseconds. Assuming similar MREA performance, the simulation of Figure 3.2 was rerun with a 10 millisecond time constant - giving the results shown in Figure 3.3. Firstly, note that some oscillations have appeared at the onset of the crash event (0.025 sec) as well as once the MREA has finished stroking (0.140 sec). These are due to the dynamics of the coupled nonlinear biodynamic model and are more pronounced because of the energy absorber time delay. Because of this time delay, the total force (3<sup>rd</sup> plot) is no longer perfectly limited to the 14.5 g stroking load. Alternatively, a slight tracking error has appeared that increases this force beyond its desired limit established in Figure 3.2. The peak force values increase beyond the load limits by 10.8%, 12.2%, and 12.4% for the 95<sup>th</sup> percentile male, 50<sup>th</sup> percentile male, and 5<sup>th</sup> percentile female, respectively. The root-mean-square (RMS) of the tracking errors are 7.3%, 8.1% and 10.0%, respectively. These tracking errors are likely acceptable for practical application as they are likely well within the realm of error for the 14.5 g injury tolerance criteria. Furthermore, predicted lumbar loads of 7,717 N, 6,521 N and 4,194 N are still well below the limits for the 95<sup>th</sup> percentile male, 50<sup>th</sup> percentile male, and 5<sup>th</sup> percentile female, respectively [4], [41].

To further test the sensitivity of the MREA time response, simulations using a 20 millisecond time constant were also performed (Figure 3.4). It can be seen in Figure 3.4 that the tracking error has not changed significantly. For this case, the peak force values increase beyond the load limits by 10.6%, 11.3%, and 14.0% for the 95<sup>th</sup> percentile male, 50<sup>th</sup> percentile male, and 5<sup>th</sup> percentile female, respectively. The RMS tracking errors are 7.1%, 7.6%, and 10.4%, respectively. These tracking errors have not changed significantly from this increase in the MREA time delay. This shows that MREA time constants less than 20 ms, which are realizable in practical MREAs or MR dampers [46], should not hinder practical implementation.

### *3.2 Notched-Profile or VPEA Control*

As discussed in Section 1.2.1 FPEAs use a notched load-stroke profile to increase the average deceleration of the occupant while maintaining spinal loads within a humanly tolerable range [3]. This notched profile reduces the dynamic overshoot of the “springs” of the occupant’s body and results in a more efficient use of suspension stroke [3]. These FPEAs, however, have a factory-established load-stroke profile and therefore cannot adapt to occupant weight.

Using MREAs, however, the system can automatically adapt the force levels in the notched profile to the occupant’s weight and essentially become variable-profile energy absorbers (VPEA). Figure 3.5 shows an example notched profile to which an MREA can be controlled to adapt to occupant weight. In this profile, the initial spike is set to 16 g times the occupant mass, the notch load is set to 12.5 g times the occupant mass, and the hold load is set to 16 g times the occupant mass. It should be noted that, with an MREA, the profile (i.e., load values and the deflection

at which they occur) can be easily varied by simply changing parameters in the controller – no hardware changes are necessary. The controller algorithm would set the desired control load,  $F_{VPEA}$ , based upon real-time measurements of the MREA stroke,  $x$  as follows:

$$F_{VPEA} = \begin{cases} G_s M & \text{if } x \leq \delta_n \\ G_n M & \text{if } \delta_n < x < \delta_h \\ G_h M & \text{if } x \geq \delta_h \end{cases} \quad (3.4)$$

where,  $G_s$ ,  $G_n$ , and  $G_h$ , are the desired deceleration values at the spike, notch, and hold, respectively,  $M$  is the effective occupied seat mass (manually set or measured), and  $\delta_n$  and  $\delta_h$  are the stroke thresholds at which the load changes. The controller can then modulate the MREA yield force real time to follow this desired load. As discussed above, MREA yield force modulation may be performed using a simple load tracking control algorithm or by using the MREA force model. In this study, the Bingham plastic force model is used as an example, therefore the yield force is varied using the following simple equation:

$$F_y = F_{VPEA} - C_p v, \quad (3.5)$$

### 3.2.1 Analytical Results

Figure 3.6 shows the MR damper time response for this VPEA control. Firstly, in the top plot it is seen that the stroke utilized is approximately 25mm less than that for VLEA control (Figure 3.2). Also in this figure, it can be seen that the MREA yield force (middle plot) is modulated to give a notched total MREA force (bottom plot). Furthermore, in these simulations, the peak lumbar loads predicted during this simulation are 7,664 N, 6,227 N, and 3,959 N for the 95<sup>th</sup> percentile male,

50<sup>th</sup> percentile male, and 5<sup>th</sup> percentile female, respectively. Not only are these lumbar loads within the humanly tolerable range per [4] and [41], but they are very close to those predicted using the VLEA control. The fact that the lumbar loads have remained the same, but less stroke was utilized shows that the notch-profile has, in fact, performed as designed.

### 3.2.1 Effect of MR Damper Time Response

As done above, the effect of MR damper time response is evaluated. Firstly, a time delay of 10 ms is analyzed. Figure 3.7 plots the resulting load-stroke profile with this time delay. It can be seen that, while the initial spike and notch are still apparent, they are not as clearly defined as in Figure 3.5 because of this time delay. As was done for the VLEA control, above, the tracking errors were calculated using this time delay. The average errors were calculated to be 11.0% , 9.8%, and 8.4%, and the peak errors were calculated to be 17.3%, 14.3%, 13.6%, respectively for the 95<sup>th</sup> percentile male, 50<sup>th</sup> percentile male, and 5<sup>th</sup> percentile female occupants. Furthermore, while the peak lumbar loads have not changed much (7,668 N, 6,338 N, and 3,959 N, respectively) and are still within the tolerable range, Figure 3.8 shows that the stroke is no longer utilized efficiently. The stroke utilized is close to what was predicted for the VLEA control. This is because, assuming this time delay, the MREA cannot react quickly enough to sharply modulate the force. This illustrates that, if the MREA has significant time delay, utilizing VPEA control may not be beneficial (over VLEA control) for the purposes of more efficiently utilizing available stroke.

In order to show the effect of further increased time delay, a simulation with 20 ms delay was performed. Figure 3.9 shows the resulting load-stroke profile. The average tracking errors were calculated to be 9.2%, 9.6%, and 9.2%, and the peak tracking errors were calculated to be 11.2%, 8.9%, 13.3%, respectively, for the 95<sup>th</sup> percentile male, 50<sup>th</sup> percentile male, and 5<sup>th</sup> percentile female occupants, respectively. While these tracking errors have not increased, it can be seen that Figure 3.9 no longer resembles the notched profile of Figure 3.5 whatsoever. This is because the notch itself only lasts approximately 20 ms, so the notch is essentially filtered out. It is interesting to note, however, that in this simulation the predicted peak lumbar loads have reduced to 6,983 N, 5,725 N, and 3,759 N, respectively. Inspection of the resulting MREA time response (Figure 3.10), however, shows that this is a result of further increase stroke, which is not ideal. This further shows that, if the MREA has significant time delay, utilizing VPEA control may not be beneficial (over VLEA control) for the purposes of more efficiently utilizing available stroke.

### 3.3 Crash Load Adaptive (CLA) Control

As discussed in Chapter 1, current schemes to attenuate crash loads (FLEAs, FPEAs, and VLEAs) are limited in that they provide the same risk of injury (~20%) for all crash load levels. That is, because the EAs cannot adapt to the crash level, the same peak force is transmitted to the occupant whether it is a severe crash or a minor crash. This crash load adaptive (CLA) control scheme aims to further reduce the risk of injury during less severe crashes by lowering the MREA force to utilize the full stroke capability during each crash event.

The difficulty with such a control scheme is that landing impact loading is not known *a priori*. While the helicopter will likely have altimeter measurements through which a sink rate may be determined, it cannot be assumed that such a measurement will be available in a crash scenario. Furthermore, the vehicle sink rate is not the only factor determining the severity of the cockpit floor deceleration. Not only will this be dependent upon what is being impacted and at what angle, but as discussed in Section 1.2.1, the duration of the crash pulse is dependent upon the characteristics of the landing gear and crushing of the vehicle substructure [1], [3]. Such a controller, therefore, should base its adaptation of the MREA on real-time measurements from within the cockpit.

Since the energy that needs to be absorbed by the MREA is proportional to the square of velocity, a velocity feedback control scheme is logical. Absolute velocity measurements, however, are not easily determined since the helicopter will likely be descending at a constant rate. Accelerometer measurements, therefore, will not be useful in determining absolute velocities. Accelerometer measurements, however, can be useful in determining relative velocity (or stroking velocity) measurements once the impact occurs. Relative velocity measurements can also be determined by differentiating a linear position sensor. Using a relative velocity measurement, a practical control strategy could then be:

$$F_{CLA} = K_{CLA}v^2, \quad (3.6)$$

where  $F_{CLA}$  and  $K_{CLA}$  are the desired control force and control gain, respectively, for this crash load adaptive control. To make this control scheme also adaptive to

occupant weight, the control gain (which is in units of mass / distance) can also be proportional to the effective occupied seat mass,  $M$ :

$$K_{CLA} = Z \cdot M \quad (3.7)$$

where  $Z$  is a parameter that is tuned to achieve the desired stroking distance (in units of distance<sup>-1</sup>). As a safety precaution, a conditional statement is added to the controller to ensure that the MREA load does not exceed the 14.5 g limit. Additionally, a minimum velocity value is set in Eq. 3.6 to initiate the MREA force and thus reduce the ramp up time. Similarly to the prior control schemes, MREA yield force modulation may be performed using a simple load tracking control algorithm or by using the MREA force model. In this study, the Bingham plastic force model is used as an example, therefore the yield force is varied using the following simple equation:

$$F_y = F_{CLA} - C_p v, \quad (3.8)$$

### 3.3.1 Analytical Results

Figure 3.11 plots the MREA time response for this CLA control. This plot show simulations resulting from a 50<sup>th</sup> percentile male occupant to three different crash levels: 1) severe: 42 ft/sec sink rate and 51 g peak acceleration, 2) medium: 30 ft/sec sink rate and 30 g peak acceleration, and 3) minor: 21 ft/s sink rate and 20 g peak acceleration. The top plot of Figure 3.11 shows that the full stroke is utilized for all crash load levels. This is achieved by modulating the MREA yield force (middle plot) to track the desired MREA total force (bottom plot). While it is not very meaningful since this is a time-based control scheme rather than deflection-based, Figure 3.12 shows the resulting load-stroke profile for comparison purposes.

The peak lumbar loads calculated in this simulation are 5,733 N, 3,923 N, and 2,673 N, respectively, for the severe, medium, and minor crash levels. These values are much lower than those for the 50<sup>th</sup> percentile male using VLEA control (6,405 N), which uses the 14.5 g load limiting criteria to yield a 20% risk of injury for all crash levels. The peak seat decelerations calculated for these controlled simulations are 14.5 g, 10.4 g, and 6.8 g for the severe, medium, and minor crash levels, respectively. According to pp. 69 in Ref. [4] (included herein as Figure 3.13), these correspond to injury risks of 20%, 0%, and 0%, respectively, for U.S. Army aviators. From these results, it can clearly be seen that CLA control provides enhanced protection by eliminating injury risk to lower crash levels.

In order to illustrate that this CLA control can adapt to both occupant mass and crash load level, a simulation was run to compare a 95<sup>th</sup> percentile male in a minor crash, a 50<sup>th</sup> percentile male in a medium crash, and a 5<sup>th</sup> percentile female in a severe crash. Figure 3.14 shows the resulting MREA time response. It can be seen that for each of these cases, the full stroke is again utilized by adjusting the MREA yield force. The resulting lumbar loads are 3,118 N, 3,923 N, and 3,914 N, respectively – all within the humanly tolerable range for each occupant per Ref. [41]. Furthermore, the peak seat decelerations for these simulations were 6.7 g, 10.4 g, and 14.7 g, respectively – again correlating to 0%, 0%, and 20% injury risk, respectively per Figure 3.13. This demonstrates that this control algorithm provides enhanced occupant protection by adapting to occupant weight and crash load level.

### 3.3.2 Effect of MR Damper Time Response

As done above, the effect of MR damper time response is evaluated for this control scheme. Figure 3.15 shows the MREA time response for CLA control assuming a 10 ms time delay and a 50<sup>th</sup> percentile male occupant. Compared to Figure 3.11, it can be seen that there is very little effect on performance – each simulation simply uses slightly more stroke than without time delay, which can be adjusted for with the control gain. The lumbar loads have also decreased to 5,627 N, 3,420 N, and 2,620 N, respectively for the severe, medium, and minor crash load levels. Finally, the resulting peak decelerations are 14.6 g, 10.2 g, and 6.8 g, respectively – again corresponding to injury risks of 20%, 0%, and 0%.

Figure 3.16 shows the MREA time response for CLA control assuming a 20 ms time delay and a 50<sup>th</sup> percentile male occupant. It can be seen that with this added time delay, the system uses even more stroking distance, but each simulation still uses approximately the same amount of stroke. Because of this additional stroke usage, the peak lumbar loads for these simulations have decreased to 5,355 N, 3,425 N, and 2,504 N, for the severe crash, medium crash, and minor crash, respectively. Additionally, the peak seat decelerations are 14.4 g, 10.2 g, and 6.7 g, respectively, which correlate to injury risks of 20%, 0%, and, 0%. This further shows that, while MREA time delay causes the use of additional stroke over an MREA with no time delay, the ability to adapt to crash level is not hindered. Furthermore, by adjusting the control gains, the stroke used can be adjusted to make up for this time delay effect.

### 3.4 *Summary and Conclusions*

In this chapter, three schemes to which an MREA-based suspension can be controlled are presented and simulated. The first of these realizes the MREAs as automatically adapting variable load energy absorbers (VLEAs) with the MREA yield force being modulated to limit the seat deceleration to a constant value (14.5 g, for instance). This control scheme allows for unattended and continuously proportional adaptation to occupant weight. It was also shown that while MREA time delay adds some error in tracking the limit load, the predicted lumbar loads are maintained within a humanly tolerable range.

Next, a control scheme which realizes MREAs as variable profile energy absorbers (VPEAs) was presented. This control scheme adapts a notched load-stroke profile to varying occupant weight. It is shown that such a control scheme can be implemented to reduce the stroke utilized by taking advantage of the dynamics of the human body. It is shown, however, that the inclusion of MREA time delay cancels this stroke reducing capability because it requires rapid force modulation.

Finally, a crash load adaptive (CLA) control scheme is presented which automatically adapts to both occupant weight and crash load level. This controller feeds back real-time stroking velocity measurements and calculates a control force that is proportional to both occupant mass and the square of the stroking velocity. It is shown that this control scheme allows the full suspension stroke to be utilized for each crash scenario, regardless of occupant weight and crash load level. By always utilizing the full suspension stroke, the load transmitted to the occupant is always minimized. This allows the risk of injury to be significantly reduced or eliminated for

lower crash load levels. This is a significant improvement over conventional EAs which always transmit a 14.5 g stroking load, corresponding to a 20% risk of injury. It is also shown that, while the control gain must be adjusted to account for MREA time delay, the ability to adapt to crash level is not hindered by this effect.

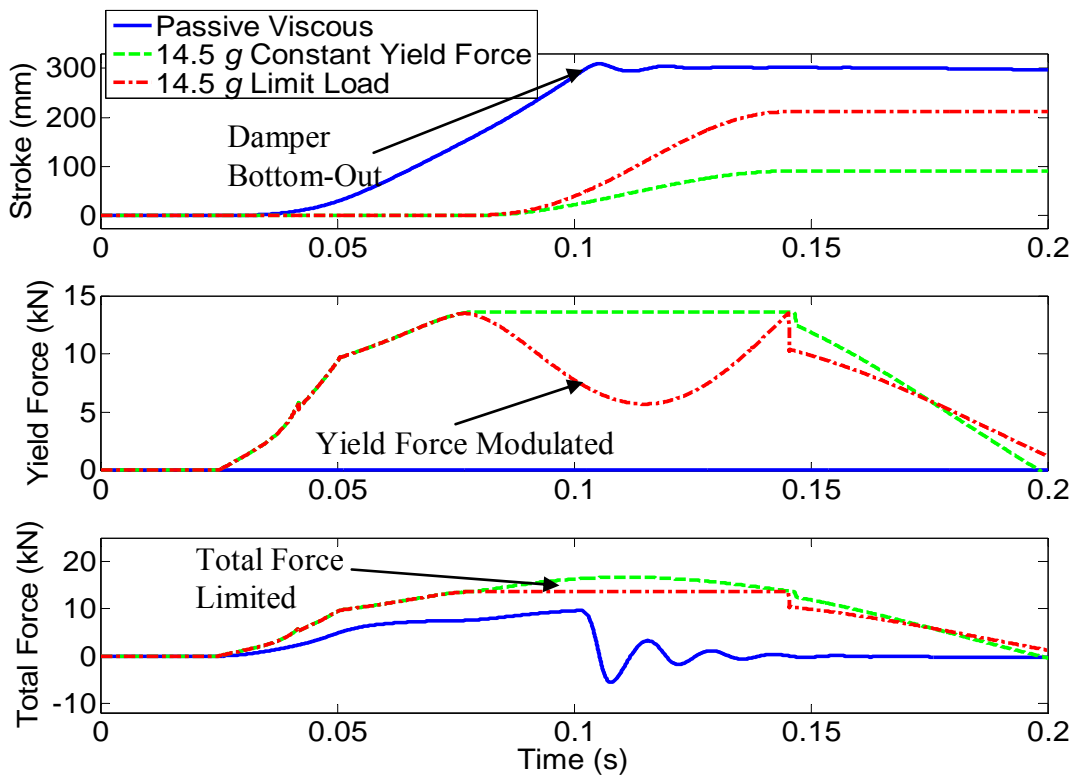


Figure 3.1: MREA Time Response for Passive Viscous, Constant Yield Force, and Load Limiting Control

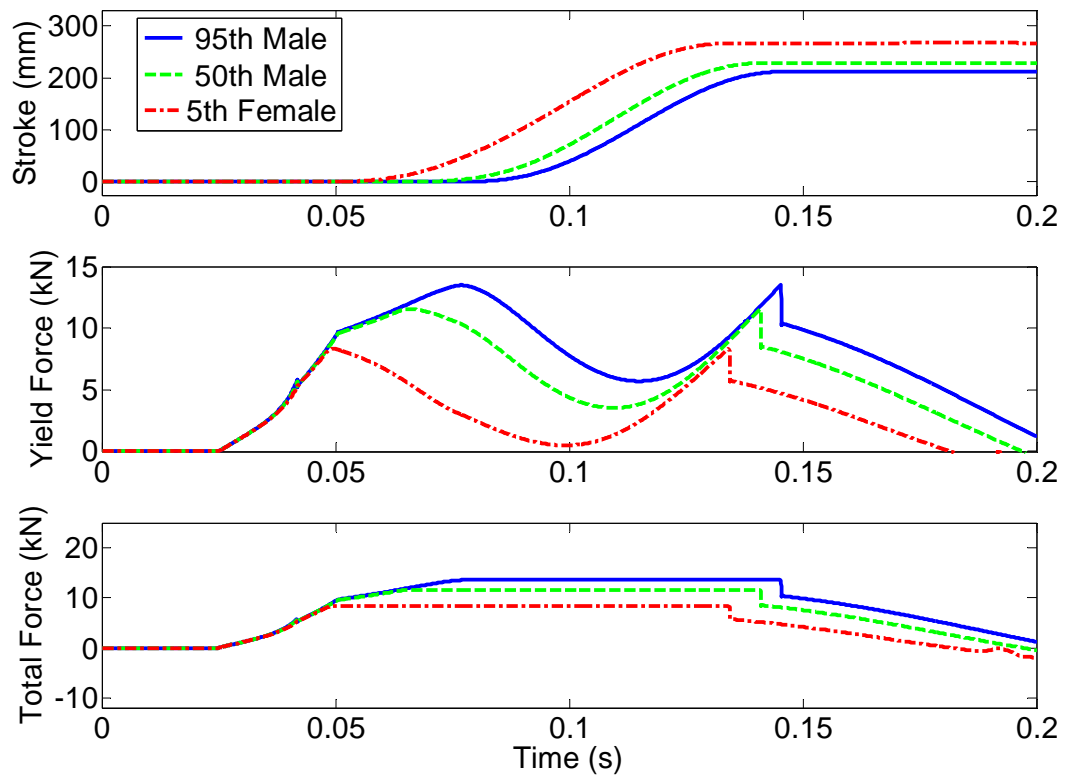


Figure 3.2: MREA Time Response for Load Limiting Control and Varying Occupant

Weight

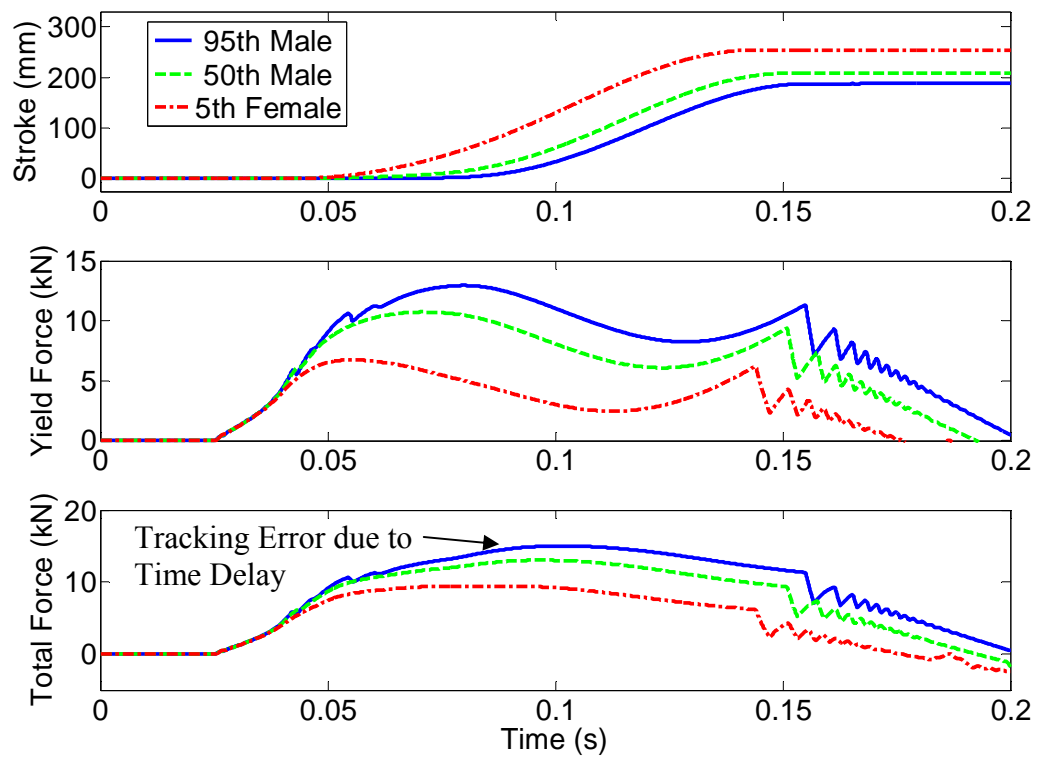


Figure 3.3: MREA Time Response for Load Limiting Control and 10 ms Time Constant

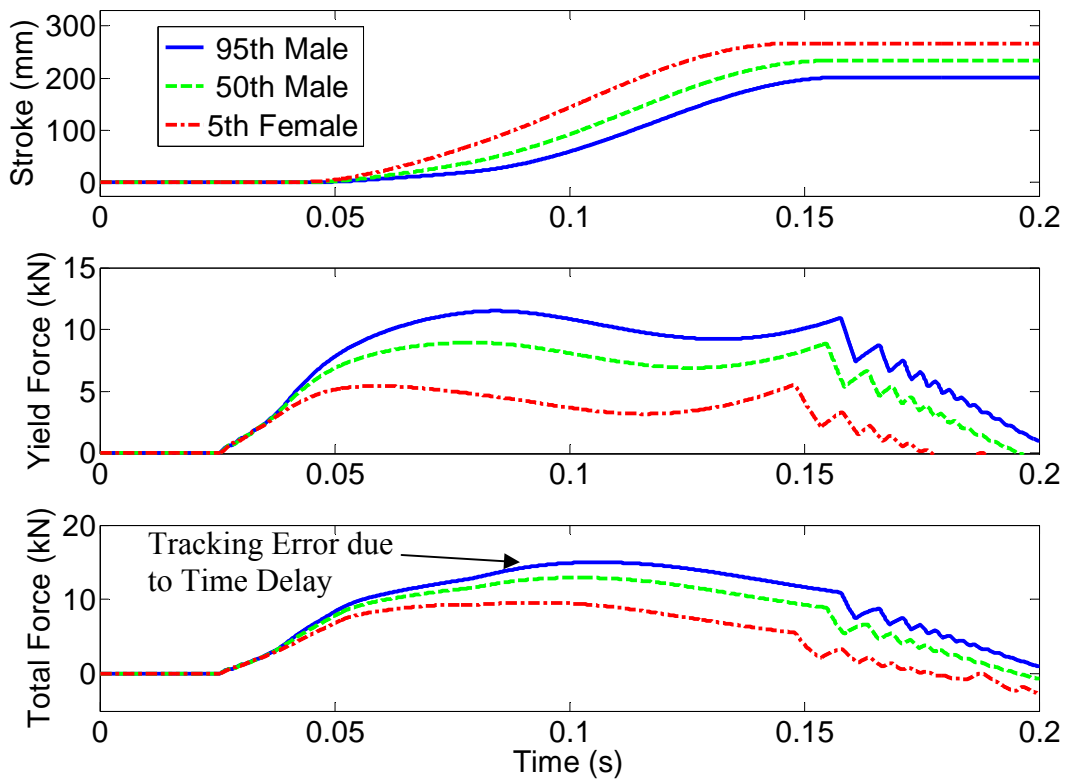


Figure 3.4: MREA Time Response for Load Limiting Control and 20 ms Time Constant

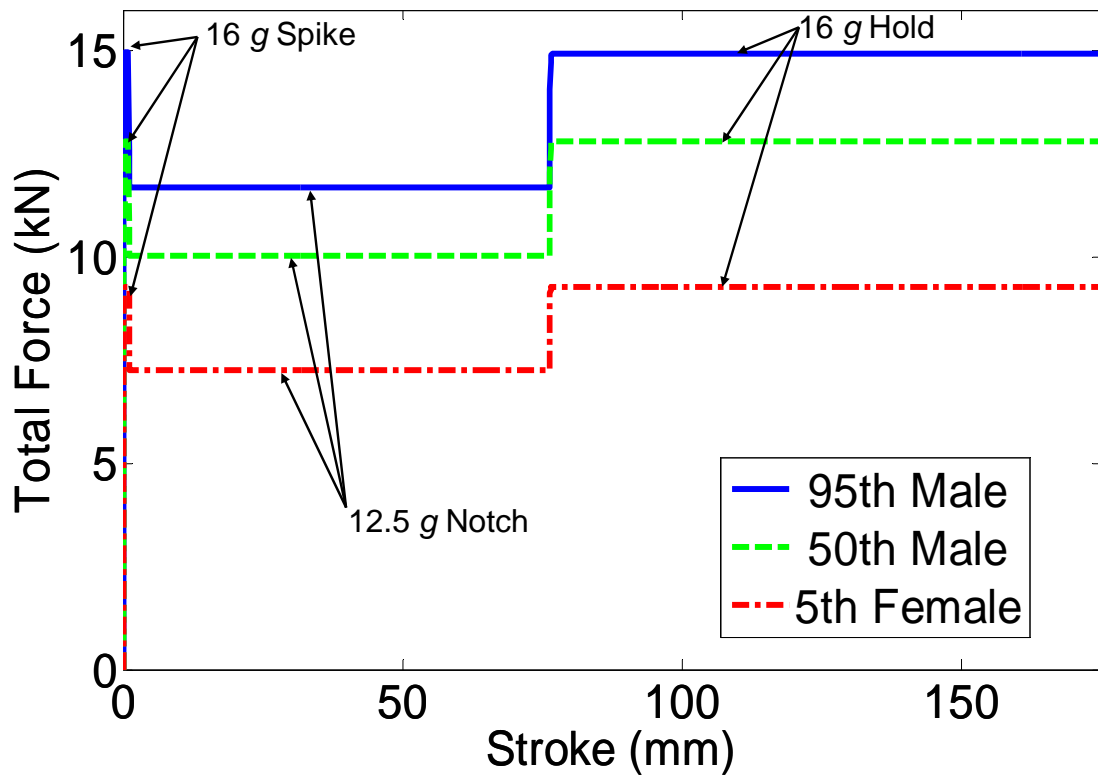


Figure 3.5: Notched Profiles for VPEA Control

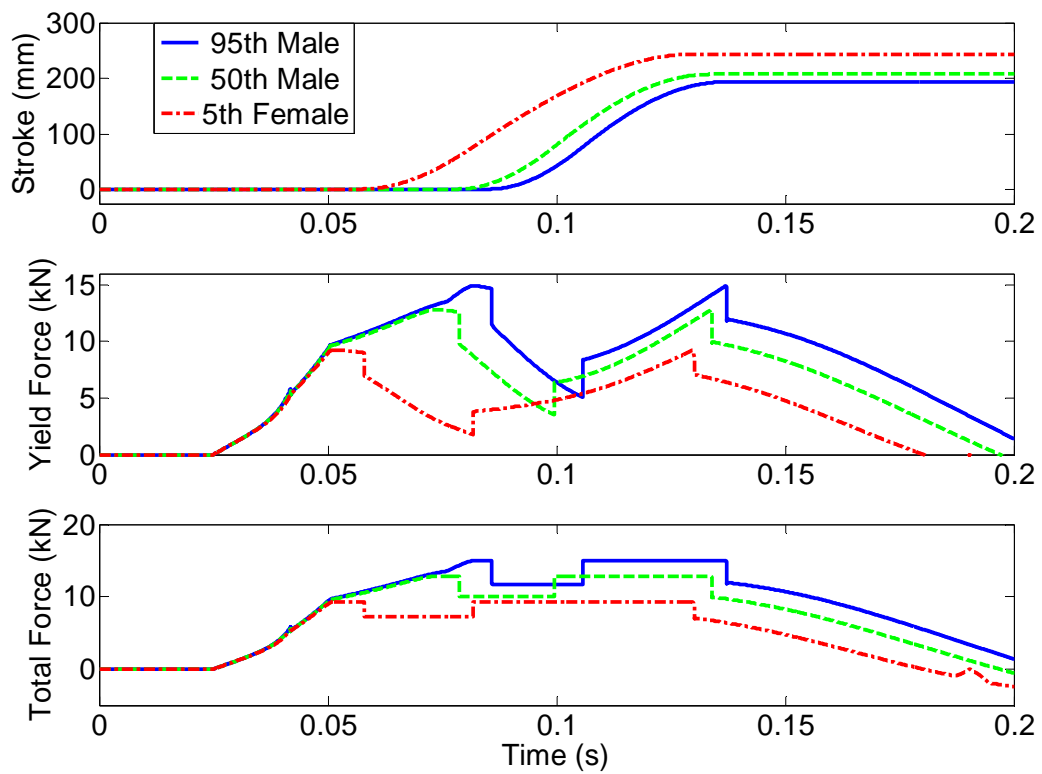


Figure 3.6: MREA Time Response for VPEA (Notched-Profile) Control

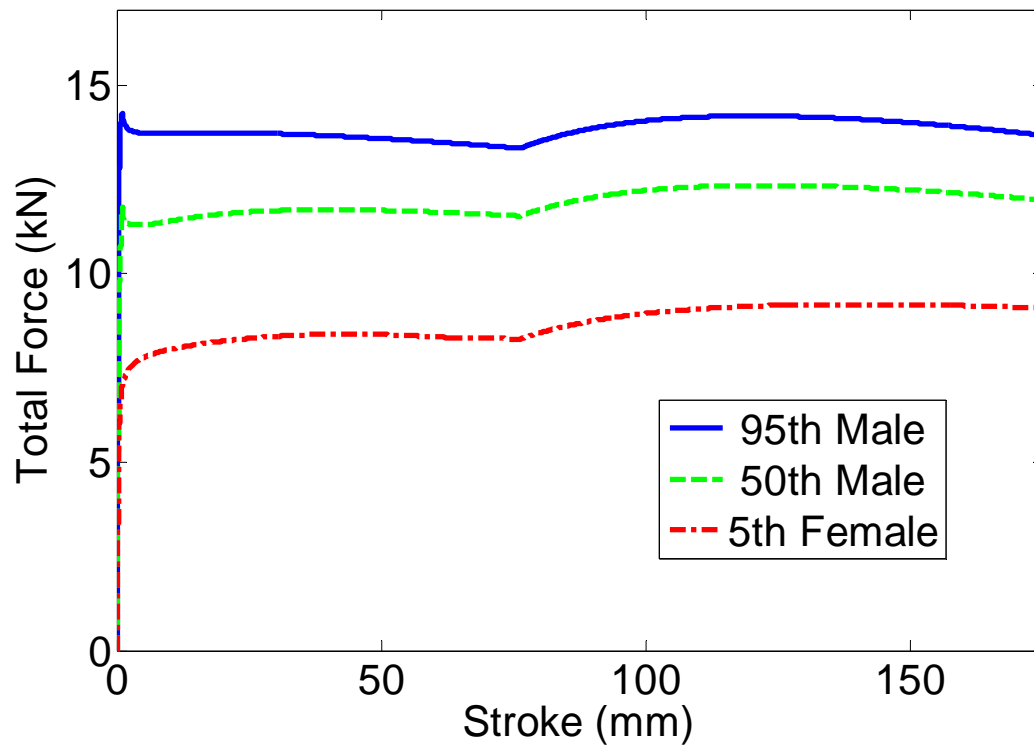


Figure 3.7: Effect of 10 ms Time Delay on Notched Load-Stroke Profile

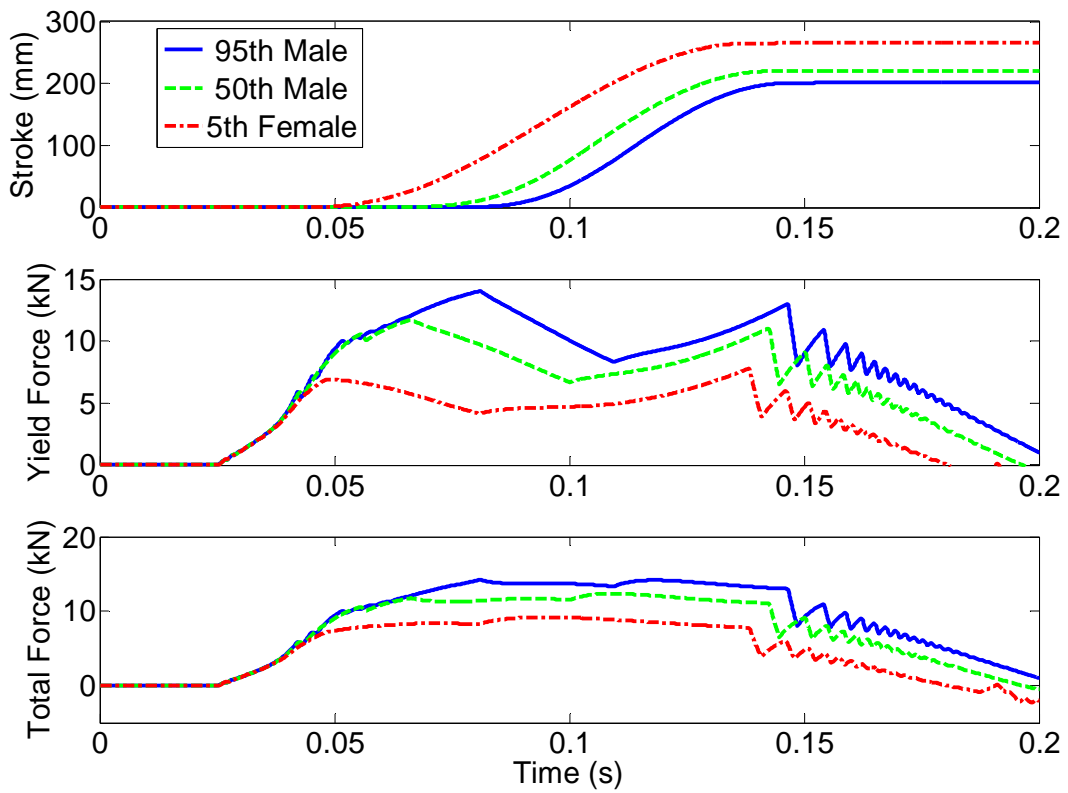


Figure 3.8: MREA Time Response for VPEA Control with 10 ms Time Delay

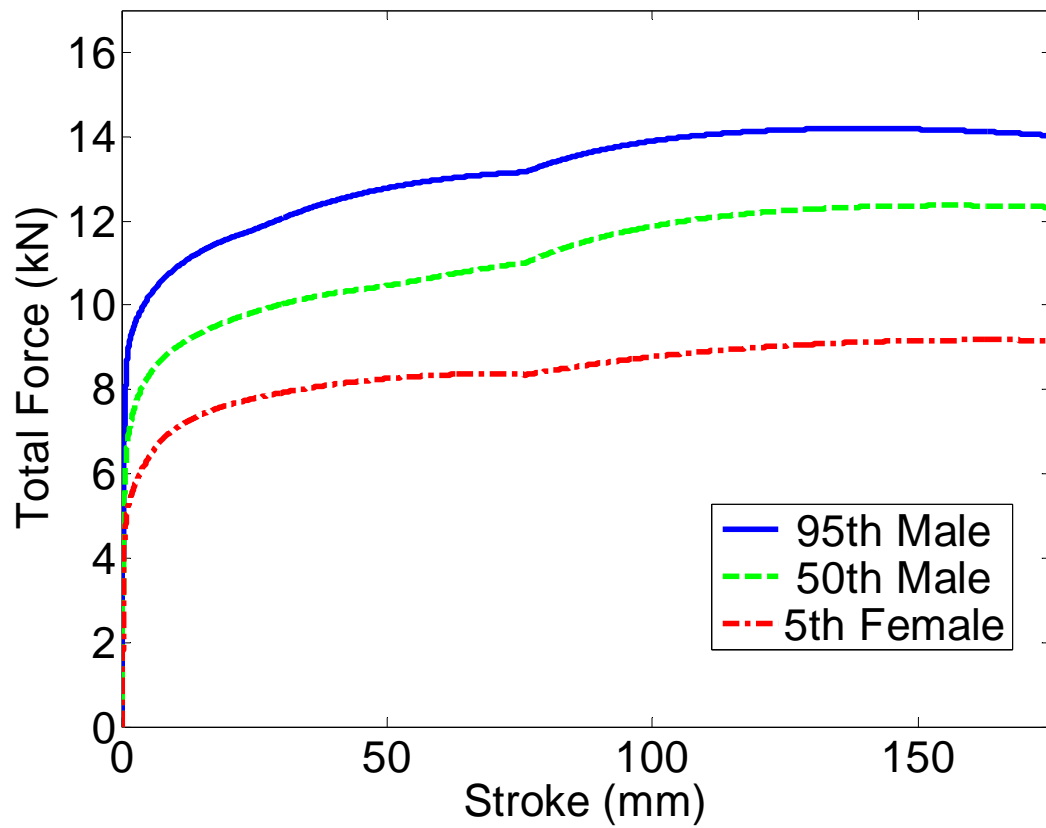


Figure 3.9: Effect of 20 ms Time Delay on Notched Load-Stroke Profile

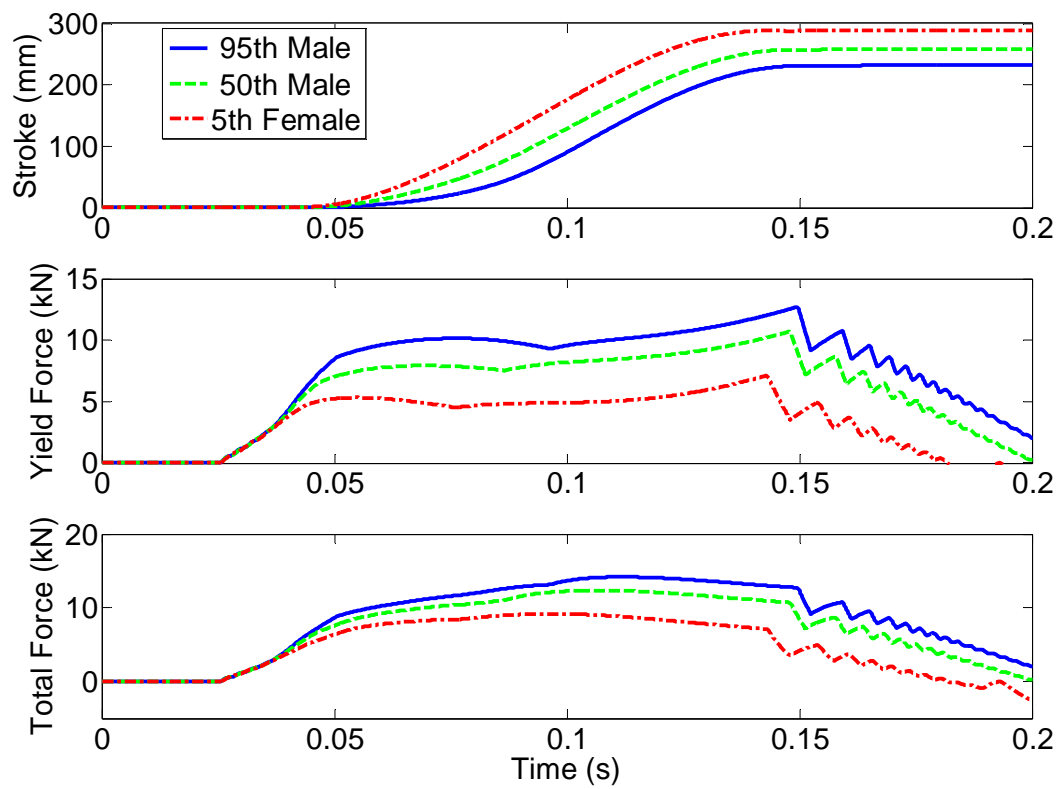


Figure 3.10: MREA Time Response for VPEA Control with 20 ms Time Delay

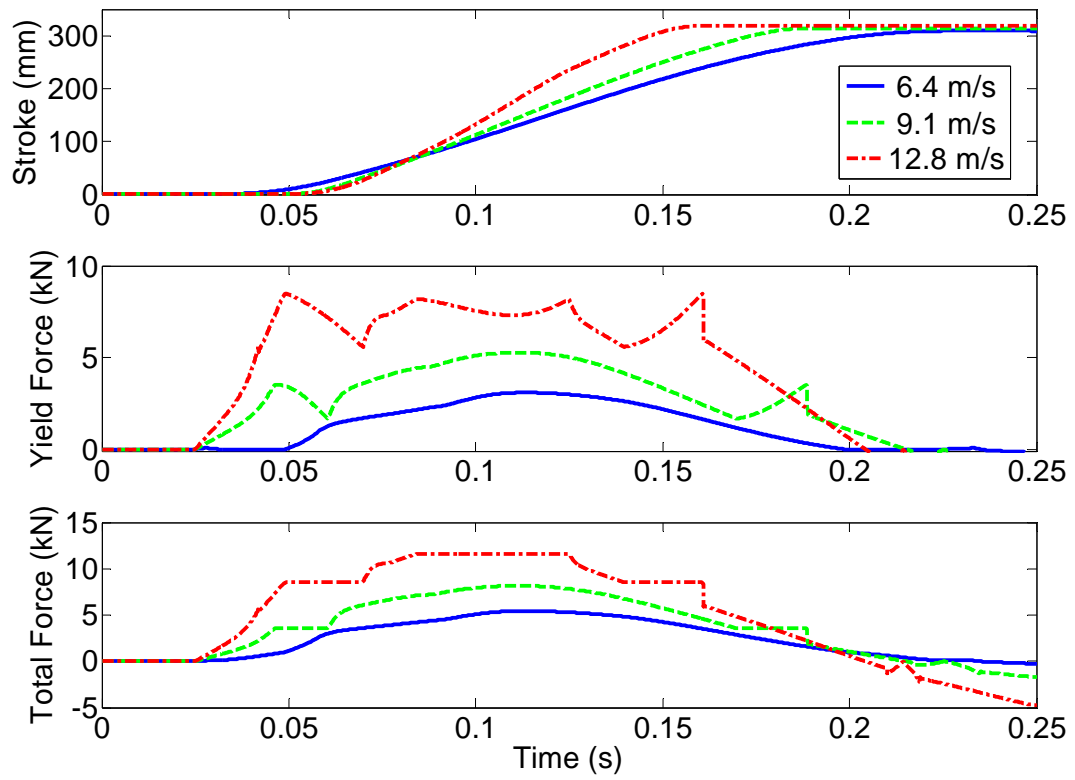


Figure 3.11: MREA Time Response for Crash Load Adaptive Control

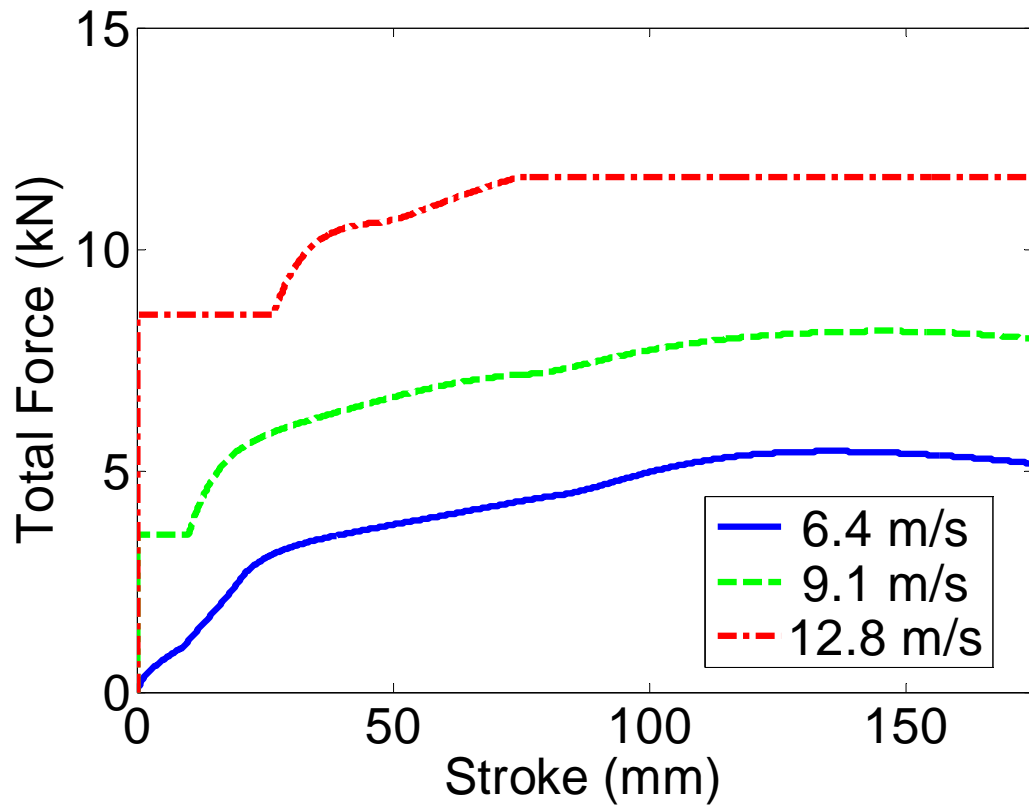


Figure 3.12: Load-Stroke Profile Resulting from Crash Load Adaptive Control

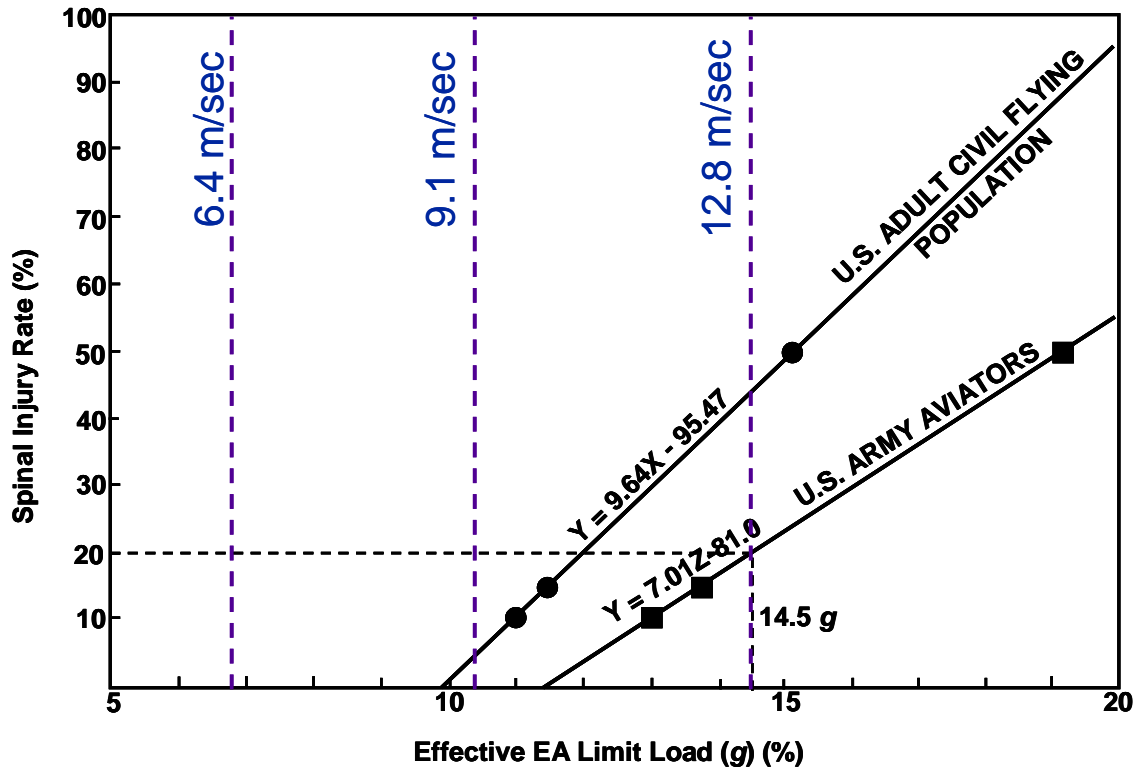


Figure 3.13: Correlation between EA Limit Load (g) and Spinal Injury Risk [4]

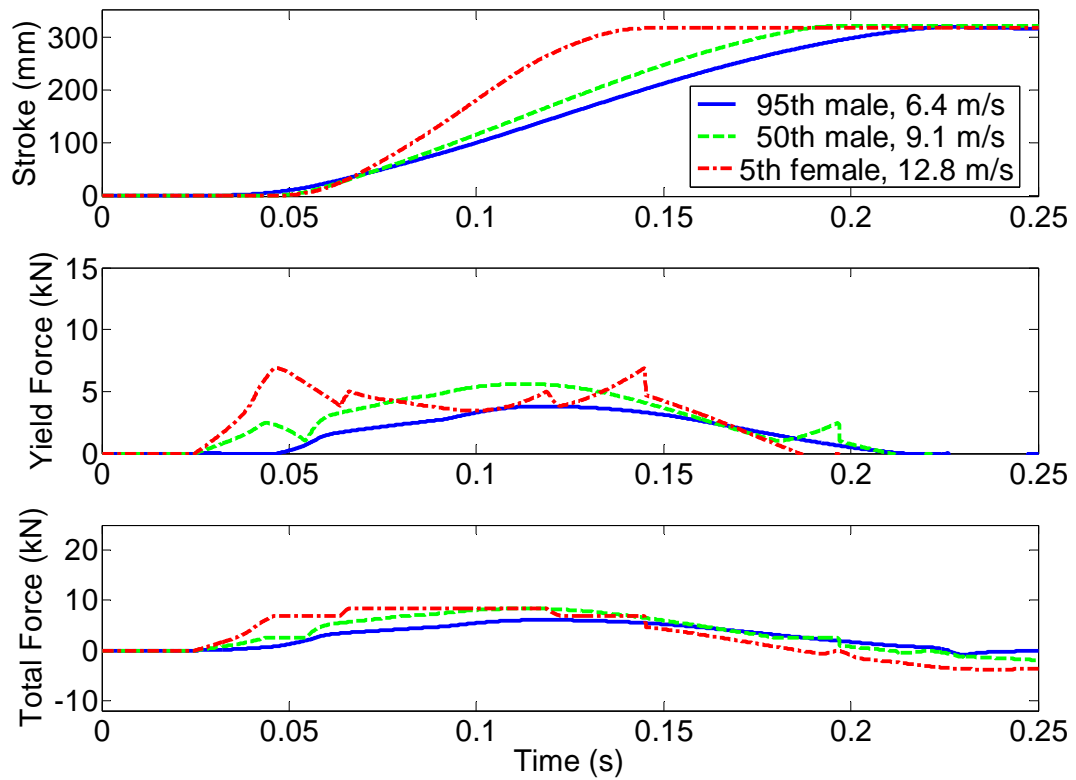


Figure 3.14: MREA Time Response for Crash Load Adaptive Control for Varying Occupant Weight and Crash Level

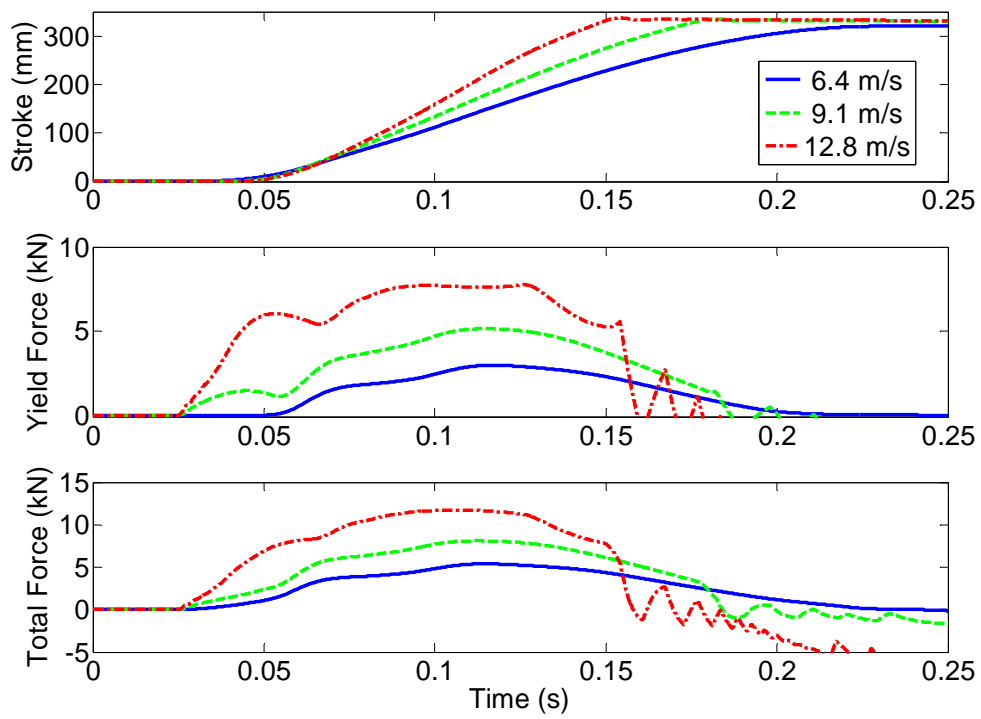


Figure 3.15: MREA Time Response for Crash Load Adaptive Control with a 10 ms Time Delay

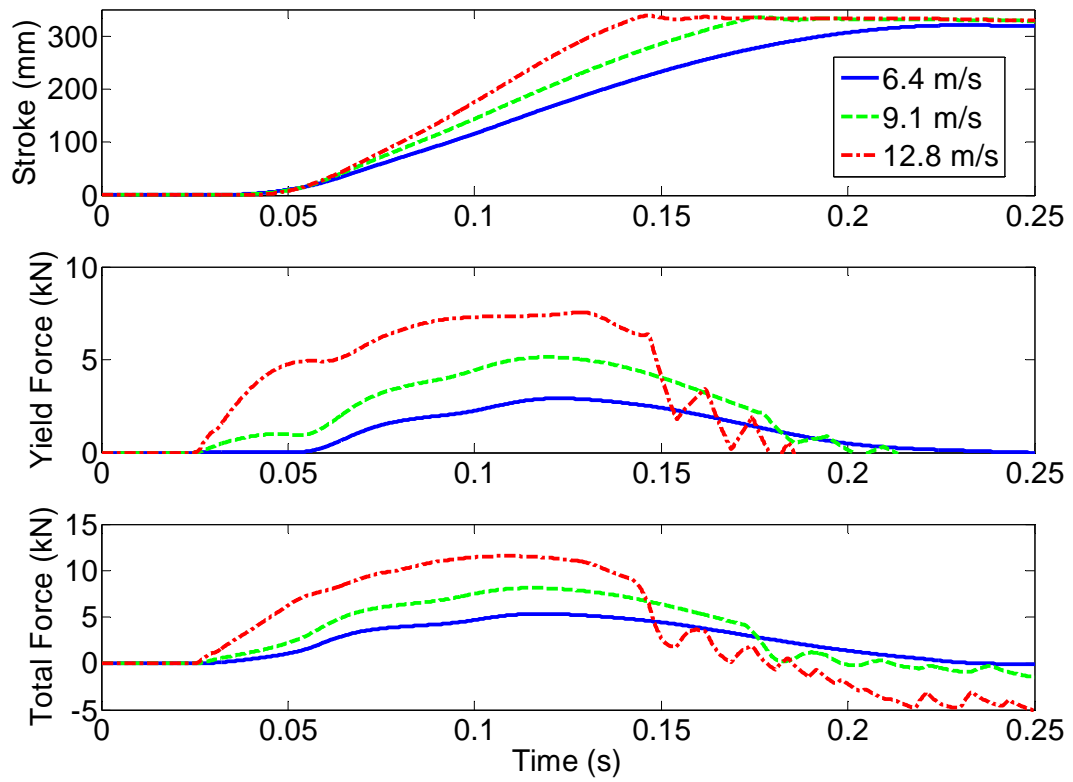


Figure 3.16: MREA Time Response for Crash Load Adaptive Control with a 20 ms Time Delay

## **Chapter 4:       Semi-Active Magnetorheological Helicopter Crew Seat Suspension for Vibration Isolation**

This chapter addresses the goal of isolating the occupant from harmful cockpit vibrations. It was shown in Chapter 2 that an MR damper designed solely for the purposes of vibration isolation can be integrated into the current crashworthy SH-60 crew seat with minimal weight impact. This option, therefore, was deemed the most practical for near-term implementation into the fleet. MR dampers were designed, fabricated, tested, characterized, and integrated into the unarmored SH-60 crew seat such that the original crashworthy capabilities were maintained. Then, utilizing semi-active control, experimental vibration testing were performed to evaluate the system performance in isolating cockpit vibrations.

### *4.1   Integration into the Unarmored SH-60 Seahawk Crew Seat*

In Section 2.2, MR dampers were optimally designed for the purposes of isolating cockpit vibration. While these MR dampers significantly reduce vibration, they are not capable of mitigating shock loads. These MR dampers, therefore, must be integrated into the crew seat in such a way that they do not interfere with the operation of the FLEAs. One method of doing this is to couple them in series with the existing inversion-tube FLEAs, as shown in Figure 4.1\*. In this configuration, the MR dampers are mounted within the two fixed vertical columns to which the seat rollers attach. The MR damper connects to the inversion tube energy absorbers via a

---

\*Patent Pending

spring and spring cap. The opposite ends of the FLEAs were then attached to the base of the stroking seat. This allows for the seat to stroke under normal operating vibratory conditions when the force levels are not high enough to stroke the FLEAs. At a tuned base input level (2 g), the spring cap bottoms out on the top of the fixed vertical column and the MR damper is taken out of the load path. This allows the inversion tube FLEAs to operate as originally designed when a crash/shock event occurs – with the FLEA load being transmitted directly to the fixed vertical columns. Finally, a crossbeam has been added which spans between the two spring caps. The purpose of this crossbeam is to react the lateral component of the loads transmitted through the FLEAs (and moments generated by them) against one another, thereby reducing friction in the system. This retrofit requires only minor modifications to the fixed vertical columns (remove old FLEA attachment points and add new MR damper mounting fixtures) and provides the ability to effectively isolate vibration while preserving crashworthy capabilities.

#### *4.2 MR Damper Characterization*

Prior to implementing semi-active control, the MR dampers had to be tested to verify their performance and characterize their dynamic parameters. Dynamic testing under steady-state sinusoidal loading was performed using an MTS 810 24.466kN (5000 lb) servo-hydraulic material testing machine. A displacement LVDT sensor was used for displacement measurement and a load cell measured the force. Fittings were designed to hold the damper securely in place. A DC power supply was used to provide current control during testing and was connected to the magnetic coil leads.

The normal range of the applied current was between 0A and 1.5A, and the maximum applied voltage was 10V DC.

The MR dampers were tested over a range of realistic frequencies (from quasi-static to 4/rev of rotor RPM) and amplitudes ranging from 2.5 mm to 10 mm (0.1 to 0.4 inches). At each of these 11 combinations of frequency and amplitude, the MR damper was energized with 0, 0.25, 0.5, 0.75, 1.0, and 1.5 Amps of applied current. All tests were performed at room temperature (25° C). Force vs. displacement data was recorded for each of these 66 cases. Figure 4.2 shows example raw force vs. displacement data taken in these tests for this MR damper design. From this data, the force vs. velocity curves were also generated. Sample force vs. velocity curves are shown in Figure 4.3.

The goal of MR damper characterization was to determine the parameters  $C_p$  and  $F_y$  of the Bingham plastic MR damper force model (Eq. 2.1) as a function of current applied to the magnetic coil. As an example, Figure 4.4 plots a fitted Bingham-plastic model against the results for 1 Hz, 5 mm amplitude excitation with the solid lines representing the Bingham-plastic approximation. It can be seen that the off-state MR damper yield force,  $F_y(0A)$ , is nonzero (36N) because of friction at the rod seal and piston ring. This Bingham-plastic force model approximation was made for each MR damper test case. The resulting yield forces and post-yield viscous damping were plotted in Figure 4.5 and Figure 4.6, respectively, against the current applied to the magnetic coil.

In these plots, the trends can be fitted with a cubic polynomial functions:

$$F_y = 65I^3 - 218I^2 + 269I + 36, \quad (4.1)$$

$$C_p = 0.37I^3 - 1.28I^2 + 1.59I + 0.45, \quad (4.2)$$

where  $I$  is the applied current (in Amps) and the  $C_o$  and  $F_y$  are in units of N-s/mm and N, respectively. By solving these cubic functions, a semi-active controller can calculate the amount of current that needs to be applied for a given desired force and measured piston velocity. The solid lines in Figure 4.3 show this model plotted against the test data. In these plots, the signum function in the Bingham plastic force model (Eq. 2.1) is approximated using a hyperbolic tangent function as shown in Eq. (4.3) to give a smooth transition through the yield region at low speed. As shown in Figure 4.3, the MR damper yield force and post-yield damping are well represented using this model.

$$F_{MR} = C_p v + F_y \tanh\left(\frac{v}{0.1}\right) \quad (4.3)$$

#### 4.3 Semi-Active Control

In 1974, Karnopp *et al.* introduced a simple, yet effective vibration isolation strategy that is realized by connecting a fictitious damper between the sprung mass and the stationary sky [22]. In this control scheme, known as skyhook control, the damper exerts a force tending to reduce the *absolute* velocity of the sprung mass. This differs from conventional dampers, which exert forces that tend to reduce the *relative* velocity between the sprung mass and the base. While conventional dampers reduce the resonant response, it is at the cost of increased high frequency response. This is because, at high frequency inputs, they tend to stiffen the suspension when a soft suspension is desired. The skyhook algorithm, however, effectively achieves a combination of resonance damping and high frequency isolation [22]. For an MR

damper installed in place of a conventional damper, this control strategy essentially turns the damper on to the desired force (linearly proportional to sprung mass absolute velocity) when it is the same sign as relative velocity and turns the damper off when they are opposite, ensuring that the force is always dissipative:

$$F_{sky} = \begin{cases} C_{sky} v_s, & \text{if } v_s \cdot v \geq 0 \\ 0 & \text{if } v_s \cdot v < 0 \end{cases} \quad (4.4)$$

For this study, the skyhook control gain,  $C_{sky}$ , was determined by assuming critical equivalent viscous damping at resonance:

$$C_{sky} = 2\zeta_{sky}\omega_n M, \quad (4.5)$$

where  $\zeta_{sky} = 1.0$ .

Using a simple SDOF simulation, the semi-active control performance for the MR suspension can be predicted. Figure 4.7 shows the simulated SDOF frequency response for the three cases: 1) unenergized MR dampers (Field off), 2) constant maximum energized MR dampers (Constant Field), and 3) skyhook control. This particular case is for the 50<sup>th</sup> percentile male aviator (77.5 kg) and the suspension properties described above. In this simulation, the off-state viscous damping ratio, friction force, and maximum yield force determined from the MR damper testing are utilized. It can be seen that in the Field off case, there is a high resonant peak around 4.5 Hz. In the constant field case, this resonance is well damped, but the high frequency isolation is very poor. The skyhook control case, however, combines resonance damping with desirable high frequency isolation performance. This simulation estimates that the MR suspension with skyhook control will reduce the

floor vibrations transmitted to the seat by 77% and 91% for the 4P (blade passing) and 8P (2<sup>nd</sup> blade passing harmonic) frequencies, respectively.

#### 4.4 *Experimental Setup*

The retrofitted SH-60 crew seat was installed into the Vertical Axis Shock and Vibration Test Stand at the University of Maryland Smart Structures Laboratory (Figure 4.8). This test facility has provisions for simulating up to 6.4 m/s sink rate (21 ft/s) crashes as well as floor vibration via a MTS model 242 portable hydraulic actuator. Tri-axial accelerometers were mounted to the base of the trolley to record input motion as well as on the seat pan and seat back to record resulting seat motion as shown in Figure 4.9. This crew seat design is known to be prone to vertically-induced longitudinal rocking because of the offset,  $d$ , between the center of gravity (CG) of the stroking seat and where it attaches to the fixed vertical columns as shown in Figure 4.9. The experimental accelerometer placement allows for measurement of both pure vertical vibrations as well as this rocking motion of the seat. These accelerometers were connected to both a dSpace Rapid Prototyping System (for control) and Siglab Data Acquisition System (to collect frequency response data) via the accelerometer signal conditioner. The seat trolley was vibrated using the MTS model 242 portable hydraulic actuator. This hydraulic actuator was controlled using the Siglab system to provide a sinusoidal base excitation with constant input acceleration amplitude of 0.2 g while sweeping from 2 to 20 Hz.

A Matlab Simulink control diagram which implemented the aforementioned skyhook control algorithm was uploaded to the dSpace system. Accelerometer signals were then fed to the accelerometer signal conditioner and then into the dSpace

controller. The dSpace controller then determined the desired electric current to be applied to the MR dampers (based upon the control algorithm, measured accelerometer signals, and the MR damper model) and then supplied this control current to the MR dampers via a current amplifier.

The tests used “dead weight” in the seat. A combination of steel and/or sand bag weights were attached to the seat to simulate the *effective* mass for 5<sup>th</sup> percentile female (46.7 kg), 50<sup>th</sup> percentile male (68.5 kg), and 95<sup>th</sup> percentile male (83.0 kg) occupants with equipment (13.6 kg) [1]. Four sine sweep tests were performed for each of these three occupant weights: 1) unmodified SH-60 crew seat 2) field off (no magnetic field applied to MR damper), 3) Constant 0.5 A (damper on, but uncontrolled with a constant magnetic field of 0.5A), and 4) skyhook control. In addition to varying occupant weight, two additional sets of sine sweeps were performed for the 50<sup>th</sup> percentile male to examine the sensitivity of the cushion and of higher (0.4 g) input acceleration, respectively. For each of these tests, acceleration data from the seat and base were recorded for generation of transmissibility plots (frequency response) in the below section.

#### 4.5 Experimental Results and Discussion

Figure 4.10 shows the rear seat pan transmissibility data measured from the Siglab data acquisition system for the 50<sup>th</sup> percentile male and without the use of a soft cushion. It can be seen in this plot that, for the unmodified seat, there was a large resonance seen between 6 Hz and 11 Hz. Figure 4.11 and Figure 4.12, however, show that this was actually the result of two separate rocking modes. Besides observations during the test, this was evidenced by the fact that there is coupling

between the seat top longitudinal acceleration and the base (Figure 4.11). This coupling is due to the fact that the occupant CG is forward of the fixed vertical columns, to which the seat is mounted (Figure 4.9), and thus creates a moment under vertical base excitation. The levels of these two rocking modes and visual observations during the test suggest that the first of these two rocking modes (at 6 Hz) is a rigid body mode due to the large clearances between the seat rollers and the columns. The second rocking mode, however, was due to the seat pan bending down away from the seat back – which explains why the front seat pan vertical transmissibility (Figure 4.12) was very high at the second rocking modal frequency.

Next, the effects of installing the suspension system were examined. Starting with the un-energized (Field Off) system, it can be seen in Figure 4.11 that the spring and damper added the tuned resonance around 4 Hz. While this increases the transmissibility at the rotor RPM (1P), the rocking modes and the blade passage frequency (4P), where the majority of the rotor-induced vibration and associated discomfort occurs, were significantly reduced. The fact that the rocking modes were also reduced is further evidenced in Figure 4.10 and Figure 4.12. The rocking modes were reduced because the vertical transmissibility is reduced – thus reducing the moment due to the CG offset discussed above.

The effect of activating the SAMSS system was then examined. At a constant applied current of 0.5A, the tuned passive resonance was nearly completely eliminated and the rocking modes were again observed (albeit to a slightly lesser magnitude). This is because the high MR constant damper force tends to lock up the damper – causing it to behave similarly to the unmodified seat.

Finally, it can be seen in these plots that when the semi-active (skyhook) control was implemented, the resonance was significantly reduced while maintaining the desirable high frequency isolation performance of the Field Off system. Figure 4.11 shows that the controlled SAMSS system reduces the 4P vertical vibration transmitted to the occupant by 77%, which is 61% better than the original seat. It should be noted that the 77% reduction of the vertical 4P floor vibration matches the predictions made in Section 4.3. This shows that, while the SDOF system does not capture the complex rocking dynamics of the seat, it can give a very good estimate of vertical attenuation and is useful for system design. Additionally, Figure 4.10 and Figure 4.12 show seat top longitudinal and front seat pan vertical transmissibilities at the second rocking mode are reduced by 85% and 80%, respectively. These reductions come at a slight sacrifice to transmissibility at the 1P frequency (8% increase) which is acceptable because these frequencies are rarely experienced during typical helicopter vibration (only if there is a very significant blade imbalance).

Figure 4.13 shows example time history data taken while the controlled system was near its fundamental vertical resonance. The top plot in this figure shows the absolute seat velocity measured versus the relative velocity measured between the seat and the floor. The middle plot in this figure shows how the skyhook control force is proportional to the absolute velocity, except for when it is set to zero because it is the opposite sign of the relative velocity (per Eq. 4.4). The bottom plot in Figure 4.13 shows the electric current applied to the MR dampers which is calculated by the controller by combining Eqs. (1), (5), and (6), and solving for electric current,  $I$ , given the desired control force,  $F_{sky}$ , and relative (piston) velocity,  $v$ .

The effect of varying occupant weight was also considered. Figure 4.14 shows the rear seat pan vertical transmissibility for the 5<sup>th</sup> percentile female and a 0.2 g amplitude floor excitation. In this plot, not only have the resonant frequencies increased due to the lowered mass, but the tuned vertical resonance for the unenergized system is less pronounced. Additionally, the performance of the controlled system at the 4P frequency has worsened (71% attenuation of floor vibrations, 45% improvement over unmodified seat). These effects are likely due to the friction in the system that is not as easily overcome by the reduced inertial forces induced by the lighter occupant. Conversely, for a 95<sup>th</sup> percentile male occupant (Figure 4.15), the tuned vertical resonance for the unenergized system is slightly more pronounced, and the performance of the controlled system at the 4P frequency has improved (78% attenuation of floor vibrations, 69% improvement over unmodified seat). This is again typical of friction in the system which is more easily overcome by the higher inertial force induced by the heavier occupant. As a final verification that friction was affecting system performance, the 50<sup>th</sup> percentile male occupant condition was tested at 0.4 g amplitude floor excitation. These results (Figure 4.16) show much more pronounced tuned vertical resonance for the unenergized system and improved performance of the controlled system at the 4P frequency (85% attenuation of floor vibrations, 71% improvement over unmodified seat). In this case, the additional inertial force provided by the increased excitation allows the friction to be more easily overcome, which improves performance.

Finally, the effect of the soft seat cushion was evaluated. The test results utilizing a soft seat cushion under a 50<sup>th</sup> percentile occupant mass for a 0.2 g

amplitude floor excitation are shown in Figure 4.17. Firstly, it can be seen that the rocking modes are much less significant – even for the unmodified seat. This is because the isolation provided by the seat cushion reduces the moment due to the CG offset and thereby reduces the amount of bending in the seat pan. The addition of the MR suspension, however, still provides an additional reduction in these rocking modes. Additionally, the controlled system performance at the 4P frequency is maintained – 76% attenuation of floor vibrations, which is a 70% improvement over the unmodified seat in this same condition.

Table 4.1 summarizes the key response reductions as compared to the unmodified SH-60 Seahawk crew seat. In general, it is shown that the vertical vibration isolation performance at the 4P increases with occupant weight and input excitation levels. As explained above, this is likely due to friction in the system which is more easily overcome by a heavier occupant. The inclusion of a soft seat cushion also shows improved isolation of vertical 4P vibrations, but the reduction in the rocking modes are less significant. As explained above, this is because the soft seat cushion provides some natural isolation to these rocking modes and the benefit of the suspension is less pronounced.

#### 4.6 *Summary and Conclusions*

This chapter has explored the use of magnetorheological (MR) dampers in a semi-active seat suspension system for helicopter crew seats to enhance occupant comfort and reduce health issues resulting from whole body vibration. MR dampers were designed, fabricated, and retrofitted into a tactical SH-60 Seahawk crew seat. This MR damper was implemented in series with the existing fixed load energy

absorbers (FLEAs) such that the crashworthiness capability of the seat was not impaired. A skyhook control algorithm was utilized and performance was evaluated both analytically and experimentally. Experimental test results have shown that this system reduced the dominant rotor-induced vertical vibration (4 per rev) transmitted to a 50<sup>th</sup> percentile male aviator by 76%, which is a 61-70% improvement over the unmodified SH-60 crew seat, depending upon whether a soft seat cushion is utilized. Furthermore, these experimental tests also show that this system significantly reduces vertically-induced seat rocking that occurs as a result of an offset center of gravity in the crew seat design. In this chapter it was also shown that, while the dynamics of a tactical vehicle seat may be complex, a SDOF model can be a valuable tool for MR damper design and performance predictions.

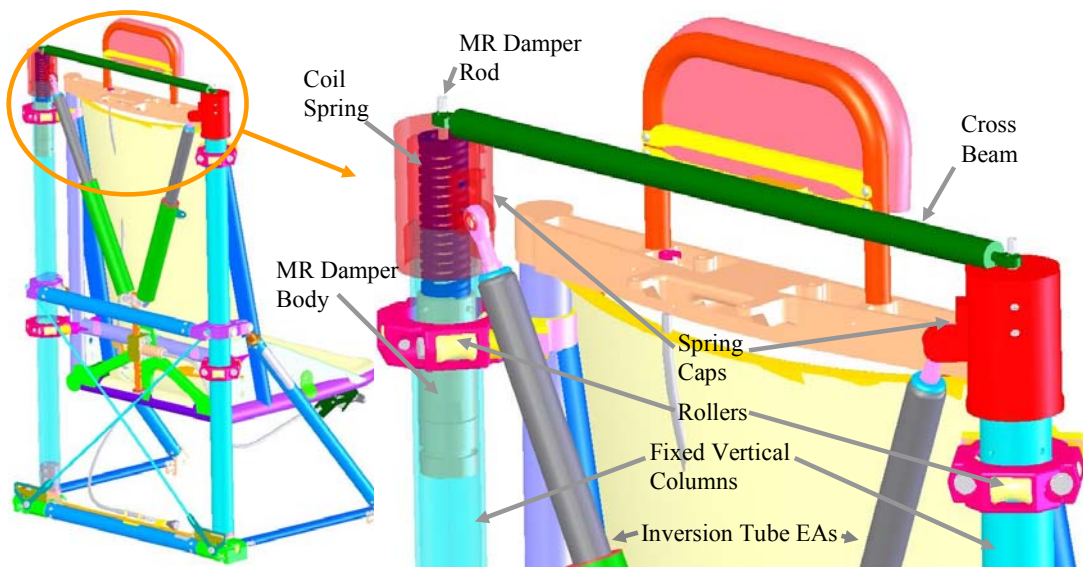


Figure 4.1: MR Dampers Retrofitted into SH-60 Crew Seat in Series with Inversion  
 Tube FLEAs\*

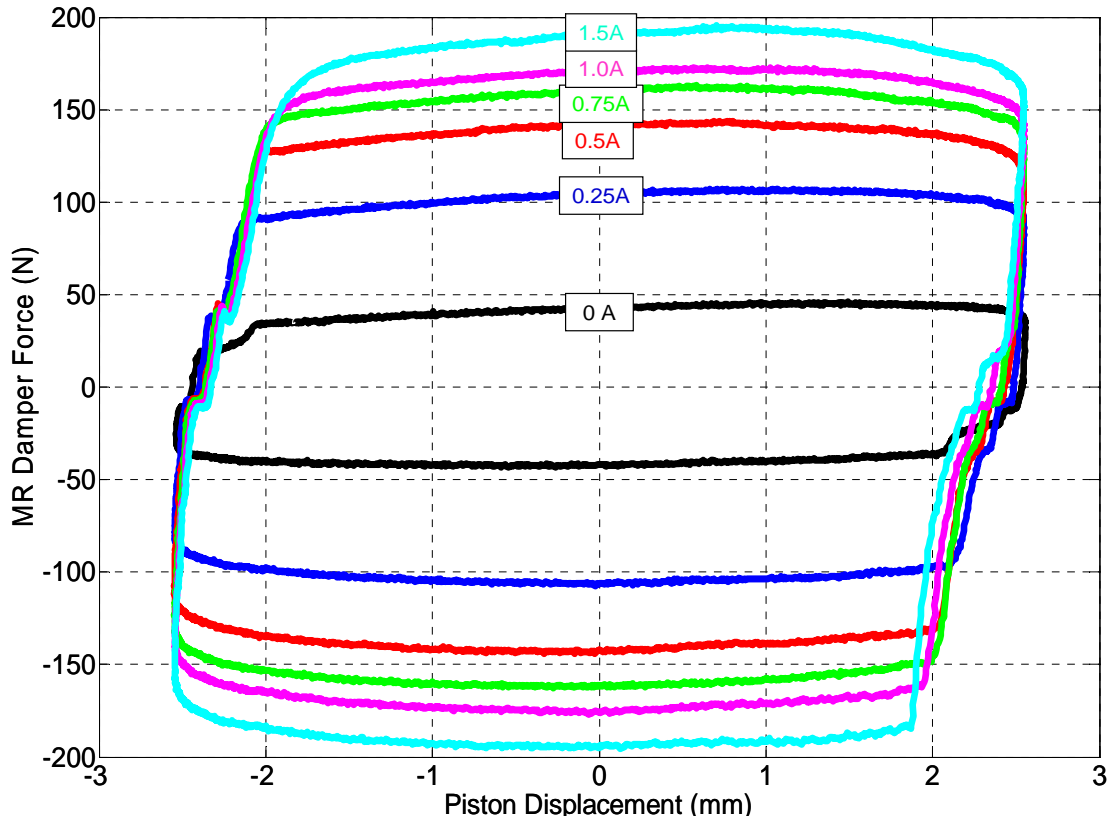


Figure 4.2: Raw Force vs. Displacement Data for 1 Hz, 2.5 mm Amplitude Excitation

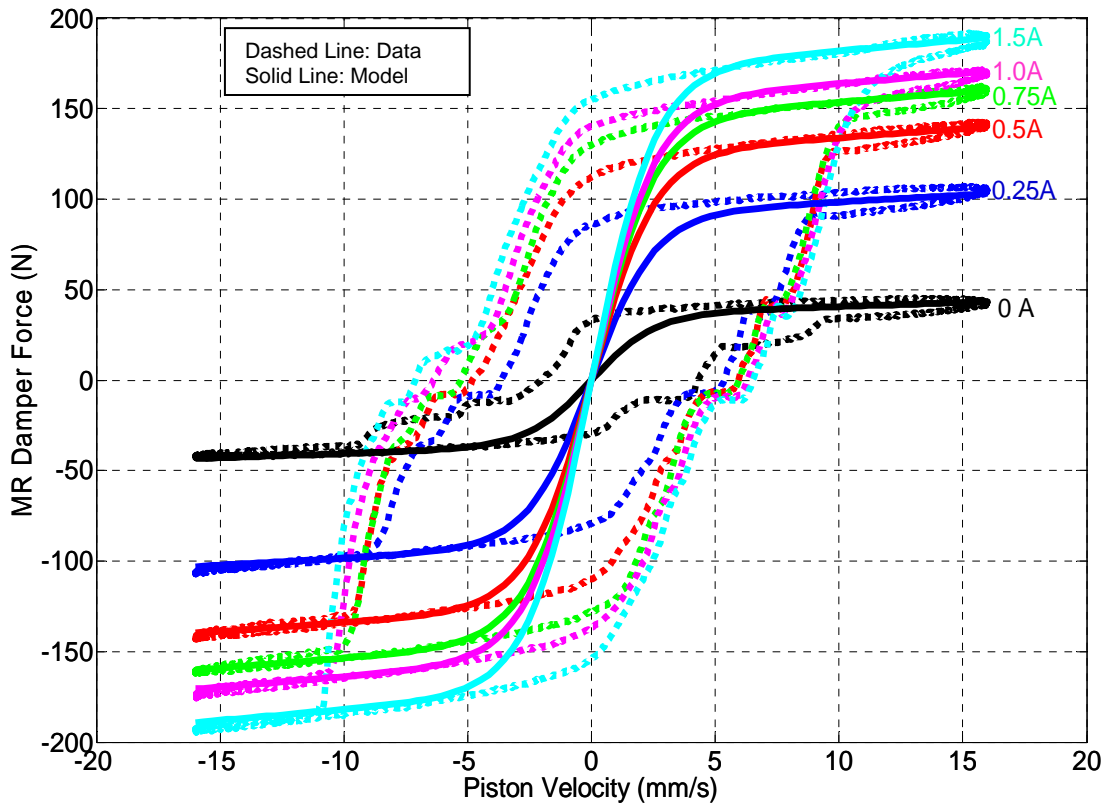


Figure 4.3: Force vs. Piston Velocity Data for 1 Hz, 2.5 mm Amplitude Excitation

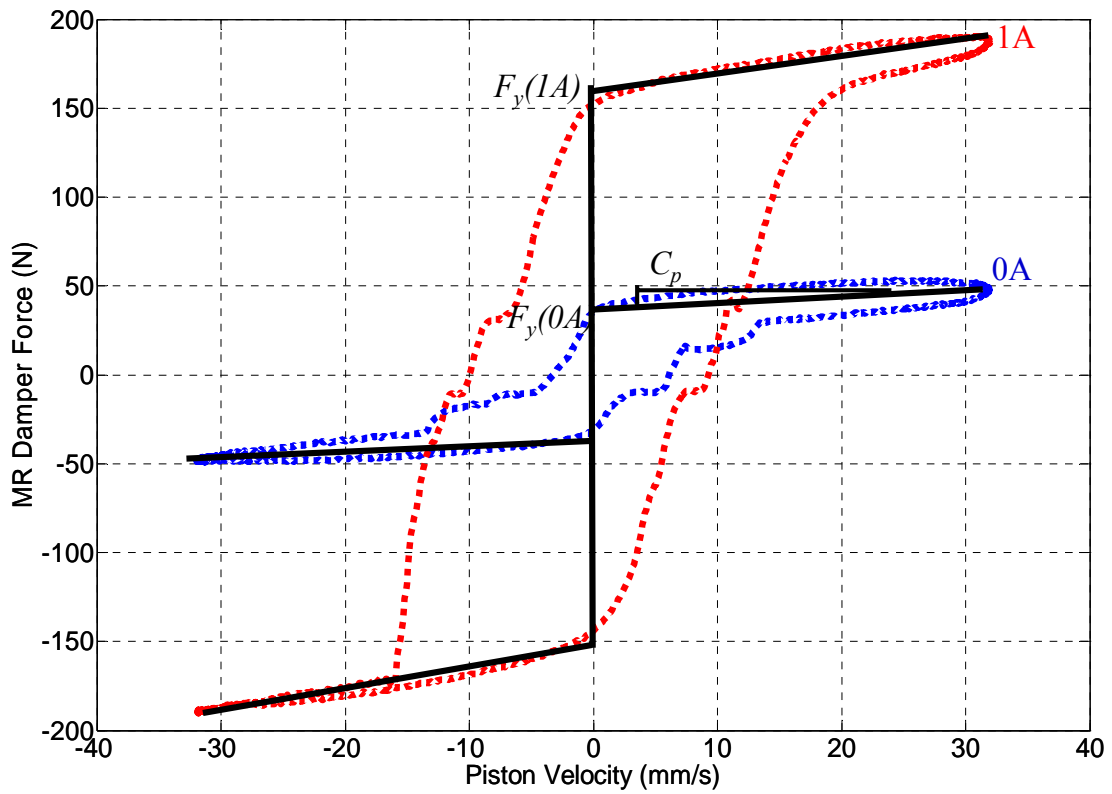


Figure 4.4: Fitting Bingham Plastic Model to MR Damper Results for 1 Hz, 5 mm Amplitude Excitation

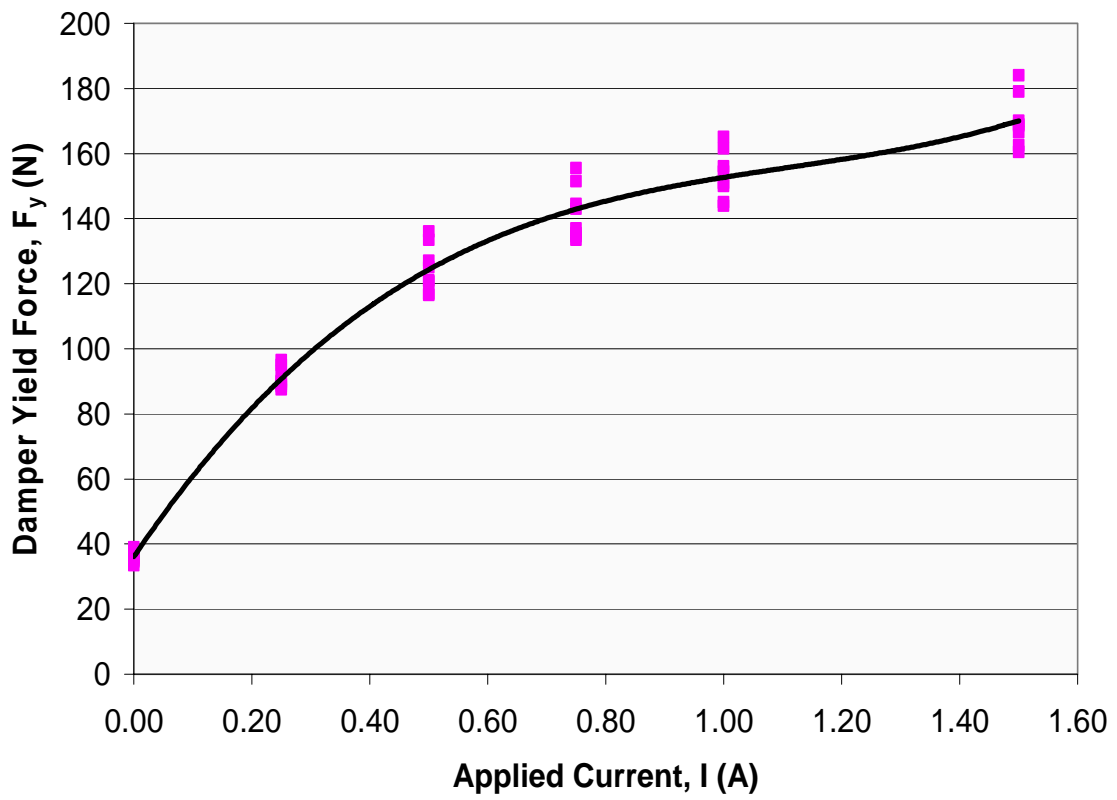


Figure 4.5: Fitting Cubic Function to Yield Force,  $F_y$ , vs. Applied Current

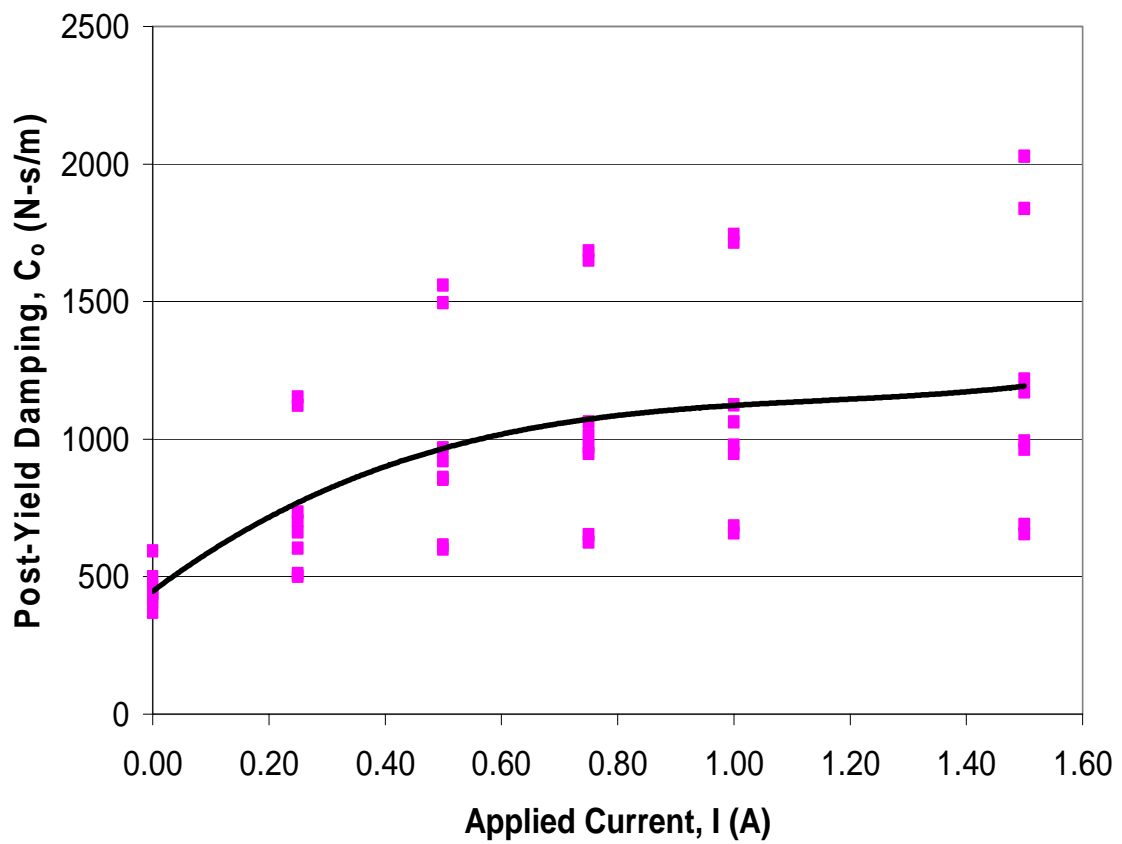


Figure 4.6: Fitting a Cubic Function to Post-yield Damping,  $C_p$ , vs. Applied Current

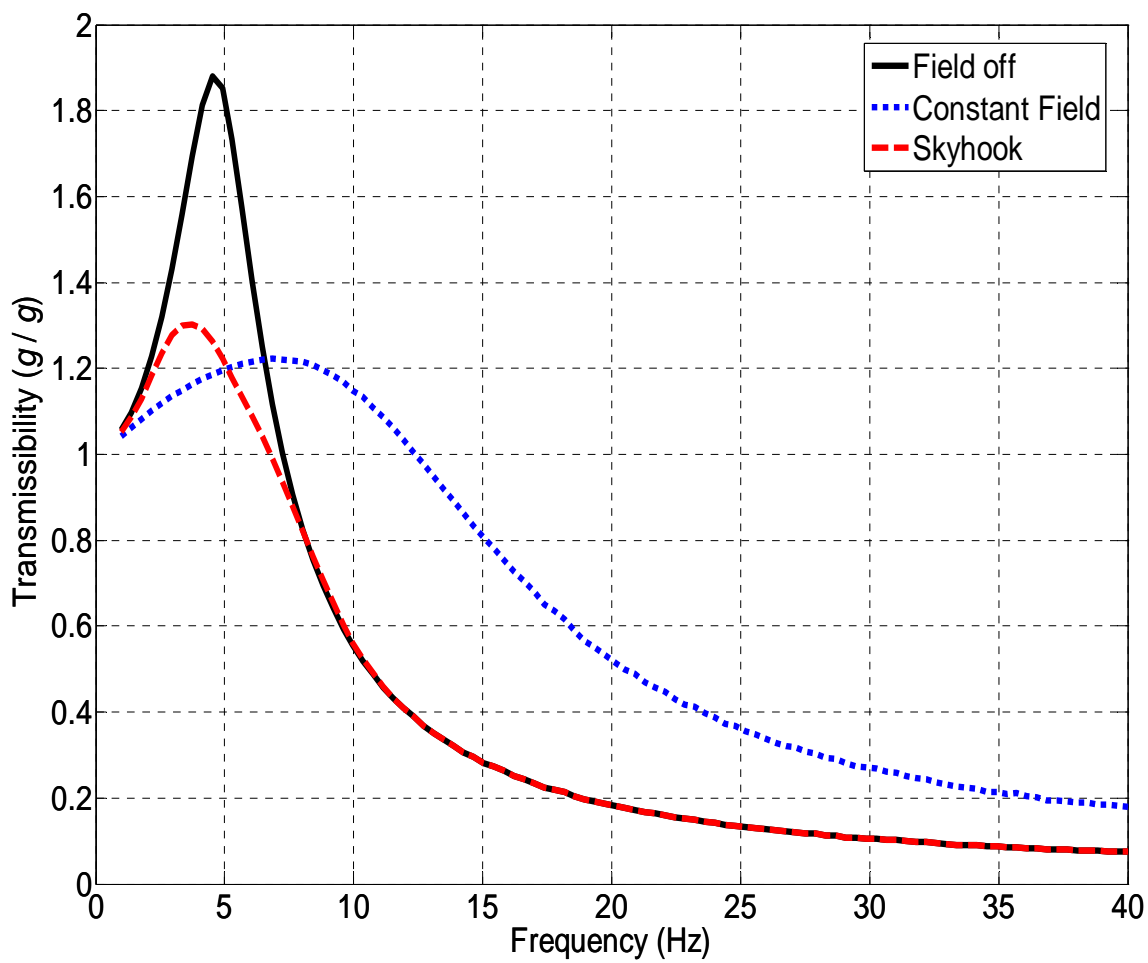


Figure 4.7: SDOF skyhook Control Performance Prediction for 50<sup>th</sup> Percentile Male  
Crew Seat Occupant

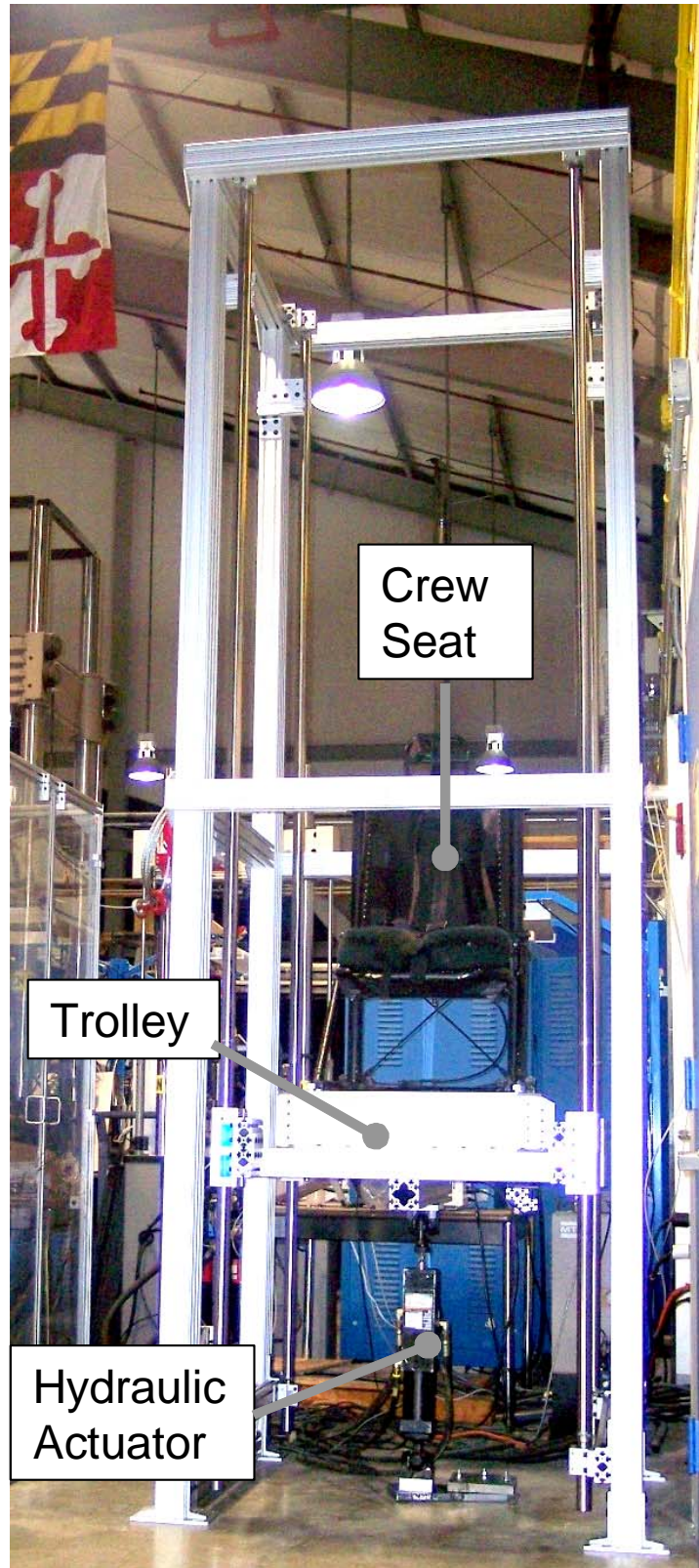


Figure 4.8: Crew Seat Installed in Vertical Axis Shock and Vibration Test Stand

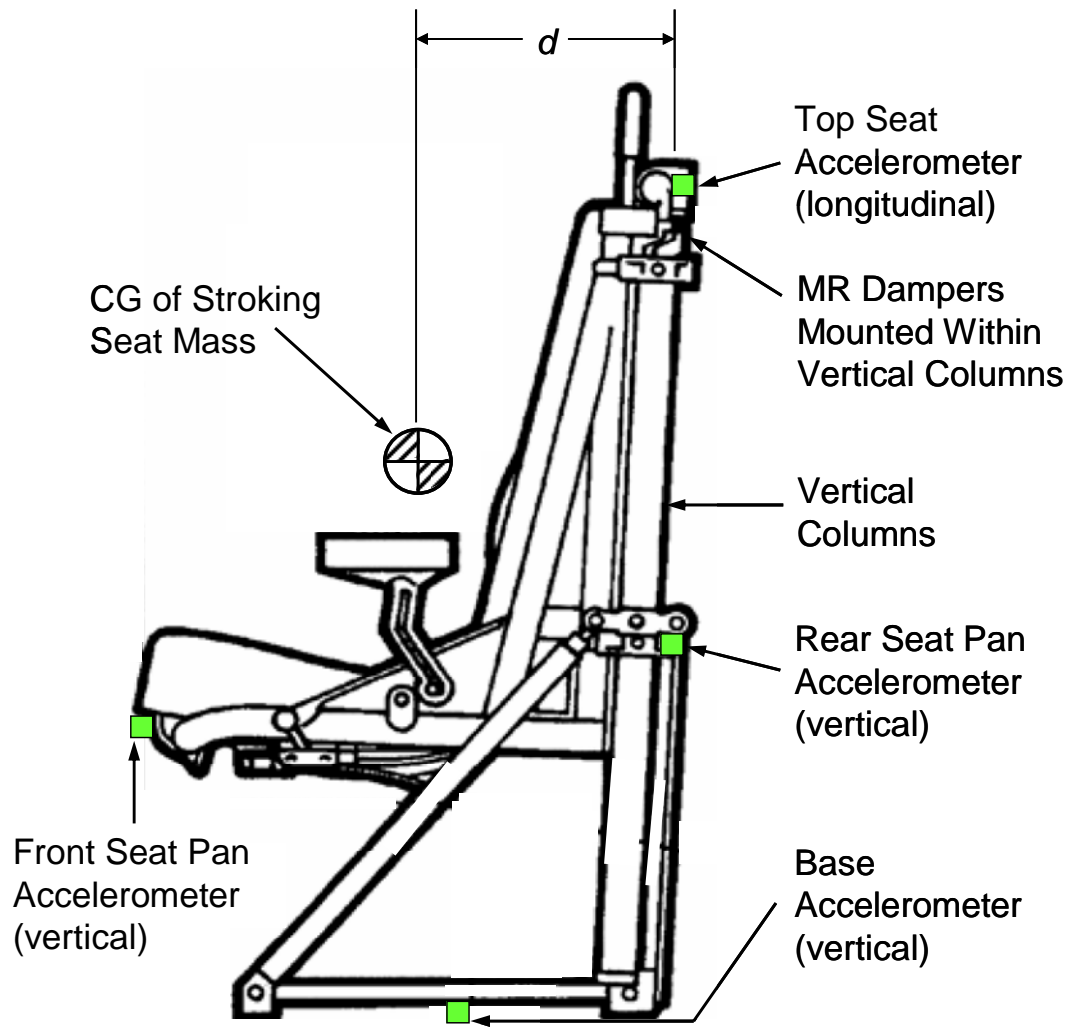


Figure 4.9: Accelerometer Placement on Seat

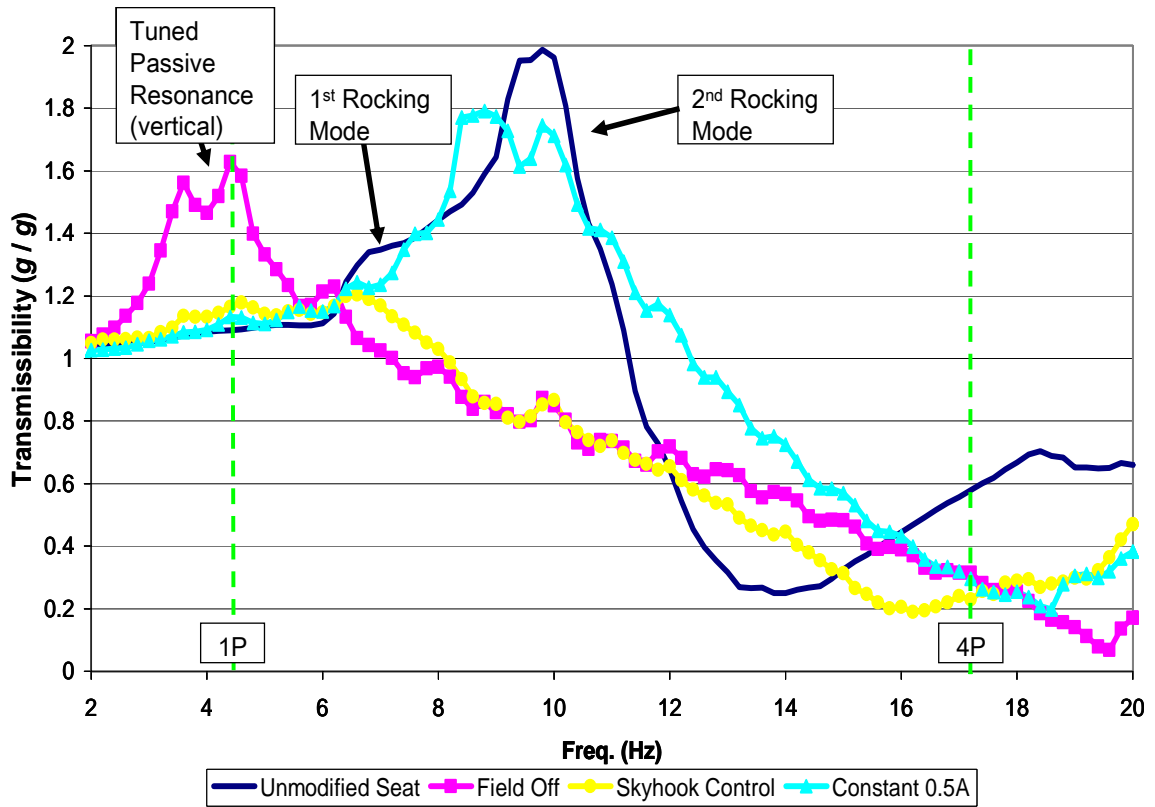


Figure 4.10: Rear Seat Pan Vertical Transmissibility for 50th Percentile Male, 0.2 g Excitation

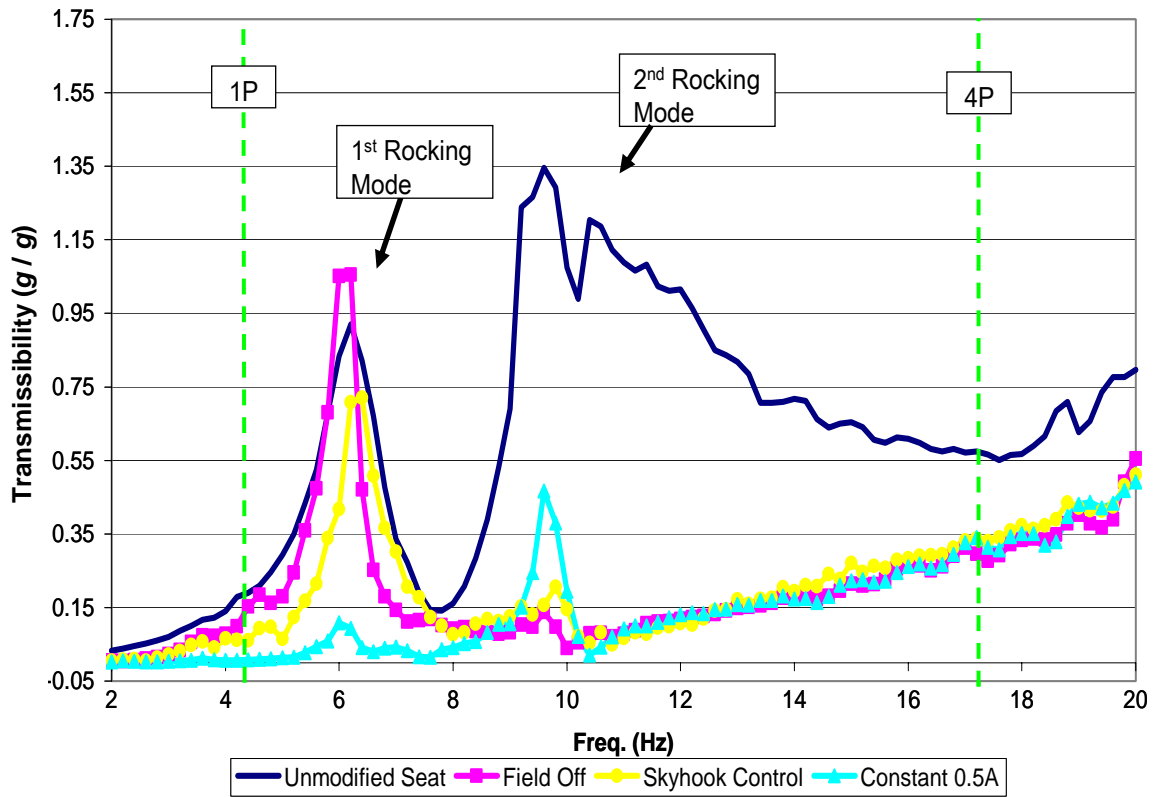


Figure 4.11: Seat Top Longitudinal Coupling Transmissibility for 50th Percentile

Male, 0.2 g Excitation

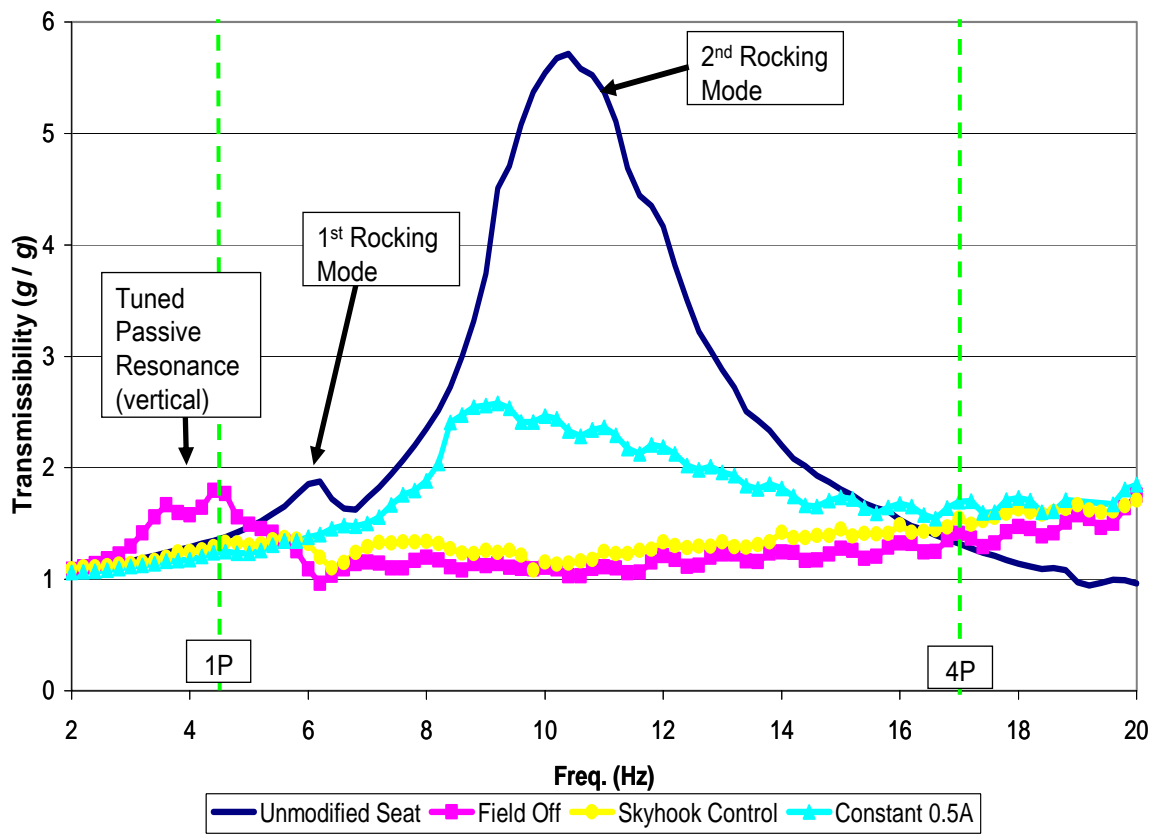


Figure 4.12: Front Seat Pan Vertical Transmissibility for 50<sup>th</sup> Percentile Male, 0.2 g Excitation

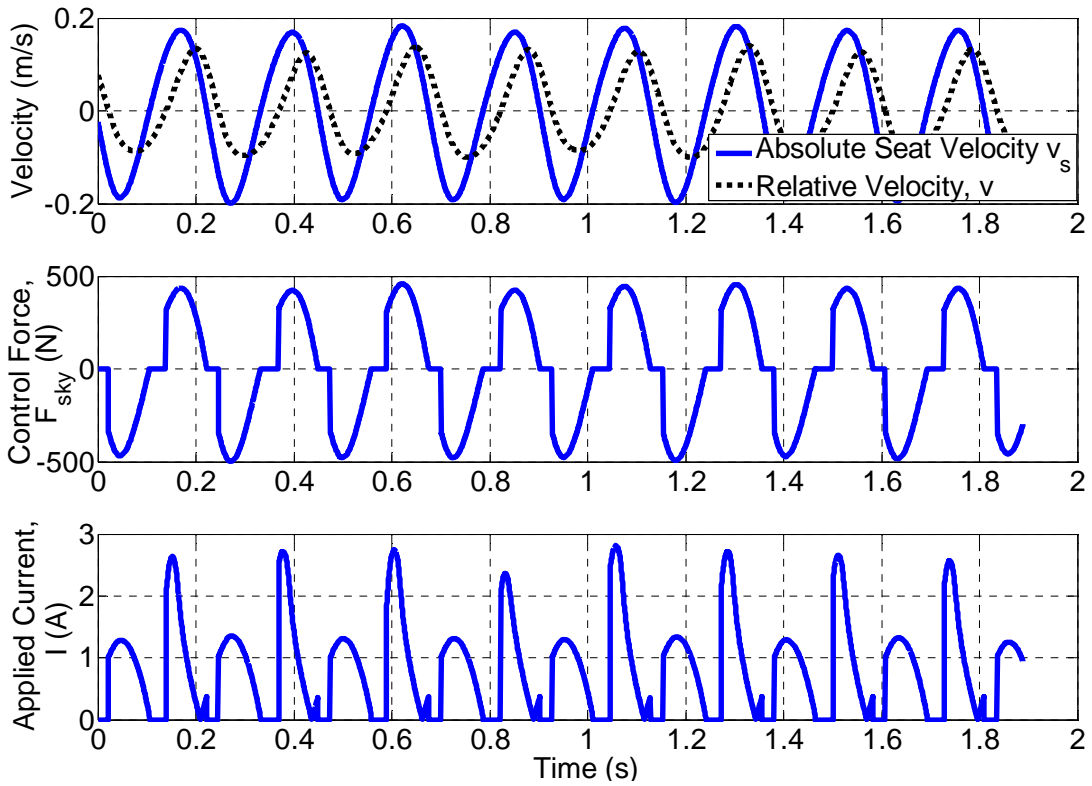


Figure 4.13: Time History Data near Resonance, 50<sup>th</sup> Percentile Male, 0.2 g

Amplitude Floor Excitation

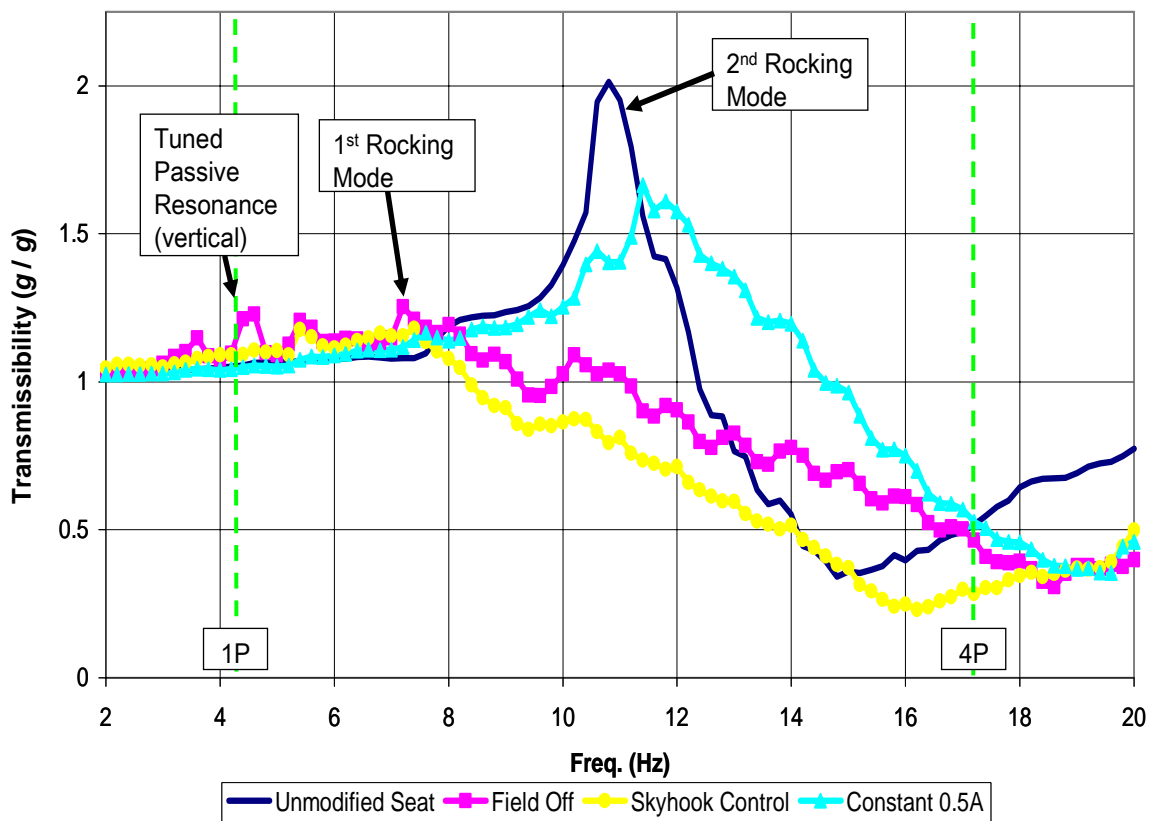


Figure 4.14: Rear Seat Pan Vertical Transmissibility for 5th Percentile Female, 0.2 g Excitation

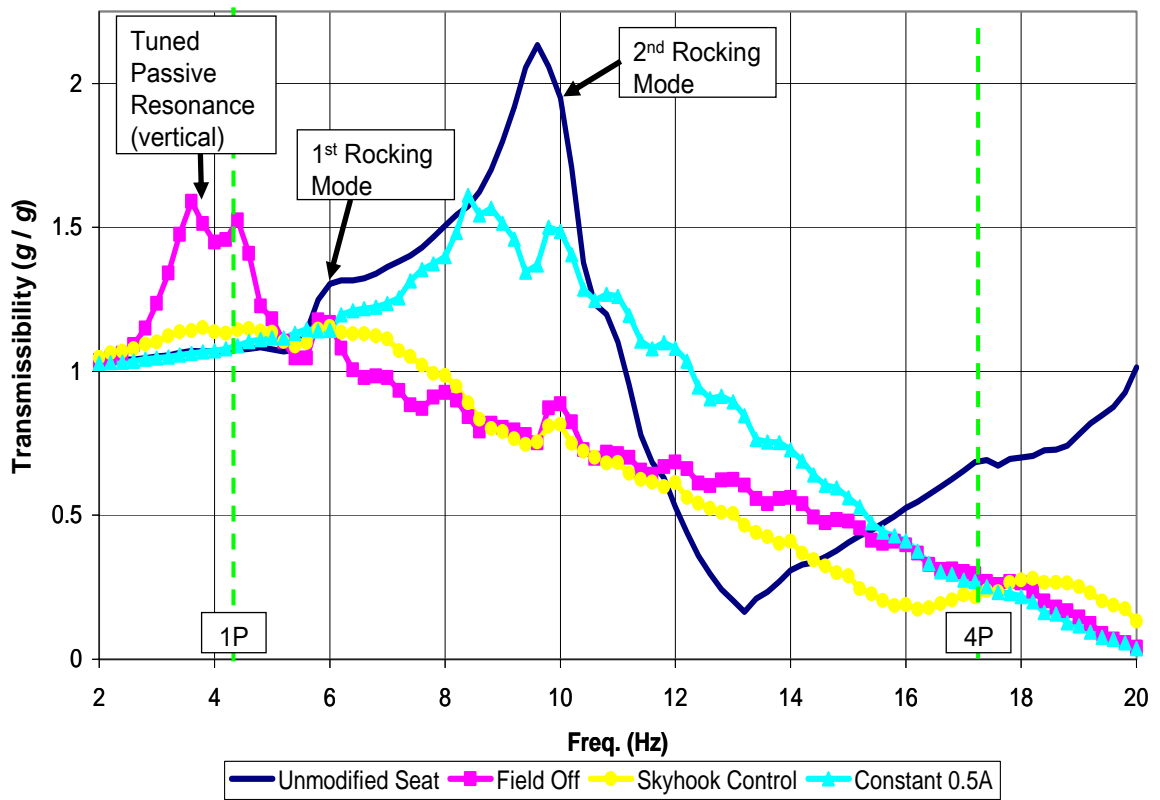


Figure 4.15: Rear Seat Pan Vertical Transmissibility for 95th Percentile Male, 0.2 g Excitation

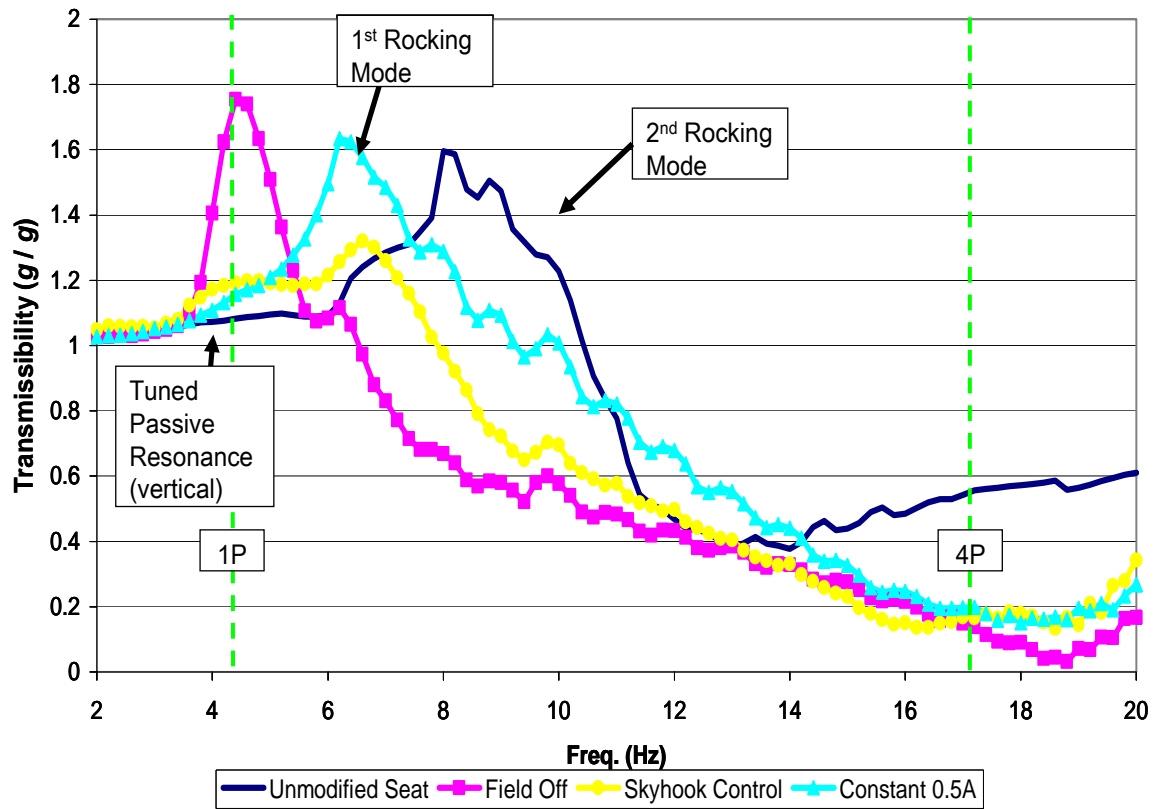


Figure 4.16: Rear Seat Pan Vertical Transmissibility for 50th Percentile Male, 0.4 g Excitation

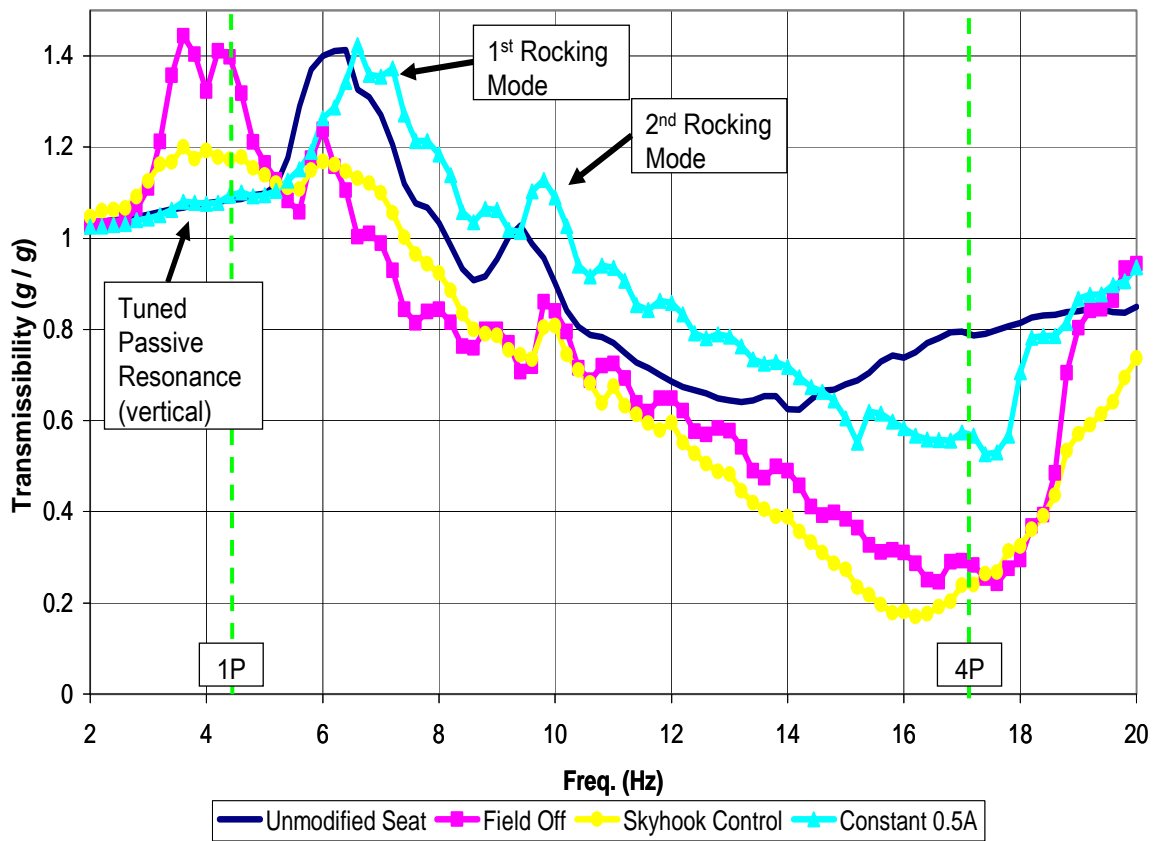


Figure 4.17: Rear Seat Pan Vertical Transmissibility for 50th Percentile Male, 0.2 g Excitation, with Cushion

Table 4.1: Summary of Key Response Reductions Compared to Unmodified SH-60

Crew Seat

<b>Occupant / Condition</b>	<b>5th %ile Female, 0.2 g</b>	<b>50th %ile Male, 0.2 g</b>	<b>95th %ile Male, 0.2 g</b>	<b>50th %ile Male, 0.4 g</b>	<b>50th %ile Male w/ Cushion, 0.2 g</b>
<b>4P, vertical</b>	45%	61%	69%	71%	70%
<b>Seat rocking, longitudinal</b>	93%	85%	88%	88%	46%
<b>Seat rocking, vertical</b>	82%	80%	82%	75%	25%
<b>1P, vertical</b>	-5%	-8%	-8%	-10%	-9%

## **Chapter 5: Summary, Conclusions, & Recommendations for Future Work**

This research focused on the use of magnetorheological energy absorbers (MREAs) for enhanced occupant protection during harsh or crash landings as well as isolation of the occupant from harmful cockpit vibrations. It was shown that the capabilities of the current state-of-the-art helicopter crew seat energy absorption systems are highly limited because they cannot optimally adapt to the individual crash scenario (i.e. both occupant weight and crash load level). Additionally, current energy absorbers (EAs) currently act as stiff members until their tuned load threshold is reached – thereby providing no means of isolating the occupant from harmful cockpit vibrations. MREAs provide the capability of optimally protecting the occupant by utilizing the same (full) stroke in each crash, regardless of occupant weight or crash level, to transmit the lowest load possible to the occupant and therefore minimize the risk of injury. Furthermore, MREAs have the added capability of being able to isolate the occupant from cockpit vibrations, thereby increasing comfort, reducing vibration induced health risks, and increasing crew exposure times.

### *5.1 Original Contributions*

As mentioned earlier, this research represents the first known in-depth investigation into the use of an MR-based suspension for rotorcraft seats to provide both enhanced occupant protection during harsh vertical landings as well as isolation of cockpit vibrations. As such, there are a number of original contributions to the field. These contributions are listed in the following three subsections.

### 5.1.1 Investigation of MR Dampers for Enhanced Crashworthiness and Vibration Isolation of Helicopter Crew Seats

This research effort began with an in-depth investigation into the feasibility of such a system for both enhanced crashworthiness and vibration isolation. Key challenges in designing a magnetorheological energy absorber (MREA)-based seat suspension system for both enhanced occupant protection and vibration isolation were identified. Furthermore, relations were made between MREA design parameters (maximum force, dynamic range, etc.) and resulting performance. Three MREA design options were considered: one optimized solely for vibration isolation, one for enhanced occupant protection, and one that is simultaneously capable of both enhanced occupant protection and vibration isolation. Resulting metrics such as performance, capabilities, weight, and size are compared, and the benefits and sacrifices associated with each of these designs were discussed.

Key contributions of this study are:

1. By using a single-degree-of-freedom (SDOF) seat suspension model, it was shown that low off-state viscous damping and low friction are key elements in effective design of MR seat suspensions for vibration isolation. It was shown that using such a design strategy, an MR damper can be designed to significantly reduce the vibration transmitted to the occupant with minimal weight impact. Experimental results have shown that such a system will reduce 4P floor vibrations by 76% of 4/rev floor vibrations while only adding 1.8 kg (4.0 lb) to the seat. This is only a net weight gain of 8% and 3% for the unarmored and armored SH-60 Seahawk crew seats, respectively. Furthermore, it was shown that such MR dampers can be retrofitted into current rotorcraft seat designs in such a

manner (in series with FLEA/VLEAs) that their crashworthy capabilities are preserved.

2. Using a lumped-parameter biodynamic seat model with the capability of estimating occupant lumbar load response, an MR seat suspension was designed for the purposes of enhanced occupant protection. It was shown that MREAs can be designed to retrofit FLEAs and VLEAs in rotorcraft seats and provide enhanced occupant protection by adapting to occupant weight and load level. These MREAs can utilize the full stroking capability of the seat for each harsh landing in order to minimize the load transmitted into the occupant. Using conventional MR valve designs, however, this enhanced performance comes at a cost of a slightly higher weight penalty of 6.7 kg (14.7 lb), which is an increase of 29% and 12% to the unarmored and armored SH-60 Seahawk crew seats, respectively. Because of stroke limitations and high viscous damping levels, however, such a design does not have appreciable capability to isolate the occupant from cockpit vibrations.

3. It was shown that, with an increase in MREA dynamic range and stroke capability, an MR seat suspension is capable of achieving the dual goals of enhanced occupant protection and vibration isolation. An MREA was designed which will provide the capability of adapting to occupant weight and load levels during a crash or harsh landing and also provide 50% reduction in 4P cockpit vibrations. Using conventional MR damper technology, however, this enhanced performance comes at a cost of increased weight penalty – 21.4 kg (47 lb) or 93% and 40% of the unarmored and armored SH-60 crew seats, respectively. Practical

implementation, therefore, is hindered by a sacrifice to size and weight resulting from conventional MR damper technology.

#### 5.1.2 Control of MREAS for Adaptive Crashworthiness

In order to further illustrate the benefits gained with an MREA-based suspension for enhanced crashworthiness, three schemes to which such a suspension can be controlled were developed and analyzed:

1. The first of these realized the MREAs as automatically adapting variable load energy absorbers (VLEAs) with the MREA yield force being modulated to limit the seat deceleration to a constant value (14.5 g, for instance). This control scheme allows for unattended and continuously proportional adaptation to occupant weight. It was also shown that while MREA time delay adds some error in tracking the limit load, the predicted lumbar loads were maintained within a humanly tolerable range.

2. Next, a control scheme which realizes MREAs as variable profile energy absorbers (VPEAs) was presented. This control scheme adapts a notched load-stroke profile to varying occupant weight. It was shown that such a control scheme can be implemented to reduce the stroke utilized by taking advantage of the dynamics of the human body. It was shown, however, that the inclusion of MREA time delay cancels this stroke reducing capability because the notched load-stroke profile requires rapid force modulation.

3. Finally, a crash load adaptive (CLA) control scheme was presented which automatically adapts to both occupant weight and crash load level. This controller feeds back real-time stroking velocity measurements and calculates a

control force that is proportional to both occupant mass and the square of the stroking velocity. It was shown that this control scheme allows the full suspension stroke to be utilized for each crash scenario, regardless of occupant weight and crash load level. By always utilizing the full suspension stroke, the load transmitted to the occupant was always minimized. This allows the risk of injury to be significantly reduced or eliminated for lower crash load levels. This is a significant improvement over conventional EAs which always transmit a 14.5 g stroking load, corresponding to a 20% risk of injury. It was also shown that, while the control gain must be adjusted to account for MREA time delay, the ability to adapt to crash level was not hindered by this effect.

#### 5.1.3 Semi-Active Magnetorheological Helicopter Crew Seat Suspension for Vibration Isolation

Because the option of using an MR suspension to address only vibration isolation has a very low weight penalty, it was deemed the most practical for near-term implementation into the fleet. As such, the use of magnetorheological (MR) dampers in a semi-active seat suspension system for helicopter crew seats to enhance occupant comfort and reduce health issues resulting from whole body vibration was further explored. The issue of vibration isolation of rotorcraft crew seats has not been explored in the past for two primary reasons: 1) the primary focus of rotorcraft seat suspension design has been on occupant protection during a crash using energy absorbers that cannot provide vibration isolation; and 2) passive vibration isolation systems cannot be designed to provide adequate performance because the cockpit vibration spectrum is very broad in frequency and a passive resonance is inevitable. This research has shown, however, that a semi-active MR suspension can effectively

isolate higher frequency vibrations while suppressing resonance conditions. Furthermore, it was shown that MR dampers can be implemented in series with the existing fixed load energy absorbers (FLEAs) such that the crashworthiness capability of the seat was not impaired.

MR dampers were designed, fabricated, and retrofitted into a tactical SH-60 Seahawk crew seat. A skyhook control algorithm was utilized and performance was evaluated both analytically and experimentally. Experimental test results demonstrated that this system reduced the dominant rotor-induced vertical vibration (4 per rev) transmitted to a 50<sup>th</sup> percentile male aviator by 76%, which is a 61-70% improvement over the unmodified SH-60 crew seat, depending upon whether a soft seat cushion was utilized. Furthermore, these experimental tests also showed that this system significantly reduces vertically-induced seat rocking that occurs as a result of an offset center of gravity in the crew seat design. Finally, it was also shown that, while the dynamics of a tactical vehicle seat may be complex, a SDOF model can be a valuable tool for MR damper design and performance predictions.

## *5.2 Future Work*

While this research has successfully shown the feasibility and benefits of semi-active magnetorheological seat suspensions for rotorcraft applications, a number of key challenges remain that should be addressed prior to practical implementation. The following subsections outline areas of future research and development through which this technology's state of readiness can be further advanced.

### 5.2.1 MREA Design

While this research has shown that MREAs can be designed to address both vibration isolation and enhanced occupant protection during harsh vertical landings, significant challenges remain before they can be implemented into the fleet. A major hurdle associated with this practical implementation of MREAs involves the MREA design itself. As discovered in this research, using conventional MR technology the enhanced occupant protection capabilities come at a sacrifice of increased device weight. Since weight reduction is a key goal in rotorcraft applications, crashworthy MREAs using current MR technology may not be particularly attractive. Furthermore, since the onset of crash loads are very rapid, the time response (delay) of MREAs may also be a concern. Future studies, therefore, should focus on new MREA designs and MR valve configurations to reduce weight and response time. The aim of such configurations might be to decouple the stroke capability from the MR valve such that the MR valve size is reduced. Also, since MR fluid is inherently heavy, the reduction in the volume of MR fluid utilized would provide a weight advantage. Finally, implementing a design which utilizes a smaller MR coil will also improve MREA time response. Other details that must be addressed prior to practical implementation include environmental considerations such as the effects of corrosive environments (marine, salt fog) and temperature, as well as, electronic considerations such as electromagnetic interference (EMI). Addressing such details as weight, performance, and environmental considerations will make this technology significantly more attractive for both military and commercial rotorcraft applications.

## 5.2.2 MREA Control Experimentation & Refinement

In this research, three MR seat suspension designs were developed, one solely for vibration isolation, one solely for crashworthiness, and one to address both of these goals in a single device. In addition to this, three MREA control strategies were developed and analyzed to provide enhanced occupant protection during harsh vertical landings or crashes. Only one MR seat suspension design – that for solely vibration isolation – was able to be fabricated and experimentally tested as a part of this research, however, and therefore these MREA control strategies remain untested. Future research, therefore, should involve the fabrication of an MREA and experimental verification and refinement of these MREA control strategies. In particular, the crash load adaptive (CLA) control strategy holds particular promise in significantly advancing the state-of-the-art for occupant protection because it can automatically adapt to crash load level and occupant weight to provide minimized risk of injury. Experimental testing and refinement of this control strategy as well as development of other similar control schemes will significantly advance this field of research and provide key demonstrations to the benefits of MREA-based rotorcraft seat suspensions. Such experiments may involve low sink rate testing using the Vertical Axis Shock & Vibration Test Stand at the University of Maryland or high speed testing using horizontal sled testing facilities at Armor Holdings Aerospace and Defense Group in Phoenix, AZ, or the Naval Air Warfare Center – Aircraft Division in Patuxent River, MD.

### 5.2.3 Refinement of MR Seat Suspension for Vibration Isolation

This research has shown great success in isolating the crew from harmful cockpit vibrations by retrofitting an unarmored SH-60 Seahawk crew seat with MR dampers. A number of efforts remain, however, that can improve performance and ready this technology for practical implementation.

The first improvement that can be made to this system is to reduce weight. The hardware that was fabricated and tested as part of this research was a proof-of-concept and was not weight optimized. Through the use of lower density materials and optimized structural designs, it is estimated that this system will have a significant weight reduction (~60%) down to approximately 5 lbs. Further weight reduction may be achieved if the MR damper design is refined to reduce the volume of fluid and thickness of the hydraulic cylinders and end caps.

Next, a performance improvement may be possible if friction in the system is reduced. It was shown in Chapter 4 that there was some performance limitation, especially for lighter occupants, due to friction in the MR damper rod seals and at the piston ring. The choice of lower friction materials or coatings may reduce this friction and provide better overall system performance. This issue may also be addressed by designing an MR damper that does not require sliding contact points.

Finally, in order to further ready this system for practical implementation, a number of other considerations should be addressed. Firstly, the control electronics should be developed into an economical, compact, modular form that can be mounted within the seat assembly and will meet environmental requirements. This may be done using MEMS accelerometers and low-cost microcontroller chips. Also, the

system should undergo qualification testing to ensure that the retrofit MR dampers do not interfere with crew operations or the original crashworthiness capabilities. Another beneficial study would be to evaluate other rotorcraft seats and explore other retrofit options. Determining as much commonality in components between seats as possible would be highly beneficial for reducing cost of a production system. Finally, details such as corrosion, temperature, electromagnetic interference, etc., should be addressed prior to practical implementation. Once these improvements are made and details addressed, this technology will be very attractive for both military and commercial rotorcraft applications to improve comfort, reduce fatigue, and extend allowable mission times for the crew.

#### 5.2.4 Applicability to Other Vehicle Seats

While this research has focused on rotorcraft seats, this technology holds great promise for other vehicle seat applications. MR seat suspension technology is particularly attractive for vehicles such as boats and ground vehicles because they are not as sensitive to weight as aircraft. For boat seats, this technology could be used to mitigate the repetitive shock due to high speed travel in a sea state. Such an MR suspension could adapt to occupant weight and to the shock level to optimally protect the occupant's spine during the harshest of sea states and improve comfort and reduce fatigue in calmer seas. This is particularly attractive for fast attack boats such as the Mark V Special Operations Craft in which Navy Seals are being continually injured.

This technology is also applicable to ground vehicles that experience varying levels of vibration and shock excitations. An MR seat suspension could isolate the occupant from low amplitude vibrations while on road or on flat terrain as well as

mitigate higher amplitude shocks experienced when traversing off-road terrain. For military ground vehicles, such a system could also optimally protect the occupant from ballistic shock such as mine blasts. Such a semi-active system may be attractive because it is a single solution that addresses multiple areas of concern: reduction in whole body vibration, mitigation of off-road shocks, and protection of the occupant during ballistic shock.

MR seat suspensions could be designed and fabricated for these applications and tested in the laboratory using hardware-in-the-loop simulations to determine the effectiveness for such a system. Control algorithms may be developed specifically to address issues such as repetitive shock and varying excitation levels such that the system will automatically adapt and provide optimal occupant protection. Multi-mode controllers may be necessary such that the controller will automatically adjust itself to the real-time measured environment. Successfully experimental demonstration of this technology will make it very attractive to a myriad of vehicle markets.

## Bibliography

- [1] Desjardins, S. P., Zimmerman, R. E., Bolukbasi, A. O., and Merritt, N. A., “Aircraft Crash Survival Design Guide Vol. IV – Aircraft Seats, Restraints, Litters, and Cockpit/Cabin Delethalization,” Aviation Applied Technology Directorate, USAAVSCOM Technical Report 89-D-22D, 1989, pp. 45-58, 83-109, and 165.
- [2] Choi, Y. T., and Wereley, N. M., “Biodynamic Response Mitigation to Shock Loads Using Magnetorheological Helicopter Crew Seat Suspensions,” *Journal of Aircraft*, Vol. 42, (5), 2005, pp. 1288-1295.
- [3] Desjardins, S. P., “The Evolution of Energy Absorption Systems for Crashworthy Helicopter Seats,” *Journal of the American Helicopter Society*, Vol. 51, (2), 2006, pp. 150-163.
- [4] Coltman, J. W., Van Ingen, C., Johnson, N. B., and Zimmerman, R. E., “Aircraft Crash Survival Design Guide Vol. II – Aircraft Crash Design Impact Conditions and Human Tolerance,” Aviation Applied Technology Directorate, USAAVSCOM Technical Report 89-D-22B, 1989, pp. 29-87.
- [5] Bongers, P. M., Hulshof, C. T. J., and Dijkstra, L., et al, “Back Pain and Exposure to WBV in Helicopter Pilots, Exposure for MH-60S Pilots,” *Ergonomics*, Vol. 33, 1990, pp. 1007-1026.
- [6] Harrer, K. L., Yniguez, D., Majar, M., Ellenbecker, D., Estrada, N., and Geiger, M., “Whole Body Vibration Exposure for MH-60S Pilots” *Proceedings of the Forty Third Annual SAFE Association Symposium*, Salt Lake City, Utah, October 24-26, 2005, pp. 303-314.

- [7] Shanahan, D. F., Mastroiane, G., and Reading, T. D., "Back Discomfort in U.S. Army Military Helicopter Aircrew Member," *Backache and Back Discomfort*, Neuilly-sur-Siene, France: AGARD; AGARD-CP-378, Vol. 21, 1986, pp. 10-25.
- [8] Hiemenz, G. J., Hu, W., and Wereley, N. M., "Investigation of MR Dampers for Enhanced Crashworthiness and Vibration Isolation of Helicopter Crew Seats," *Proceedings from the 63<sup>rd</sup> Annual AHS Forum*, Virginia Beach, VA, May, 2007.
- [9] Kamath, G. and Wereley, N., "Modeling the Damping Mechanism in Electrorheological Fluid Base Dampers," M3D III: Mechanics and Mechanisms of Material Damping ASTM STP 1304, pp. 331-348, 1997.
- [10] Pang L., Kamath, G., and Wereley N., "Analysis and Testing of a Linear Stroke Magnetorheological Damper," in *Proceedings of SPIE Conference on Passive Damping and Isolation*, vol. 3327-25, (San Diego, CA), March 2-3, 1998.
- [11] Lindler J., and Wereley N. M., "Double Adjustable Shock Absorbers Using Electrorheological Fluids." *Journal of Intelligent Material Systems and Structures*. Vol. 10, No. 8, August, 1999, pp. 652–657.
- [12] Kamath G. and Wereley, N., "Influence of Pre-Yield Behavior on Dynamic Response of Systems Using ER and MR Dampers," in *Proceedings of the 7<sup>th</sup> International Conference on ER Fluids and MR Suspensions*, (Honolulu, HI), July 19-23, 1999.

- [13] Wereley, N., Pang, L. and Kamath, G., "Idealized Hysteresis Modeling of Electrorheological and Magnetorheological Dampers," *Journal of Intelligent Material Systems and Structures* 9, pp. 642-649, August, 1998.
- [14] Wereley, N. M., and Pang, L., "Nondimensional Analysis of Semi-Active Electrorheological And Magnetorheological Dampers Using Approximate Parallel Plate Models," *Smart Materials and Structures*, Vol. 7, (5), 1998, pp. 732-743.
- [15] Hong, S. R., Choi, S.B., Choi, Y.-T. and Wereley, N. M., "Nondimensional Analysis for Effective Design of Semi-Active Electrorheological Damping Systems," *IMEchE Part D Journal of Automobile Engineering*, Vol. 217, No. 12, pp. 1095–1106.
- [16] Mao, M., Choi, Y.-T., and Wereley, N. M., "Effective Design Strategy for a Magneto-Rheological Damper Using a Nonlinear Flow Model," *Smart Structures and Materials 2005: Damping and Isolation*, SPIE, Vol. 5760, pp. 446-455.
- [17] Hartog, J., "Forced Vibrations with Combined Coulomb and Viscous Friction," *Journal of Applied Mechanics*, 1953.
- [18] Hiemenz, G. J., and Wereley, N. M., "Seismic Response of Civil Structures Utilizing Semi-Active ER and MR Bracing Systems," *Journal of Intelligent Materials and Structures*, Vol. 10, (8), 1999.
- [19] Leitmann, G., "Semi-Active Control for Vibration Attenuation," *Journal of Intelligent Material Systems and Structures* 5, pp. 841-846, November 1994.

- [20] Dyke, S., Spencer Jr., B., Sain, M., and Carlson, J., "Seismic Response Reduction Using Magnetorheological Dampers," in Proceedings of the IFAC World Congress, vol. L, pp. 145-150, (San Francisco, CA), June 30-July 5, 1996.
- [21] Dyke, S., Spencer Jr., B., Sain, M., and Carlson, J., "Experimental Verification of Semi-Active Structural Control Strategies Using Acceleration Feedback," in Proceedings of the 3rd International Conference on Motion and Vibration Control, vol. III, pp. 1-9, (Chiba, Japan), Sept. 1-6, 1996.
- [22] Karnopp, D., Crosby, M. and Harwood, R., "Vibration Control Using Semi-Active Force Generators," Journal of Engineering for Industry, Vol. 96, (2), 1974, pp. 619-626.
- [23] Miller, L. R., An Approach to Semi-active Control of Multi-Degree-of-Freedom Systems, 1988 (Ph.D. Thesis, North Carolina State University, Raleigh, N.C.).
- [24] Carter, A. K., Transient Motion Control of Passive and Semi-active Damping for Vehicle Suspensions, 1998 (M.S. Thesis, Virginia Polytechnic Institute and State University, Blacksburg, Virginia).
- [25] Koo, J. H., and Ahmadian, M., "A Qualitative Analysis of Groundhook Tuned Vibration Absorbers for Controlling Structural Vibrations," Journal of Multibody Dynamics, Special Edition for June 2002.
- [26] Goncalves, F. D., and Ahmadian, M., "A Hybrid Control Policy for Semi-Active Vehicle Suspensions," Shock and Vibration, Vol. 10, 2003, pp. 59-69.

- [27] Hong, K.S., Sohn, H. C., and Hedrick, J. K., "Modified Skyhook Control of Semi-Active Suspensions: A New Model, Gain Scheduling, and Hardware-in-the-Loop Tuning," *ASME Journal of Dynamic Systems, Measurement, and Control*, Vol. 124, March 2002, pp. 158-167
- [28] Ahmadian, M, Song, X., and Southward, S. C., "No-Jerk Skyhook Control Methods for Semiactive Suspensions," *ASME Journal of Vibration and Acoustics*, Vol. 126, Oct. 2004, pp. 580-584.
- [29] Hiemenz, G. J., Choi, Y.-T., and Wereley, N. M., "Seismic Control of Civil Structures Utilizing Semi-Active MR Braces," *Journal of Computer-Aided Civil and Infrastructure Engineering*, Vol. 18, 2003, pp. 31-44.
- [30] Wu, X., and Griffin, M. J., "A Semi-Active Control Policy to Reduce the Occurrence and Severity of End-Stop Impacts In A Suspension Seat with an Electrorheological Fluid Damper," *Journal of Sound and Vibration*, Vol. 203, (5), 1997, pp. 781-793.
- [31] Choi, S. B., Choi, J. H., Nam, M. H., Cheong, C. C., and Lee, H. G., "A Semi-Active Suspension Using ER Fluids for a Commercial Vehicle Seat," *Journal of Intelligent Material Systems and Structures*, Vol. 9, (8), 1999, pp. 601-606.
- [32] Choi, S. B., Nam, M. H., and Lee, B. K., "Vibration Control of MR Seat Damper for Commercial Vehicles," *Journal of Intelligent Material Systems and Structures*, Vol. 11, (12), 2000, pp. 936-944.
- [33] Park, C., and Jeon, D., "Semi-Active Vibration Control of A Smart Seat with an MR Fluid Damper Considering Its Time Delay," *Journal of Intelligent Material Systems and Structures*, Vol. 13, (7/8), 2002, pp. 521-524.

- [34] Liu, X. X., Shi, J., Li, G., Le, X., Zhao, B., Yue, M., Liu, J., Bai, G. and Ke, W., "Biodynamic Response and Injury Estimation of Ship Personnel to Ship Shock Motion Induced by Underwater Explosion", Proceedings of the 69th Shock and Vibration Symposium, Shock and Vibration Information Analysis Center, Richmond, VA, Vol. 18, 1998, pp. 1-18.
- [35] Zong, Z., and Lam, K. Y., "Biodynamic Response of Shipboard Sitting Subject to Ship Shock Motion," Journal of Biomechanics, Vol. 35, No. 1, 2002, pp. 35-43.
- [36] Gunston, T., and Griffin, M. J., "The Isolation Performance of a Suspension Seat Over a Range of Vibration Magnitudes Tested With An Anthropodynamic Dummy And Human Subjects," Inter-noise '99, Proc. 28<sup>th</sup> Int. Congress and Exposition on Noise Control Engineering, Florida, U.S.A., December 1999, pp. 949-954.
- [37] Boileau, P. E., Rakheja, S., and Wu, X., "A Body Mass Dependent Mechanical Impedance Model for Applications in Vibration Seat Testing," Journal of Sound and Vibration, Vol. 253, (1), 2002, pp. 243-264.
- [38] Hiemenz, G. J., Choi, Y. T., and Wereley, N. M., "Semi-Active Control of a Vertical Stroking Helicopter Crew Seat for Enhanced Crashworthiness," AIAA Journal of Aircraft, Vol. 44, No. 3, May-June 2007, pp. 1031-1034.
- [39] Hiemenz, G. J., Hu, W. and Wereley, N. M., "Semi-Active Magnetorheological Helicopter Crew Seat Suspension for Vibration Isolation," Proceedings from the 15th AIAA/ASME/AHS Adaptive Structures Conference, Waikiki, HI, April 2007.

- [40] Bousman, W. G., "Putting the Aero Back into Aeroelasticity," NASA/TM-2000-209589, USAAMCOM-TR-00-A-005, March 2000.
- [41] "Crash Protection Handbook – Crew Systems," Department of Defense Joint Services Specification Guide, JSSG-2010-7, 1998, pp. 34.
- [42] Wereley, N. M., Hiemenz, G. J., Hu, W., Wang, G, and Chen, P., "Adaptive Energy Absorption System for a Vehicle Seat," U.S. Patent Application No. 11/670,773, Feb. 2007.
- [43] J. Lindler and N. M. Wereley, "Analysis and Testing of Electrorheological Bypass Dampers," Journal of Intelligent Material Systems and Structures. Vol. 10, (5), 1999, pp. 363-376.
- [44] Facey, W. B., Rosenfeld, N. C., Choi, Y. T., Wereley, N. M., Choi, S. B., and Chen, P. C., "Design and Testing of a Compact Magnetorheological Impact Damper for High Impulsive Loads," International Journal of Modern Physics Part B, Vol. 19 (7-9), 2005, pp. 1549-1555.
- [45] Chen, P. and Wereley, N., "Magnetorheological Damper and Energy Dissipation Method," U.S. Patent No. 6,694,856B1, Feb. 2004.
- [46] Choi Y.-T. and Wereley N. M., "Comparative Analysis of the Time Response of Electrorheological and Magnetorheological Dampers Using Nondimensional Parameters," Journal of Intelligent Material Systems and Structures, Vol. 13, No. 7/8, 2002 pp. 443-452.